THE FLORIDA STATE UNIVERSITY

FAMU-FSU COLLEGE OF ENGINEERING

A CONCENTRATED SOLAR THERMAL ENERGY SYSTEM

By

C. CHRISTOPHER NEWTON

A Thesis submitted to the
Department of Mechanical Engineering
in partial fulfillment of the
requirements for the degree of
Master of Science

Degree Awarded:
Spring Semester, 2007

The members of the Committee approve the Thesis of C. Christopher Newton defended on December 14, 2006.

_____
Anjaneyulu Krothapalli
Professor Directing Thesis

_____
Patrick Hollis
Outside Committee Member

_____
Brenton Greska
Committee Member

The Office of Graduate Studies has verified and approved the above named committee members.

This thesis is dedicated to my family and friends for their love and support.

ACKNOWLEDGEMENTS

I would like to thank Professor Anjaneyulu Krothapalli and Dr. Brenton Greska for their advisement and support of this work. Through their teachings, my view on life and the world has changed.

I would also like to give special thanks to Robert Avant and Bobby DePriest for their help with the design and fabrication of the apparatus used for this work. Also, I would like to thank them for teaching myself, the author, the basics of machining.

Mike Sheehan and Ryan Whitney also deserve mention for their help with setting up and assembling the apparatus used in this work.

The help and support from each of these individuals mentioned was, and will always be greatly appreciated.

TABLE OF CONTENTS

LIST OF TABLES

LIST OF FIGURES

ABSTRACT

Solar thermal technology is competitive in some very limited markets. The most common use for solar thermal technology has been for water heating in sunny climates. Another use is for power production, such as the Vanguard system and the Shannendoah Valley Parabolic dish system. However, due to the complex design and costs of production and maintenance, solar thermal systems have fallen behind in the world of alternative energy systems.

The concentrated solar thermal energy system constructed for this work follows that of the conventional design of a parabolic concentrator with the receiver placed along the line between the center of the concentrator and the sun. This allows for effective collecting and concentrating of the incoming solar irradiation. The concentrator receives approximately 1.064 kW/m^2 of solar insolation (dependent upon time of year), which is concentrated and reflected to the receiver. By concentrating the incoming radiation, the operating temperature of the system is increased significantly, and subsequently increases the efficiency of the conversion from sunlight to electricity. For the current system, with a concentration ratio of 96, the concentrator is theoretically capable of producing temperatures upwards to 712 degrees centigrade. However, due to degradation of the optics and other various factors, temperatures as high as 560 degrees centigrade have been achieved. It was found that the collector (concentrator + receiver) yields an efficiency of 95.6 percent.

The system converts this concentrated solar energy to electric energy by use of a Rankine cycle which is operated intermittently; determinant by operating temperature. The efficiency of the Rankine cycle for this system was determined to be 3.2 percent, which is 10.3 percent of its Carnot Efficiency.

The system has a solar to electric power conversion of 1.94 percent with a peak electric power production of 220 Watts.

The rousing point for this particular system is the simplicity behind the design, with it being simple enough to be maintained by an ordinary bicycle mechanic. This makes the system versatile and ideal for use in off-grid and less tech-savvy areas. This work serves mostly as a proof of concept.

CHAPTER 1

BACKGROUND

1.1 Introduction

Even in today's world market, with all of the vast technology advancements and improvements, there are still people who live in darkness at night and use candle light or kerosene lamps to study. These people have the knowledge that electricity exists; however, the area in which they reside lacks the infrastructure and resources for such an amenity. Also, throughout the world, the demand for useable energy is increasing rapidly, with electricity being the energy of choice. This electricity production, however, does not come free. There is cost associated with the infrastructure for setting up new power production facilities and the rising cost and lack of natural resources such as oil, coal, and natural gas. One solution is to steer away from conventional methods and look for novel, alternative, renewable, energy resources, such as solar energy.

The sun is an excellent source of radiant energy, and is the world's most abundant source of energy. It emits electromagnetic radiation with an average irradiance of 1353 W/m^2**1** on the earth's surface [1, 2]. The solar radiation incident on the Earth's surface is comprised of two types of radiation – beam and diffuse, ranging in the wavelengths from the ultraviolet to the infrared (300 to 200 nm), which is characterized by an average solar surface temperature of approximately 6000°K [3]. The amount of this solar energy that is intercepted is 5000 times greater than the sum of all other inputs – terrestrial nuclear, geothermal and gravitational energies, and lunar gravitational energy [1]. To put this into perspective, if the energy produced by 25 acres of the surface of the sun were harvested, there would be enough energy to supply the current energy demand of the world.

1 The average amount of solar radiation falling on a surface normal to the rays of the sun outside the atmosphere of the earth at mean earth-sun distance, as measured by NASA [1].

When dealing with solar energy, there are two basic choices. The first is photovoltaics, which is direct energy conversion that converts solar radiation to electricity. The second is solar thermal, in which the solar radiation is used to provide heat to a thermodynamic system, thus creating mechanical energy that can be converted to electricity. In commercially available photovoltaic systems, efficiencies are on the order of 10 to 15 percent, where in a solar thermal system, efficiencies as high as 30 percent are achievable [4]. This work focuses on the electric power generation of a parabolic concentrating solar thermal system.

1.2 Historical Perspective of Solar Thermal Power and Process Heat

Records date as far back as 1774 for attempts to harness the sun's energy for power production. The first documented attempt is that of the French chemist Lavoisier and the English scientist Joseph Priestley when they developed the theory of combustion by concentrating the rays of the sun on a test tube for gas collection [1]. Figure 1.1 shows an illustration of the solar concentration device used by Lavoisier.

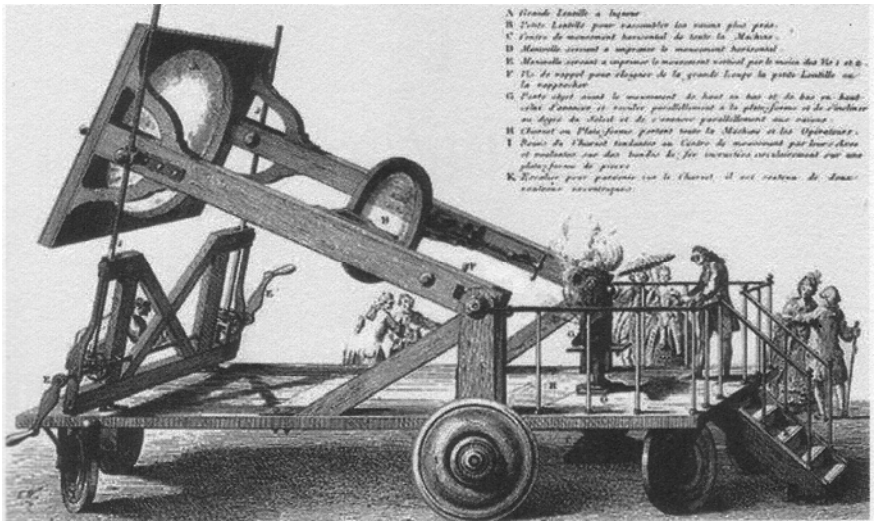

Figure 1.1: Solar furnace used by Lavoisier in 1774. (Courtesy of Bibliotheque Nationale de Paris. Lavoisier, Oeuvres, vol. 3.) [10]

About a century later, in 1878, a small solar power plant was exhibited at the World's Fair in Paris (Figure 1.2). This solar power plant consisted of a parabolic

reflector that focused sunlight onto a steam boiler located at the focus, thus producing steam that was used to operate a small reciprocating steam engine for running a printing press. In 1901, A.G. Eneas in Pasadena, California operated a 10-hp solar steam engine which was powered by a reflective dish with a surface area of 700 ft^2 (~65 m^2 or 30 feet in diameter). Between 1907 and 1913, documents also show that the American engineer, F. Shuman, developed solar-driven hydraulic pumps; and in 1913, he built a 50-hp solar engine for pumping irrigation water from the Nile near Cairo, Egypt. [10]

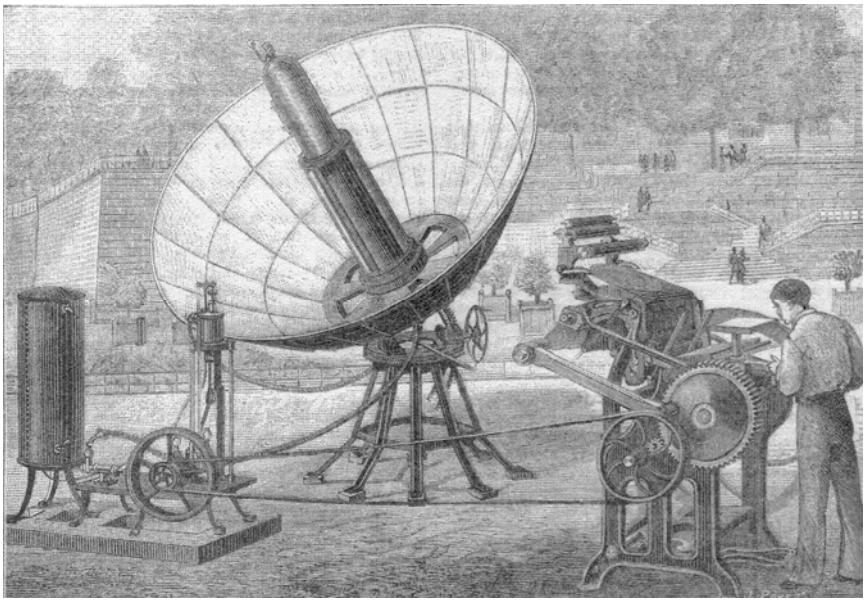

Figure 1.2: Parabolic collector powered printing press at the 1878 Paris Exposition [10]

Interest in solar energy production fell off due to advances in internal combustion engines and the increasing availability of low-cost oil in the early 1900s. Interest in solar power began to arise again in the 1960s, with the focus on photovoltaics for the space program. It wasn't until the oil embargo in 1973 that interest was once again sparked, and research began to take place for development of solar electric power [1].

1.2.1 Known Parabolic Dish Systems

In the late 1970s, Omnium-G, Inc. designed a parabolic dish collector system that would run a steam engine. The parabolic dish was 6 meters (20 feet) in diameter and was constructed from panels of polyurethane foam with a reflecting surface of anodized

aluminum [11]. The receiver for the system was of the cavity type and used a single coil of stainless steel tubing buried in molten aluminum inside of an Inconel housing. The aluminum was used as a type of latent heat storage and to provide uniform heat distribution and thermal storage once melted. The aperture of the receiver was 200mm (8 inches) in diameter, thus giving a geometric concentration ratio of 900. A double-acting reciprocating two cylinder 34 kW (45 hp) steam engine was used with the system, however, it was found to be oversized and operated at 1000 rpm with steam at 315°C and 2.5 MPa (350 psia). One main issue with this particular parabolic dish collector system was that it had a very low reflectance and a large optical error, thus it supplied less energy at the focal region than was needed to power the steam engine.

The Advanco Vanguard, shown in Figure 1.3, is another parabolic dish collector system; however, this system used a Stirling engine at the focal area for power production. Developed by the Advanco Corporation, the Vanguard collector was an 11 meter diameter (36 feet) parabolic dish which consisted of 320 foam-glass facets, each 46 by 61 cm, that had thin-glass, back-surfaced silver mirrors attached. This particular collector, paired with the United Stirling Model 4-95 MkII four-cylinder kinematic Stirling engine holds the world record for conversion of sunlight to electricity with a 31 percent gross efficiency and 29 percent net efficiency (including parasitic losses). The program, however, was cancelled due to the high cost of the concentrator and maintenance to the system [1].

A known parabolic dish based solar thermal power plant also existed in Shenandoah, Georgia. The plant consisted of 114 parabolic dish concentrators (total aperture area of 4352 m^2), and was designed to operate at a maximum temperature of 382°C and to provide electricity (450 kW_e), air-conditioning, and process steam (at 173°C). The individual parabolic concentrators were seven meters in diameter (23 feet), and constructed of stamped aluminum gores with an aluminized plastic film applied to the reflective surface [4]. The overall power cycle efficiency of the system was 17 percent, which was 42 percent of the maximum possible [4]. However, due to high costs and the amount of maintenance required, the system was decommissioned in 1990.

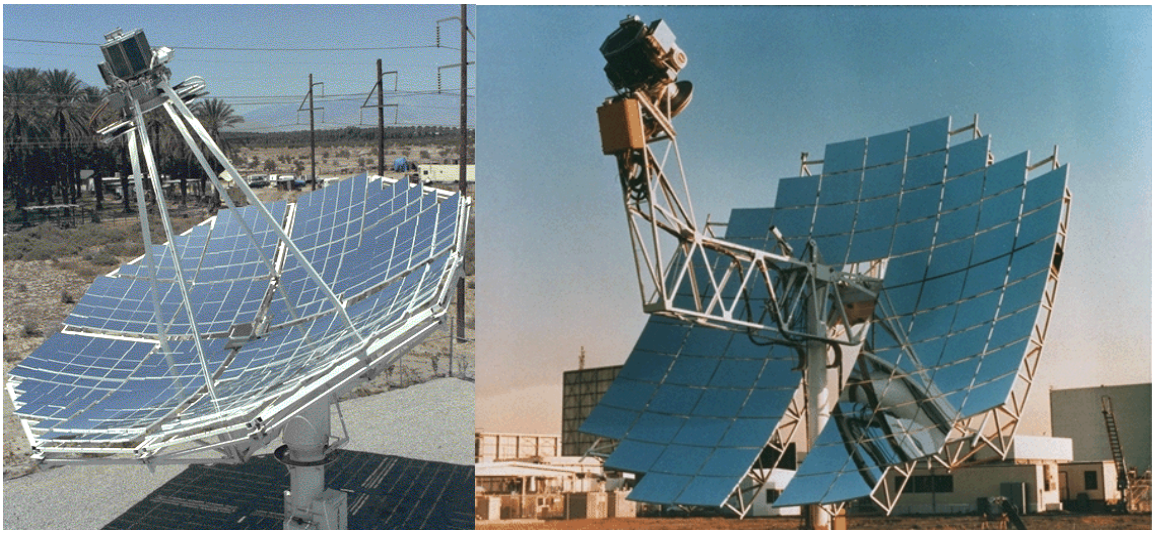

Figure 1.3: Photographs of the Vanguard (left) and McDonnell Douglas (right) parabolic concentrator systems.

Other known parabolic concentrator systems, such as Solarplant One, McDonnell Douglas Stirling Systems (Figure 1.3), Power Kinetics, Inc. Captiol Concrete Collector, the Jet Propulsion Laboratories Test-Bed Concentrators, and a few other projects in conjunction with Sandia National Laboratories, have been designed and tested in the last twenty years. In the early 1990s, Cummins Engine Company attempted to commercialize a dish-stirling system by teaming up with SunLab, but this company pulled out in 1996 to focus solely on its core diesel-engine business. It appears that Sandia National Laboratories is still currently researching new systems. The apparent downfall for the majority of the solar thermal systems mentioned here is due to the extremely high cost and high maintenance of the systems.

1.3 Solar Thermal Conversion

The basic principle of solar thermal collection is that when solar radiation is incident on a surface (such as that of a black-body), part of this radiation is absorbed, thus increasing the temperature of the surface. As the temperature of the body increases, the surface loses heat at an increasing rate to the surroundings. Steady-state is reached when the rate of the solar heat gain is balanced by the rate of heat loss to the ambient surroundings. Two types of systems can be used to utilize this solar thermal conversion:

passive systems and active systems [2]. For our purposes, an active system is utilized, in which an external solar collector with a heat transfer fluid is used to convey the collected heat. The chosen system for the solar thermal conversion at SESEC is that of the parabolic concentrator type.

1.4 Solar Geometry (Fundamentals of Solar Radiation)

In order to track the sun throughout the day for every day of the year, there are geometric relationships that need to be known to find out where to position the collector with respect to the time. In order to perform these calculations, a few facts about the sun need be known.

The sun is considered to be a sphere $13.9 \times 10^5 \, km$ in diameter. The surface of the sun is approximated to be equivalent to that of a black body at a temperature of 6000K with an energy emission rate of $3.8 \times 10^{23} \, kW$. Of this amount of energy, the earth intercepts only a small amount, approximately $1.7 \times 10^{14} \, kW$, of which 30 percent is reflected to space, 47 percent is converted to low-temperature heat and reradiated to space, and 23 percent powers the evaporation/precipitation cycle of the biosphere [1].

1.4.1 Sun-Earth Geometric Relationship

The earth makes one rotation about its axis every 24 hours and completes a rotation about the sun in approximately 365 ¼ days. The path the earth takes around the sun is located slightly off center, thus making the earth closest to the sun at the winter solstice (Perihelion), at $1.471 \times 10^{11} \, m$, and furthest from the sun at the summer solstice (Aphelion), at a distance of $1.521 \times 10^{11} \, m$, when located in the northern hemisphere [1, 2, 4]. During Perihelion, the earth is about 3.3 percent closer, and the solar intensity is proportional to the inverse square of the distance, thus making the solar intensity on December 21st about 7 percent higher than that on June 21st [3]. The axis of rotation of the earth is tilted at an angle of 23.45° with respect to its orbital plane, as shown in Figure 1.4. This tilt remains fixed and is the cause for the seasons throughout the year.

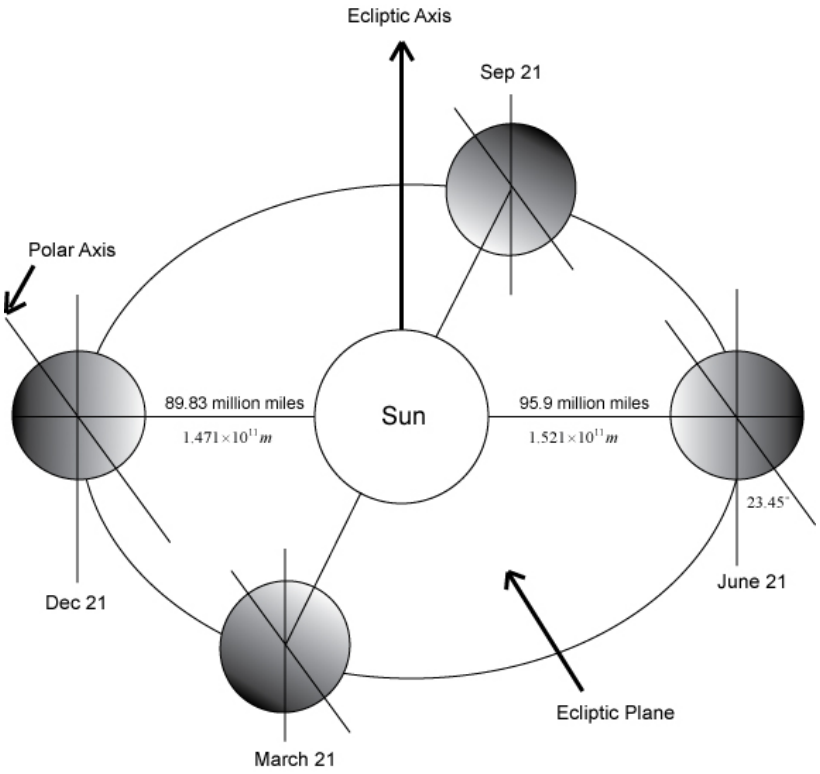

Figure 1.4: Motion of the earth about the sun.

1.4.2 Angle of Declination

The earth's equator is considered to be in the equatorial plane. By drawing a line between the center of the earth and the sun, as shown in Figure 1.6 the angle of declination, δ_s, is derived. The declination varies between -23.45° on December 21 to +23.45° on June 21. Stated simply, the declination has the same numerical value as the latitude at which the sun is directly overhead at solar noon on a given day, where the extremes are the tropics of Cancer (23.45° N) and Capricorn (23.45° S). The angle of declination, δ_s, is estimated by use of the following equation, or the resultant graph in Figure 1.5:

$$\delta_s = 23.45^\circ \sin\left[\left(360 \cdot \frac{284+n}{365}\right)^\circ\right] \qquad \textbf{(1-1)}$$

where n is the day number during the year with the first of January set as $n = 1$ [1, 2].

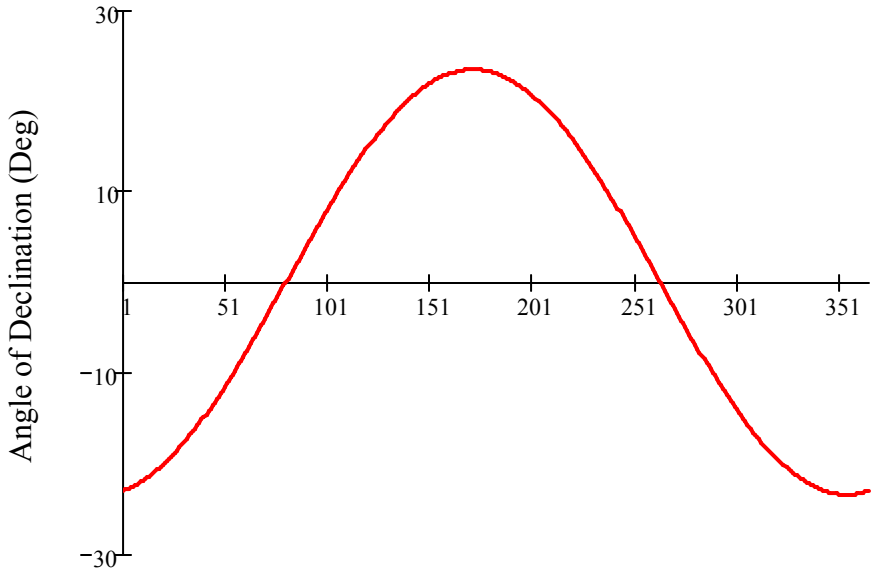

Figure 1.5: Declination Angle as a Function of the Date.

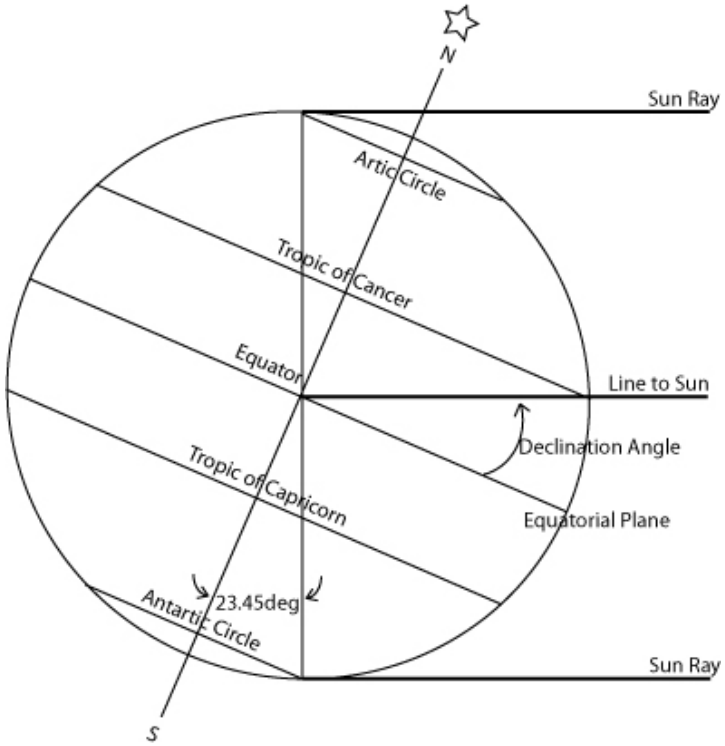

Figure 1.6: The declination angle (shown in the summer solstice position where δ = +23.45°)

In order to simplify calculations, it will be assumed that the earth is fixed and the sun's apparent motion be described in a coordinate system fixed to the earth with the origin being at the site of interest, which for this work is Tallahassee, FL at Latitude 30.38° North and Longitude 84.37° West. By assuming this type of coordinate system, it allows for the position of the sun to be described at any time by the altitude and azimuth angles. The altitude angle, α, is the angle between a line collinear with the sun's rays and the horizontal plane, and the azimuth angle, α_s, is the angle between a due south line and the projection of the site to the sun line on the horizontal plane. For the azimuth angle, the sign convention used is positive if west of south and negative if east of south. The angle between the site to sun line and vertical at site is the zenith angle, *z*, which is found by subtracting the altitude angle from ninety degrees:

$$z = 90^\circ - \alpha \qquad \textbf{(1-2)}$$

However, the altitude and azimuth angles are not fundamental angles and must be related to the fundamental angular quantities of **hour angle** (h_s), **latitude** (L), and **declination** (δ_s). The hour angle is based on the nominal time requirement of 24 hours for the sun to move 360° around the earth, or 15° per hour, basing solar noon (12:00) as the time that the sun is exactly due south [4]. The hour angle, h_s, is defined as:

$$h_s = 15^\circ \cdot (\text{hours from solar noon}) = \frac{\text{minutes from local solar noon}}{4\,\text{min/ degree}} \qquad \textbf{(1-3)}$$

The same rules for sign convention for the azimuth angle are applied for the values obtained for the hour angle, that is, the values east of due south (morning) are negative; and the values west of due south (afternoon) are positive. The latitude angle, *L*, is defined as the angle between the line from the center of the earth to the site of interest and the equatorial plane; and can easily found on an atlas or by use of the Global Positioning System (GPS).

1.4.3 Solar Time and Angles

By using the previously defined angles, the solar time and resulting solar angles can be defined. Solar time is used in predicting the direction of the sun's rays relative to a particular position on the earth. Solar time is location (longitude) dependent, and is nominally different from that of the local standard time for the area of interest. The relationship between the local solar time and the local standard time (LST) is:

$$\text{Solar Time} = LST + ET + (l_{st} - l_{local}) \cdot 4\,\text{min/degree} \qquad \textbf{(1-4)}$$

where ET is the equation of time, a correction factor that accounts for the irregularity of the speed of the earth's motion around the sun, l_{st} is the standard time meridian, and l_{local} is the local longitude. The equation of time is calculated by use of the following empirical equation:

$$ET\ (\text{in minutes}) = 9.87\sin(2B) - 7.53\cos(B) - 1.5\sin(B) \qquad \textbf{(1-5)}$$

Where B, in degrees, is defined as:

$$B = 360^{\circ} \cdot \frac{n-81}{364} \qquad \textbf{(1-6)}$$

The equation of time can also be estimated from Figure 1.7, in which Equation 1-5 is plotted to the time of year.

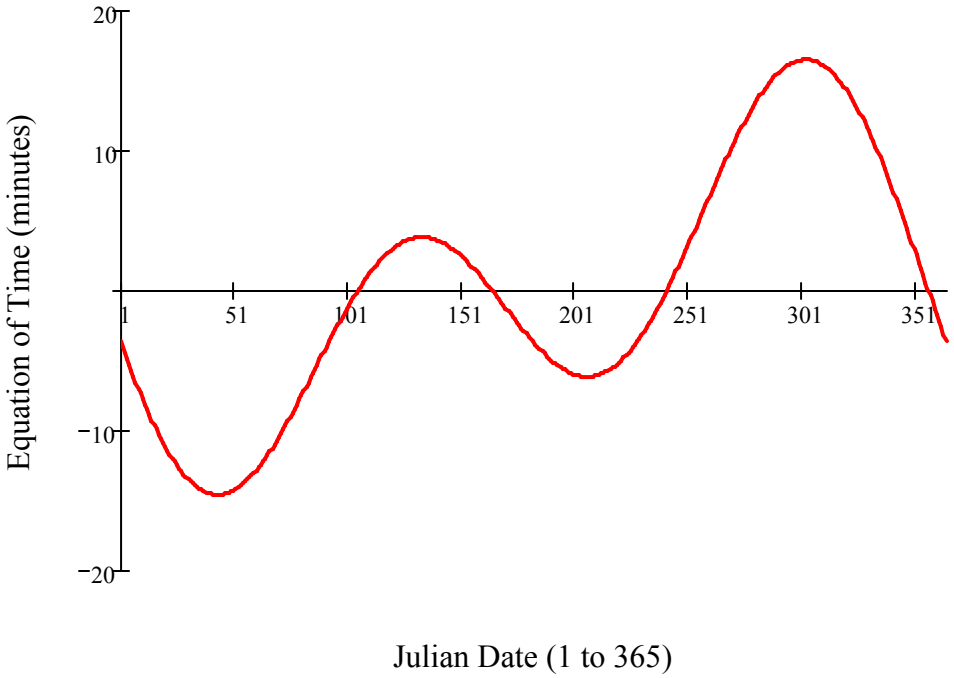

Figure 1.7: Equation of time (in minutes) as a function of the time of year.

The altitude angle, α, is calculated by use of the following equation:

$$\sin(\alpha) = \sin(L)\sin(\delta_s) + \cos(L)\cos(\delta_s)\cos(h_s) \qquad \textbf{(1-7)}$$

and the azimuth angle, α_s, is found similarly by:

$$\sin(\alpha_s) = \cos(\delta_s)\frac{\sin(h_s)}{\cos(\alpha)} \qquad \textbf{(1-8)}$$

Sunrise and sunset times can thus be estimated by finding the hour angle for when α = 0. This is done by substituting α = 0 into Equation 1-7 which results in the hour angles for sunrise (h_{sr}) and sunset (h_{ss}), represented as:

$$h_{ss} \text{ or } h_{sr} = \pm\cos^{-1}\left[-\tan(L)\cdot\tan(\delta_s)\right] \qquad \textbf{(1-9)}$$

The sunrise and sunset times are dependent on the day of the year, with the longest day being the summer solstice. The hour angle also corresponds to the time from solar noon with the hour angle changing at a rate of 15 degrees per hour. Thus the length of of the days can be estimated by use of Equation 1-10, yielding Figure 1.8.

$$\text{Day Length} = \frac{h_{ss} + h_{sr}}{15 \frac{\text{deg}}{hour}} \qquad \textbf{(1-10)}$$

However, to the eye it may appear that the calculated times are off by several minutes as to when the sun actually rises and sets. This is due to the observers' line of sight and their interpretation of sunrise and sunset. By convention, the times are solved for when the center of the sun is at the horizon.

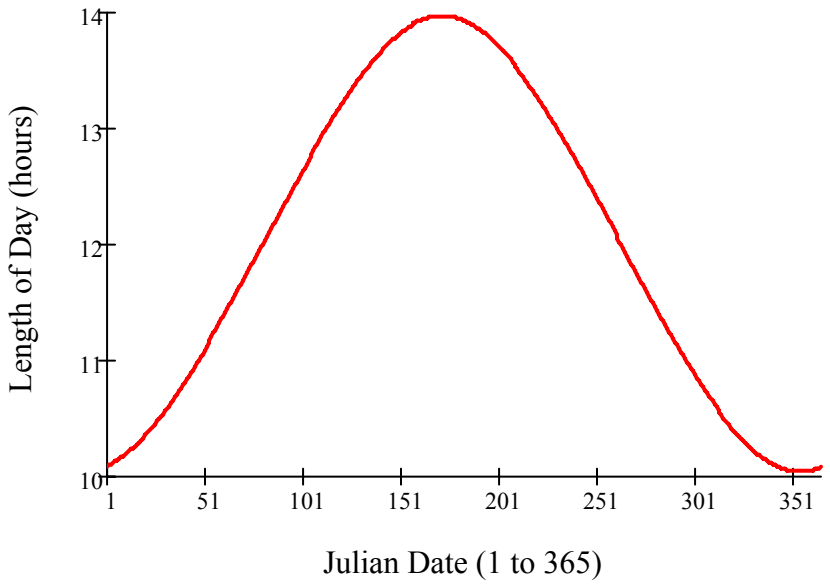

Figure 1.8: Length of day, in hours, as a function of the date.

1.5 Solar Radiation

1.5.1 Extraterrestrial Solar Radiation

Extraterrestrial solar radiation (I) is the solar radiation which falls on a surface normal to the rays of the sun outside the atmosphere of the earth. This extraterrestrial solar radiation at the mean earth-sun distance, D_0, is called the solar constant, I_0. Using the value obtained by measurements from NASA [1], the solar constant is said to be 1353 W/m^2, and the mean earth-sun distance is $1.496 \times 10^{11} m$. Because of the variation in seasonal solar radiation due to the elliptical orbit of the earth about the sun, the earth-sun distance has a variance of ±1.7 percent [1]. Thus, the extraterrestrial solar radiation, I, varies by the inverse square law, as shown in equation 1-11.

$$I = I_0 \left(\frac{D_0}{D} \right)^2 \qquad \textbf{(1-11)}$$

where D is the distance between the sun and the earth. The $(D_0 / D)^2$ factor is approximated by:

$$\left(\frac{D_0}{D} \right)^2 = 1.00011 + 0.034221\cos(x) + 0.00128\sin(x) + 0.000719\cos(2x) + 0.000077\sin(2x) \qquad \textbf{(1-12)}$$

where

$$x = \left(360 \frac{(n-1)}{365} \right) \text{deg} \qquad \textbf{(1-13)}$$

This relationship can also be approximated by:

$$I = I_0 \left[1 + 0.034 \cos\left(\left(\frac{360 \cdot n}{365.25} \right)^\circ \right) \right] \qquad \textbf{(1-14)}$$

The calculations for the extraterrestrial solar radiation are found in Appendix B. A plot for estimating the amount of the extraterrestrial solar radiation as a function of the time of year is shown below in Figure 1.9 [3].

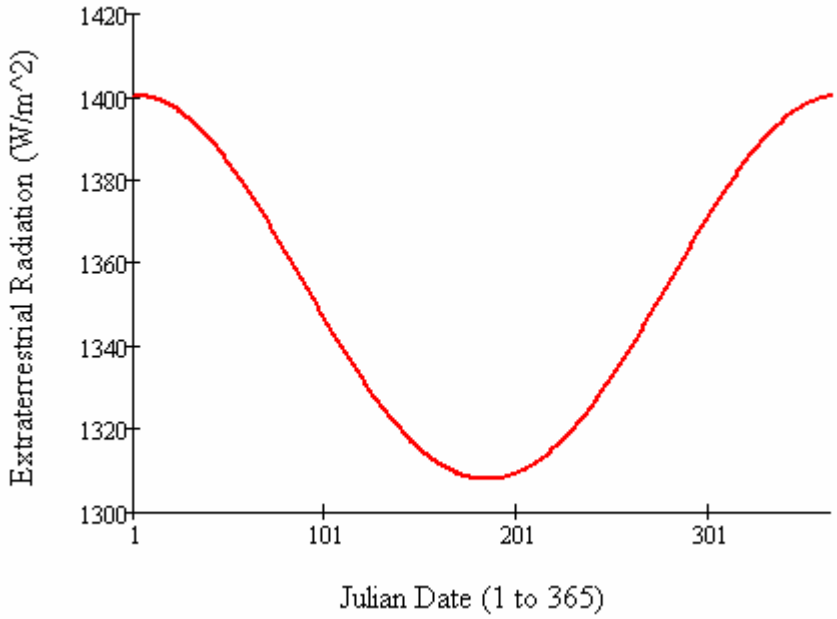

Figure 1.9: The variation of extraterrestrial radiation with time of year.

1.5.2 Terrestrial Solar Radiation

As the extraterrestrial solar radiation passes through the atmosphere, part of it is reflected back into space, part is absorbed by air and water vapor, and some is scattered. The solar radiation that reaches the surface of the earth is known as beam (direct) radiation, and the scattered radiation that reaches the surface from the sky is known as sky diffuse radiation.

Atmospheric Extinction of Solar Radiation

As the extraterrestrial solar radiation is attenuated upon entering the earth's atmosphere, the beam solar radiation at the earth's surface is represented as:

$$I_{b,N} = Ie^{-\int Kdx} \quad \textbf{(1-15)}$$

where $I_{b,N}$ is the instantaneous beam solar radiation per unit area normal to the suns rays, K is the local extinction coefficient of the atmosphere, and x is the length of travel through the atmosphere. Consider the vertical thickness of the atmosphere to be L_0 and the optical depth is represented as:

$$k = \int_0^{L_0} Kdx \qquad \textbf{(1-16)}$$

then the beam normal solar radiation for a solar zenith angle is given by:

$$I_{b,N} = Ie^{-k\sec(z)} = Ie^{-k/\sin(\alpha)} = Ie^{-km} \qquad \textbf{(1-17)}$$

where m, the air mass ratio, is the dimensionless path length of sunlight through the atmosphere. When the solar altitude angle is 90 degrees (sun directly overhead), the air mass ratio is equal to one. The values for optical depth (k) were estimated by Threlkeld and Jordan for average atmospheric conditions at sea level with a moderately dusty atmosphere and water vapor for the United States. The values for k, along with values for the sky diffuse factor, C, are given in Table 1.1. In order to amend for differences in local conditions, the equation for the beam normal solar radiation (Equation 1-17) is modified by the addition of a parameter called the clearness number, C_n. The resulting equation is:

$$I_{b,N} = C_n Ie^{-k/\sin(\alpha)} \qquad \textbf{(1-18)}$$

For ease of calculation purposes, the clearness number is assumed to be one.

Table 1.1: Average values of atmospheric optical depth (*k*) and sky diffuse factor (*C*) for average atmospheric conditions at sea level for the United States [1].

Month	Jan	Feb	Mar	Apr	May	Jun	Jul	Aug	Sep	Oct	Nov	Dec
k	0.142	0.144	0.156	0.180	0.196	0.205	0.207	0.201	0.177	0.160	0.149	0.142
C	0.058	0.060	0.071	0.097	0.121	0.134	0.136	0.122	0.092	0.073	0.063	0.057

Solar Radiation on Clear Days

The total instantaneous solar radiation on a horizontal surface, I_h, is the sum of the beam radiation, $I_{b,h}$, and the sky diffuse radiation, $I_{d,h}$.

$$I_h = I_{b,h} + I_{d,h} \qquad \textbf{(1-19)}$$

According to Threlkeld and Jordan, the sky diffuse radiation on a clear day is proportional to the beam normal solar radiation, and can thus be estimated by use of an empirical sky diffuse factor, C (see Table 1.1). Thus the total instantaneous solar radiation can be estimated by

$$I_h = I_{b,N}\cos(z) + CI_{b,N} = I_{b,N}\cos(\alpha) + CI_{b,N} = C_n Ie^{-k/\sin(\alpha)}(C + \sin(\alpha)) \qquad \textbf{(1-20)}$$

[1]. Figure 1.10 shows the variance of the total and beam insolation available throughout the year.

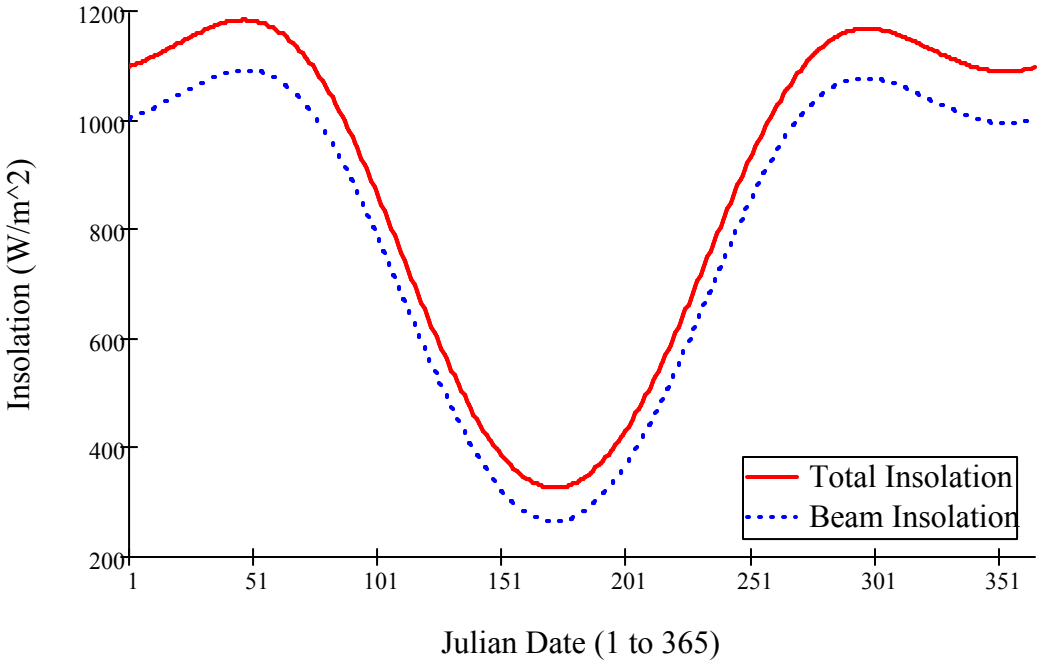

Figure 1.10: Variance of the Total Insolation compared to the Beam Insolation.

1.6 Radiative Properties

When radiation strikes a body, part of this radiation is reflected, part is absorbed, and if the material is transparent, part is transmitted. The fraction of incident radiation reflected is defined as the reflectance, $\rho_{reflectance}$, the fraction absorbed as the absorptance, $\alpha_{absorptance}$, and the fraction transmitted as the transmittance, $\tau_{transmittance}$. When it comes to solar radiation, there are two types of radiation reflection: specular and diffuse. Specular reflection is when the angle of incidence is equal to the angle of reflection, and diffuse reflection is when the reflected radiation is uniformly distributed in all directions. No real surface is either specular or diffuse, but a highly polished surface appears to approach specular reflection, where a rougher surface reflects diffusely [1]. For concentrated solar collectors, a surface capable of specular reflectance is ideal, however, in these solar collector systems, there are two important types of surfaces – selective and reflecting surfaces. Selective surfaces are a combination of high absorptance for solar radiation with a low emittance for the temperature range in which the surface emits radiation, usually used for the absorber (receiver). Reflecting surfaces, such as those

required by the solar concentrator, are surfaces with high specular reflectance in the solar spectrum. Reflecting surfaces are usually highly polished metals or metal coatings on substrates, some of which are shown in Table 1.2 with the materials reflectivity value. Under laboratory conditions, polished silver has the highest reflection for the solar energy spectrum; however, a silvered surface is expensive. Chromium plating, such as that used in the automotive industry may seem tempting, but it has shown such a low reflectance in laboratory use that it is usually no longer a consideration for solar reflectance [1]. A better choice, which makes a compromise between price and reflectivity, is the use of a reflective plastic film known as Aluminized Mylar. Aluminized Mylar is available with a high reflectance, almost as high as 96% in some cases, and is the choice for design in many solar collector projects due to the low cost, high reflectivity, and its light-weight and ease of workability. However, after long exposure to the ultraviolet rays, Aluminized Mylar tends to degrade, but new stabilizers can be added to aid in slowing the degradation of the film.

Table 1.2: Specular reflectance values for different reflector materials [1]

Material	Reflectivity (ρ)
Copper	0.75
Aluminized type-C Mylar (from Mylar side)	0.76
Gold	0.76±0.03
Various aluminum surfaces-range	0.82-0.92
Anodized aluminum	0.82±0.05
Aluminized acrylic, second surface	0.86
Black-silvered water-white plate glass	0.88
Silver (unstable as a front surface mirror)	0.94±0.02

1.7 Solar Collector/Concentrator

The solar collector is the key element in a solar thermal energy system. The function of the collector is quite simple; it intercepts the incoming solar insolation and converts it into a useable form of energy that can be applied to meet a specific demand,

such as generation of steam from water. Concentrating solar collectors are used to achieve high temperatures and accomplish this concentration of the solar radiation by reflecting or refracting the flux incident on the aperture area (reflective surface), A_a onto a smaller absorber (receiver) area, A_r. The receiver's surface area is smaller than that of the reflective surface capturing the energy, thus allowing for the same amount of radiation that would have been spread over a few square meters to be collected and concentrated over a much smaller area, allowing for higher temperatures to be obtained. These concentrating solar collectors have the advantage of higher concentration and are capable of much greater utilization of the solar intensity at off-noon hours than other types of solar concentrators. However, one of the major problems of using a 'dish-type' parabolic collector is that two-dimensional tracking is required. Most concentrating collectors can only concentrate the beam normal insolation (the parallel insolation coming directly from the sun), otherwise the focal region becomes scattered and off focus, as shown in Figure 1.11, therefore requiring the concentrator to follow the sun throughout the day for efficient energy collection. For the parabolic concentrator, continuous tracking is needed; if oriented east-west, the concentrator requires an approximate ± 30°/day motion; if north-south, an approximate 15°/hr motion. This tracking also must accommodate a ±23.5°/yr declination excursion.

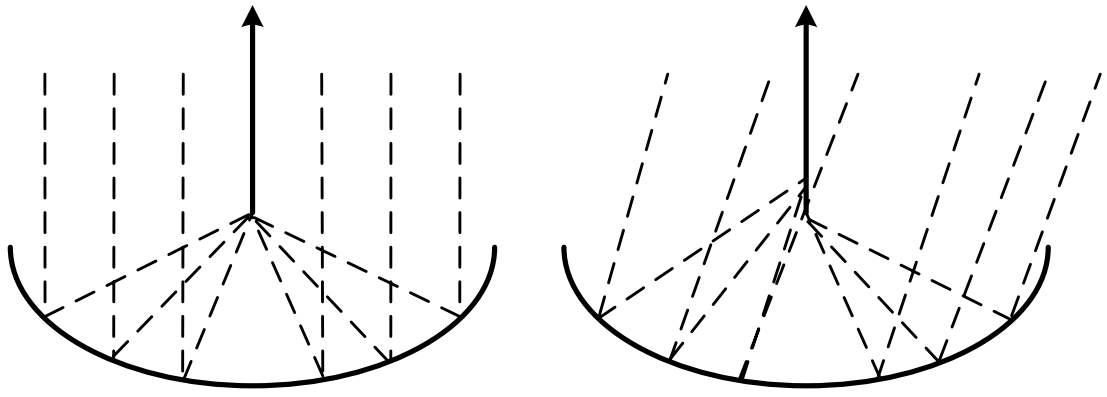

Figure 1.11: Concentration by parabolic concentrating reflector for a beam parallel to the axis of symmetry, and at an angle to the axis.

As stated previously, the concentration of solar radiation is achieved by reflecting or refracting the flux incident on an aperture area, A_a, onto a smaller receiver/absorber area, A_r. There are two ways of representing this ratio of concentration; as an optical ratio, or as a geometric ratio. An optical concentration ratio, CR_o, is defined as the ratio of the solar flux, I_r, on the receiver to the flux on the aperture, I_a, and is most often referred to as the flux concentration ratio (Equation 1-21).

$$CR_o = \frac{I_r}{I_a} \qquad \textbf{(1-21)}$$

The geometric concentration ratio, CR, is based on the ratio of the area of the aperture and the receiver.

$$CR = \frac{A_a}{A_r} \qquad \textbf{(1-22)}$$

The optical concentration ratio gives a true concentration ratio because it takes in account the optical losses from reflecting and refracting elements. However, it has no relationship to the receiver area, thus it does not give insight into thermal losses. These thermal losses are proportional to the receiver area, and since we are most interested in the thermal aspects of the system, the geometric concentration ratio will be used here.

The amount of solar radiation reaching the receiver is dependent on the amount of radiation available (sky conditions), the size of the concentrator, and several other parameters describing the loss of this radiation on its way to being absorbed. Heat loss from the receiver is separated into convection-conduction heat loss and radiation heat loss. The rate of heat loss increases as the area of the receiver and/or its temperature increases. This is why concentrators are more efficient at a given temperature than flat plate collectors, because the area in which heat is lost is smaller than the aperture area. The useful energy delivered by the collector, q_u, is given by the energy balance

$$q_u = \eta_o I_c A_a - U_c (T_c - T_a) A_r \qquad \textbf{(1-23)}$$

where η_o is the optical efficiency, U_c is the collector heat-loss conductance, T_c and T_a respectively are the temperatures of the collector and the ambient temperature, and I_c is the insolation incident on the aperture. The instantaneous collector efficiency, η_c, is thus given by

$$\eta_c = \eta_o - \frac{U_c(T_c - T_a)}{I_c}\frac{1}{CR} \qquad \textbf{(1-24)}$$

Neglecting the optical efficiency, the instantaneous efficiency, η_{inst}, of the solar thermal collector can also be simplified and defined as the ratio of the useful heat, $\dot{Q}$, delivered per aperture area, A_a, and the insolation, I_c, which is incident on the aperture.

$$\eta_{inst} = \frac{\dot{Q}}{AI_c} = \frac{\dot{q}}{I_c} \qquad \textbf{(1-25)}$$

The useful heat $\dot{Q}$ is related to the flow rate, $\dot{m}$, specific heat at a constant pressure, C_p, and the inlet and outlet temperatures, T_{in} and T_{out}, by

$$\dot{Q} = \dot{m}C_p(T_{out} - T_{in}) = \dot{m}C_p\Delta T \qquad \textbf{(1-26)}$$

[2, 12]

1.7.1 Acceptance Angle

Closely related to the concentration ratio is the acceptance angle, $2\theta_a$. The acceptance angle is defined as being the angular range over which all or most all of the rays are accepted without moving the collector [13]. The higher the concentration, the smaller the range of acceptance angles by the collector, thus an inverse relationship between the concentration and the acceptance aperture of the collector exists. As was stated in a previous section, tracking is needed for the system to maintain the high solar concentration, thus it is desirable to have a collector that has as high an acceptance angle as possible. The basic expression given by Rabl for acceptance angle is:

The maximum possible concentration achievable with a collector that only accepts all incident light rays within the half-angle, θ_a, is

$$CR_{ideal} = \frac{1}{\sin^2(\theta_a)} \qquad \textbf{(1-27)}$$

for a three dimensional collector (parabolic 'dish-type' concentrator) [13].

The derivation of this equation can be found in Appendix A.

1.7.2 Thermodynamic Limits of Concentration (Max Achievable Temperature)

As stated previously, there is a thermodynamic limit to the concentration of a concentrating solar collector, or more plainly stated, a maximum achievable temperature. From the laws of thermodynamics, $T_{abs} \leq T_s$, where T_{abs} is the temperature of the absorber (receiver) and T_s is the temperature of the sun. If T_{abs} were greater than T_s, then the system would be in violation of the second law [3]. The power absorbed by the receiver can be defined by the following equation:

$$Q_{s\to abs} = \eta_{optical} A \frac{r^2}{R^2} \sigma T_s^4 = \eta_{opitcal} A \sin^2(\theta) T_s^4 \sigma \qquad \textbf{(1-28)}$$

When using the source as the sun, the appropriate half-angle is $\theta \approx \frac{1}{4}^\circ$ [3]. The radiative power loss from the absorber is

$$Q_{abs\to amb} = \varepsilon_{abs} A_{abs} \sigma T_{abs}^4 \qquad \textbf{(1-29)}$$

where ε_{abs} is the effective emissivity of the receiver over the spectral wavelength region characteristic of a body emitting at T_{abs}. If the efficiency of the collector for capturing the incident radiation as useful energy in a transfer fluid is called η, then the heat balance on the absorber is:

$$Q_{s\to abs} = Q_{abs\to amb} + \eta Q_{s\to amb} \qquad \textbf{(1-30)}$$

To simplify the calculations, it will be assumed that there are no conductive or convective heat losses from the receiver, thus

$$(1-\eta)\eta_{optical}\sigma A\sin^2(\theta)T_s^4 = \varepsilon_{abs}A_{abs}\sigma T_{abs}^4 \qquad \textbf{(1-31)}$$

This can also be written as

$$T_{abs} = T_s\left[(1-\eta)\frac{\eta_{optical}}{\varepsilon_{abs}}CR_{theoretical}\sin^2(\theta)\right]^{1/4} \qquad \textbf{(1-32)}$$

where CR_{ideal} was defined in Equation 1-27, and $CR_{theoretical}$ is equal to the geometric concentration ratio, therefore,

$$T_{abs} = T_s\left[(1-\eta)\frac{\eta_{optical}}{\varepsilon_{abs}}\frac{CR_{theoretical}}{CR_{ideal}}\right]^{1/4} \qquad \textbf{(1-33)}$$

The maximum possible value of $CR_{\text{theoretical}}$ is CR_{ideal}, and the maximum value of T_{abs} is T_{s}. This, however, can only occur if the optics of the concentrator are perfect and no useful heat is lost or removed from the receiver. If this were the case, and considering the sun to be represented as a blackbody at 5760 K, the maximum achievable temperature at the receiver would be equivalent to that of the sun [3].

1.8 The Receiver/Absorber

The purpose of the receiver in the solar-thermal system is to intercept and absorb the concentrated solar radiation and convert it to usable energy; in this case, thermal energy which will then be converted to electrical energy via a thermodynamic cycle. Once absorbed, this thermal energy is transferred as heat to a heat-transfer fluid, such as water, Paratherm ©, ethyl-glycol, or molten salt, to be stored and/or used in a power conversion cycle.

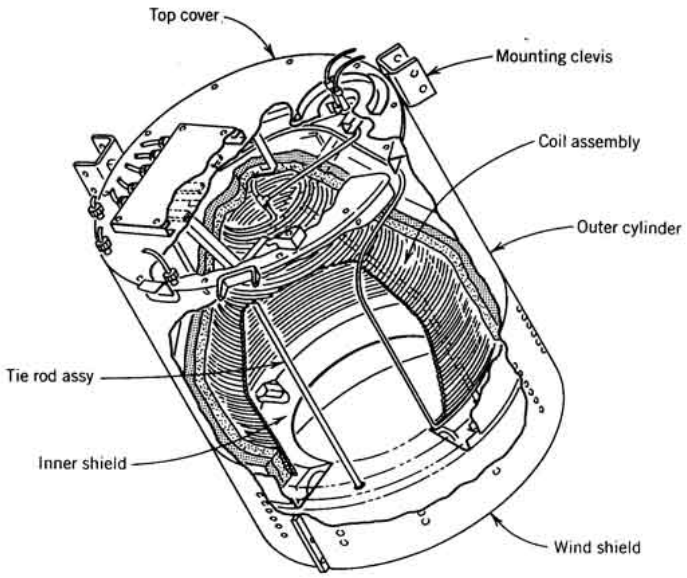

Figure 1.12: Cavity Type Receiver (Sandia National Labs)(J.T. Lyle Center)

There are two main types of receivers that are found to be used with parabolic solar concentrator systems: external (omni-directional) receivers, and cavity (focal plane) receivers, as shown in Figure 1.12. External receivers are considered to be omni-directional receivers since the absorbing surfaces are in direct view of the concentrator and depend on direct radiation absorption. Cavity type receivers, however, have an aperture through which the reflected solar radiation passes. Once inside the cavity, internal reflections ensure that the majority of the radiation that has entered the cavity is absorbed on the internal absorbing surface [11].

1.8.1 Cavity Receiver

In large scale solar concentrator projects, and commercially available solar concentrators, it is found that the cavity type receiver is most commonly used. This is due to the lower heat-loss rate compared to that of an external receiver; however, they are more expensive than external receivers. The concentrated solar radiation entering the aperture of the cavity spreads inside and is absorbed on the internal walls where the heat is then transferred to a working fluid. Any radiation that is reflected or re-radiated from the walls inside the cavity is also absorbed internally on the cavity walls resulting in a higher absorptance value of the receiver. This spreading of the solar radiation causes a reduction in the incident flux within the cavity, thus helping to prevent thermal cracking

or smelting of the internal walls. Also, because of the design of the cavity receiver, it is easier to insulate to aid in avoiding radiant and convective heat loss to the environment. [14, 15, 16]

1.8.2 External Receiver

External receivers are designed to absorb radiation coming from all directions and are the simpler of the two receiver types. The size of the receiver is determined in a process based on the amount of received solar radiation and the amount of heat loss from the receiver. Simply stated, a larger receiver will capture more reflected solar radiation, but will suffer from more radiant and convective heat loss. These receivers are nominally spherical or tubular in shape. (J.T. Lyle Center)

1.9 Heat Storage

There are three methods for storing the collected thermal energy: 1) sensible, 2) latent, and 3) thermochemical heat storage. These methods differ in the amount of heat that can be stored per unit weight or volume of storage media and operating temperatures. Thermochemical is not practical for the solar thermal system discussed in this paper, thus a discussion will be omitted. [3]

1.9.1 Sensible Heat Storage

In sensible heat storage, the thermal energy is stored by changing the temperature of the storage medium. The amount of heat stored depends on the heat capacity of the media being used, the temperature change, and the amount of storage media. Solid or liquid state media can be utilized, however, since storage occurs over a temperature interval, temperature regulation during retrieval can prove to be problematic. The most common type of sensible heat storage is that of a liquid in a drum in which heat is constantly added and is often recirculated. [3]

1.9.2 Latent Heat Storage

In latent heat storage, thermal energy is stored by a means of a reversible change of state (phase change) in the media. Solid-liquid transformations are most commonly utilized. Liquid-gas and solid-gas phase changes involve the most energy of the possible latent heat storage methods. A common media used for latent heat storage in solar thermal systems is molten salt. A good example of this is that a pint bottle of molten salt at 30°C releases 0.1515 MJ on cooling to room temperature (and will feel tepid to the touch), whereas the same bottle filled with water at 60°C only releases half the amount of heat on cooling (and is hot to the touch). This is one main advantage to latent heat storage when compared to other methods, that is has a higher heat capacity, thus allowing for a smaller thermal storage unit. [1, 17]

1.10 Rankine Cycle

The majority of power production facilities in the world are based on the Rankine cycle. The basic ideal Rankine cycle is shown in Figure 1.13, and Figure 1.14 shows the Temperature-Entropy (T-s) diagram for steam as a working fluid.

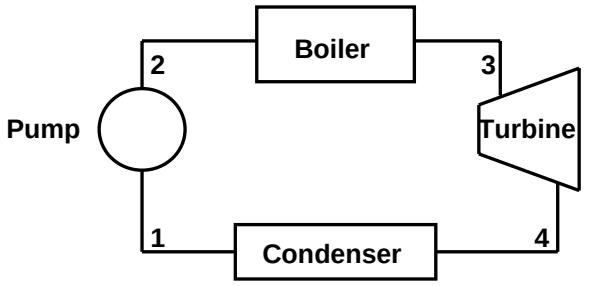

Figure 1.13: Basic Rankine Power Cycle

The ideal Rankine cycle consists of the following processes, which correlate with Figures 1.13 and 1.14:

Process

1-2 Saturated liquid from the condenser at state 1 is pumped to the boiler at state 2 isentropically

2-3 Liquid is heated in the boiler at constant pressure. The temperature of the liquid rises until it becomes a saturated liquid. Further addition of heat vaporizes the liquid at constant temperature until all of the liquid turns into saturated vapor. Any additional heat superheats the working fluid to state 3.

3-4 Steam expands isentropically through a turbine to state 4.

4-1 Steam exiting the turbine is condensed at constant pressure until it returns to state 1 as a saturated liquid.

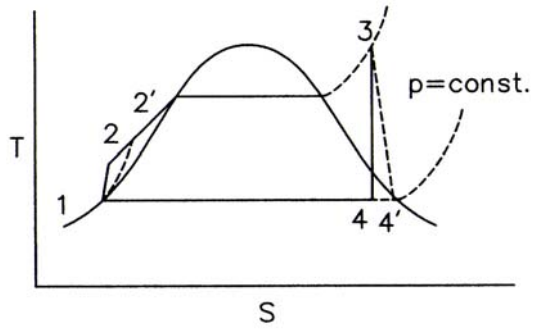

Figure 1.14: T-S Diagram of 'Ideal' and 'Actual' Rankine Cycle.

However, the pumping and the turbine expansion process in an actual Rankine cycle are not ideal. Instead, the actual processes are 1-2' and 3-4', respectively, as indicated in Figure 1.14. For the Rankine cycle, turbine efficiency ($\eta_{turbine}$), pump efficiency (η_{pump}), net work output, heat input, and cycle efficiency (η_{cycle}) can be solved for respectively by:

$$\eta_{turbine\_thermal} = \frac{h_3 - h_{4'}}{h_3 - h_4} \qquad \textbf{(1-34)}$$

$$\eta_{pump} = \frac{h_1 - h_2}{h_1 - h_{2'}} \qquad \textbf{(1-35)}$$

$$\text{Net Work Output} = (h_3 - h_{4'}) - (h_{2'} - h_1) \quad \textbf{(1-36)}$$

$$\text{Heat Input} = h_3 - h_{2'} \quad \textbf{(1-37)}$$

$$\text{Pump Work} = h_{2'} - h_1 = \frac{\upsilon(P_2 - P_1)}{\eta_{pump}} \quad \textbf{(1-38)}$$

$$\text{Cycle Efficiency} = \eta_{\text{cycle}} = \frac{\text{Net Work Output}}{\text{Heat Input}} = \frac{(h_3 - h_{4'}) - (h_{2'} - h_1)}{h_3 - h_{2'}} \quad \textbf{(1-39)}$$

where h is the enthalpy and υ is the specific volume at state 1 [23].

For comparison purposes, the Rankine cycle efficiency of standard power plants is compared with that of the systems Carnot cycle efficiency, where the Carnot efficiency is given as:

$$\text{Carnot Efficiency} = \eta_{Carnot} = 1 - \frac{T_C}{T_H} \quad \textbf{(1-40)}$$

where T_C is the condenser temperature (low rejection temperature) of the system, and T_H is the input temperature of the system (Cengel). The majority of standard steam power plants attempt to operate at an efficiency of 50 percent of its Carnot efficiency [4]. The lower efficiency of the Rankine cycle compared to that of the Carnot cycle is due to the average temperature between points 2 and 2' being less than the temperature during the evaporation stage. Even with the lower efficiency, the Rankine cycle is still used over the Carnot cycle for a few reasons. The first is due to the pumping process, where at state 1 there is a mixture of liquid and vapor. It is difficult to design a pump which can handle the mixture of water and vapor at this stage and deliver the working fluid as a saturated liquid at stage 2'. It is easier to condense the vapor completely and have the pump only handle liquid. Secondly, in the Carnot cycle, the heat transfer is at a constant temperature, therefore the vapor is superheated in process 3-3", where as in the Rankine cycle, the fluid is superheated at constant pressure in process 3-3'. Thus, in the Carnot

cycle, the pressure is dropping, which means that the heat must be transferred to the fluid (vapor at this stage) as it undergoes an expansion process in which work is done. It is very difficult to achieve this heat transfer in practice, hence why the Rankine cycle is used [23].

1.10.1 Working Fluid

In a solar Rankine cycle, the working fluid is chosen based upon the expected temperatures of the solar collection system. Steam (water) is most commonly used with the Rankine cycle due to its critical temperature and pressure of 374°C and 218 atm respectively. Thus it is usable in systems that operate at high temperatures, such as those produced by parabolic 'dish' type collector systems. When water is converted to steam, its volume is increased by approximately 1600 times [25]. This expansion is what stores the energy and produces the force to run a steam turbine. Other major advantages of steam is that it is non-toxic, environmentally safe, inexpensive, and nominally easily available.

1.10.2 Deviation of Actual Cycle from Ideal

Piping Losses

In the actual Rankine cycle, there are losses which are contributed by the piping, such as pressure drops caused by frictional effects and heat transfer to the surroundings. For example, consider the pipe connecting the turbine to the boiler. If only frictional effects occur, there will be an increase in entropy, as shown by states *a* and *b* in Figure 1.15. However, heat transferred to the surroundings at constant pressure causes a decrease in entropy, as represented by process *b-c* in Figure 1.15. Both the pressure drop and heat transfer causes a decrease in the availability of steam entering the turbine, and a decrease in the amount of energy available. [23]

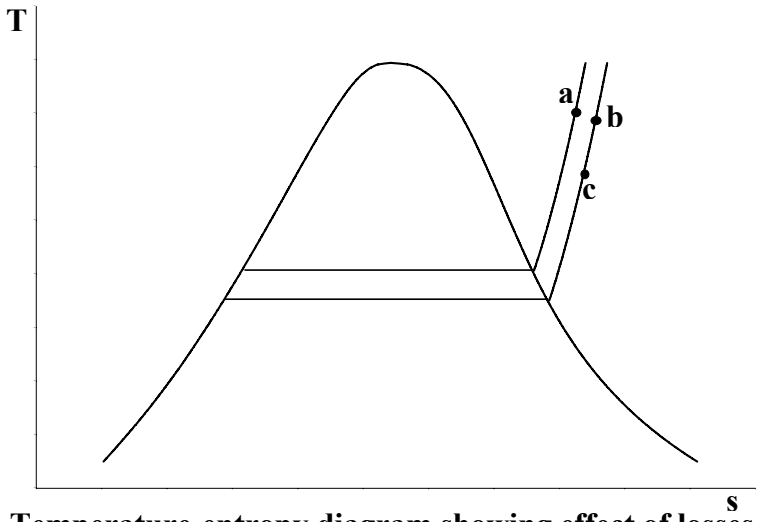

Figure 1.15: Temperature-entropy diagram showing effect of losses between boiler and turbine.

Pump and Turbine Losses

Losses in the turbine are nominally associated with the flow of the working fluid through the turbine. Heat transfer to the surroundings also plays a role, but is usually of secondary importance. These effects are basically the same as for those mentioned in the section above about piping losses. This process is shown in Figure 1.14, where point 4s represent the state after an isentropic expansion and point 4' represents the actual state leaving the turbine. Losses in the turbine are also caused by any kind of throttling control or resistance on the output shaft. Losses in the pump are similar to those mentioned here of the turbine and are due to the irreversibility associated with the fluid flow. [23, 24]

1.11 Steam Turbine

With the process steam that is generated by the solar thermal system, the internal energy of this steam must somehow be extracted. This energy can by extracted by expanding the steam through a turbine. An ideal steam turbine is considered to be an isentropic process (or constant entropy process) in which the entropy of the steam entering the turbine is equal to that of the entropy of the steam exiting the turbine. However, no steam turbine is truly isentropic, but depending on application, efficiencies

ranging from 20 to 90 percent can be achieved [30]. There are two general classifications of steam turbines, impulse and reaction turbines, as shown in Figure 1.16.

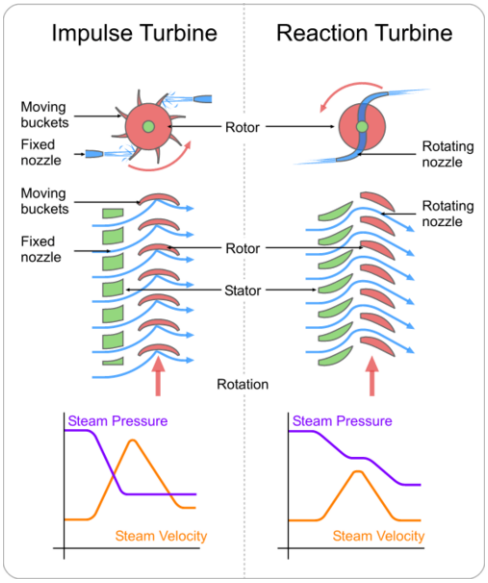

Figure 1.16: Diagram showing difference between an impulse and a reaction turbine.

1.11.1 Impulse Turbine

An impulse turbine is driven by one or more high-speed free jets. The jets are accelerated in nozzles, which are external to the turbine rotor (wheel) and impinge the flow on the turbine blades, sometimes referred to as 'buckets'. As described by Newton's second law of motion, this impulse removes the kinetic energy from the steam flow by the resulting force on the turbine blades causing the rotor to spin, resulting in shaft rotation.

1.11.2 Reaction Turbine

In a reaction turbine, the rotor blades are designed so as to be convergent nozzles, thus the pressure change takes place both externally and internally. External acceleration takes place, the same as in an impulse turbine, with additional acceleration from the moving blades of the rotor. [31]

1.11.3 Turbine Efficiency

In order to determine the efficiency of a turbine, certain assumptions have to be made. It needs to be assumed that the process through the turbine is a steady-state, steady-flow process, meaning that 1) the control volume does not move relative to the coordinate frame, 2) the state of the mass at each point in the control volume does not vary with time, and 3) the rates at which heat and work cross the control surface remain constant [23]. The repercussions of these assumptions are that 1) all velocities measured relative to the coordinate frame are also velocities relative to the control surface, and there is no work associated with the acceleration of the control volume, 2) the state of mass at each point in the control volume does not vary with time such that

$$\frac{dm}{dt} = 0 \quad \textbf{(1-41)} \qquad \text{and} \qquad \frac{dE}{dt} = 0 \quad \textbf{(1-42)}$$

resulting in the continuity equation

$$\sum \dot{m}_{inlet} = \sum \dot{m}_{outlet} \qquad \textbf{(1-43)}$$

and the first law as

$$\dot{Q} + \sum \dot{m}\left(h_{inlet} + \frac{V_{inlet}^2}{2} + gZ_{inlet} \right) = \sum \dot{m}\left(h_{outlet} + \frac{V_{outlet}^2}{2} + gZ_{outlet} \right) + \dot{W} \qquad \textbf{(1-44)}$$

and 3) the applications of equations 1-43 and 1-44 above are independent of time. Equation 1-44 can then be rearranged, yielding

$$q + h_{inlet} + \frac{V_{inlet}^2}{2} + gZ_{inlet} = h_{outlet} + \frac{V_{outlet}^2}{2} + gZ_{outlet} + w \qquad \textbf{(1-45)}$$

where

$$q = \frac{\dot{Q}}{\dot{m}} \quad \textbf{(1-46)} \qquad \text{and} \qquad w = \frac{\dot{W}}{\dot{m}} \quad \textbf{(1-47)},$$

the heat transfer and work per unit mass flowing into and out of the turbine. The efficiency of the turbine is then determined as being the actual work done per unit mass of steam flow through the turbine, w_a, compared to that work that would be done in an ideal cycle, w_s. The efficiency of the turbine [23] is then expressed as:

$$\eta_{turbine} = \frac{w_a}{w_s} \quad \textbf{(1-48)}$$

1.12 Overview

The overall objective of this project is to design a system that is capable of power generation by means of solar concentration for use in emergency and/or off-grid situations, which would be reasonably affordable for newly developing regions of the world. The system must be capable of utilizing nearby resources, such as well water, or unfiltered stream water, and must be 'simple' in design for simplicity of repairs. However, in order to reach this goal, a few key research objectives must be met. The key objectives include characterization of the dish, the receiver, and the turbine in order to determine the overall system efficiency. This characterization of the individual components of the system will allow for future work on the project for an increase in efficiency and power output.

CHAPTER 2

EXPERIMENTAL APPARATUS AND PROCEDURES

2.1 Introduction

This work was focused on the development of a system for converting incoming solar radiation to electrical energy. The system concentrated the incoming solar radiation to power a thermal cycle in which the energy was converted to mechanical power, and subsequently to electrical power. This chapter contains a description of this system and a detailed explanation of how the individual components of the system work. The design, implementation, and testing of the system were conducted at the Sustainable Energy Science and Engineering Center (SESEC) located on the campus of Florida State University in Tallahassee, Florida.

2.2 Solar Collector

To obtain the high temperatures necessary, a concentrating solar collector is needed due to solar radiation being a low entropy heat source. The type chosen was that of the parabolic 'dish' type. The parabolic dish is a 3.66 meter diameter Channel Master Satellite dish, obtained from WCTV Channel 6 of Tallahassee, Florida. The dish consists of six fiberglass, pie-shaped, sections which are assembled together to form the parabolic structure of the dish. Figure 2.1a shows one of the pie shaped panels of the dish. With the six panels assembled, shown in Figure 2.1b, the dish has a surface area of 11.7 m^2 (126.3 ft^2), with an aperture area of 10.51 m^2 (113.1 ft^2) and a focal length of 1.34 meters (52.75 inches).

Figure 2.1: a) Pie-shaped section of the dish coated in Aluminized Mylar. b) Assembled dish with surface area of 11.7 m^2.

Because the dish was originally surfaced to reflect radio waves, a new surface capable of reflecting the ultraviolet to the infrared spectrum (electromagnetic radiation between the wavelengths of 300 to 200 *nm*) was needed; basically, a surface with high visual reflectivity. Because of its low cost, ease of workability, and high reflectivity of 0.76, Aluminized Mylar was chosen as the new surface coating of the dish. For application of the Aluminized Mylar to the fiberglass panels, the mylar was cut into 152.4 x 152.4 mm (6 x 6 in) squares, and a heavy duty double sided adhesive film by Avery Denison products was used, as shown in Figure 2.2.

Figure 2.2: Application of Aluminized Mylar to Fiberglass Panels of the Dish

2.3 The Receiver

The receiver of the solar concentrator system serves as the boiler in the Rankine cycle, thus it needed to be able to handle high temperatures. This first generation receiver was designed with simplicity in mind for characterization of the system. An external type receiver was decided upon for use with the concentrator. The basis behind the design of the receiver was a standard D-type boiler, with a mud (water) drum, steam drum, and down-comers. Because of the extreme temperatures expected at the focal region, in excess of 900 K, the outer housing of the receiver was constructed of stainless steel.

The receiver consists of a stainless steel cylindrical water drum and two sets of stainless steel coils housed within a stainless steel welded tube. The outer shell of the boiler is 203.2 mm (8 in) long and 152.4 mm (6 in) in diameter, with an internal volume of 3.245 liters. The water drum is 38.1 mm (1.5 in) tall and 133.35 mm (5.25 in) in diameter, with a volume of 0.402 liters. The inner coils consists of 25.4 mm (¼-inch) stainless steel tubing, one set coiled within the other (Figure 2.3), with the outer and inner coils consisting of fourteen windings with a diameter of 133.35 mm (5.25 in) and six windings with a diameter of 63.5 mm (2.5 in), respectively.

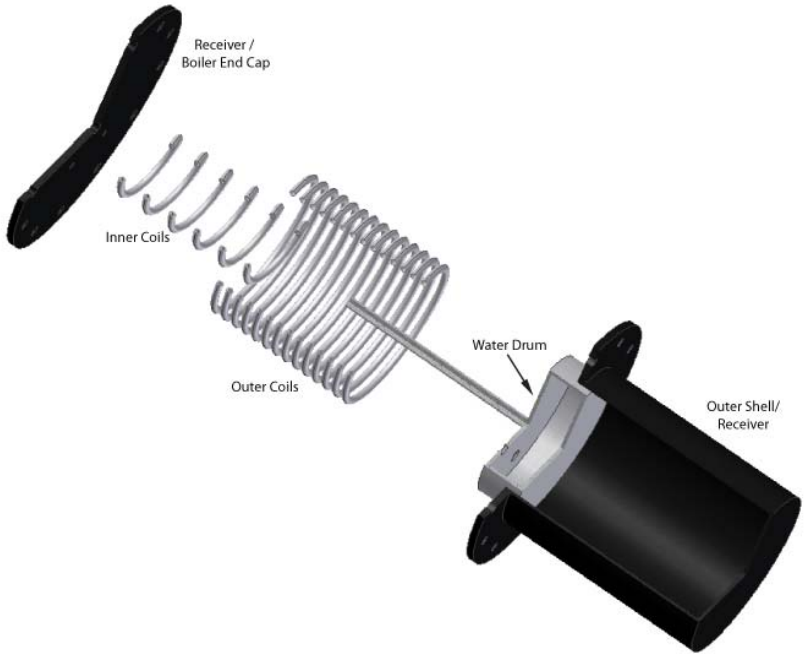

Figure 2.3: Exploded Three-dimensional layout of the receiver/boiler.

The outer shell is filled with a molten salt into which the water drum and coils are submerged. The molten salt is known as Draw Salt, which consists of a 1:1 molar ratio of Potassium Nitrate (KNO_3 - 101.11 grams per mol) and Sodium Nitrate ($NaNO_3$ - 84.99 grams per mol). There is a total of 19.39 Mols of Draw Salt in the thermal bath, Figure 2.4, which has a total mass of 3.61 kg; 1.96 kg of Potassium Nitrate and 1.65 kg of Sodium Nitrate. The Draw Salt serves as latent heat storage to allow for continuous heat transfer in the case of intermittent cloud cover and for equal thermal distribution over the water drum and the coils.

Figure 2.4: The Draw Salt mixture being mixed in the receiver.

The receiver is set up to record the inlet, outlet, and thermal bath temperatures, along with the outlet steam pressure. Three stainless steel sleeved K-type thermocouples, with ceramic connectors, are used for temperature measurements. The thermocouples are located at the inlet and exit of the receiver to measure the incoming water and exiting steam temperature. The third thermocouple is submerged halfway into the thermal Draw Salt bath. Figure 2.5 shows the location of the thermocouples on the receiver. With the receiver assembled, it was then placed at the focal region of the concentrator. The supporting structure for the receiver and the area of the receiver not subject to concentrated solar intensity was then covered with Kaowool Superwool insulation; shown in Figure 2.6.

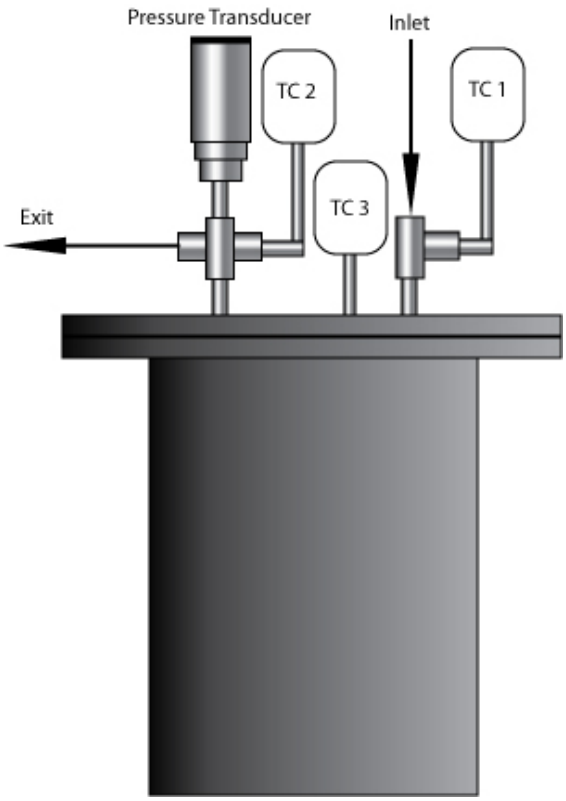

Figure 2.5: Schematic of Instrumentation of Boiler. TC1 is inlet temperature, TC2 is exit temperature, and TC3 is the temperature of the thermal Draw Salt bath. The pressure transducer measures the exit pressure of the boiler.

Figure 2.6: Receiver assembled and positioned in focal region of concentrator. Receiver and supporting structure of receiver wrapped in super wool insulation.

2.4 Steam Turbine

It was decided that a single stage impulse turbine would best meet the system requirements of simplicity and use in developing areas. Design plans were purchased from Reliable Industries, Inc. for the T-500 turbine. The impulse turbine was built in house at SESEC and modifications were made for use on the solar thermal system in this work. The design conditions are listed below in Table 2.1. Figures 2.7, 2.8, and 2.9 show the different components of the steam turbine, including the turbine blades and shaft (Figure 2.7), the housing (Figure 2.8), and the assembled turbine (Figure 2.9). The CAD drawings can be found in Appendix M.

Table 2.1: Design Conditions of the T-500 Impulse Turbine. Left: Original design parameters. Right: Modified design parameters. Gear Ratio and Output RPM is for attached gear-train.

T-500 Design Conditions	
Rotor RPM	33000
Gear Ratio	45.5:1
Output RPM	800
Steam Pressure	125 psig
Steam Flow Rate	1.512 kg/min
Mechanical Power	5 hp (3.73 kW)

T-500 SESEC Conditions	
Rotor RPM	3500
Gear Ratio	12.5:1
Output RPM	280
Steam Pressure	50 psig
Steam Flow Rate	0.292 kg/min
Mechanical Power	1.8 hp (1.34 kW)

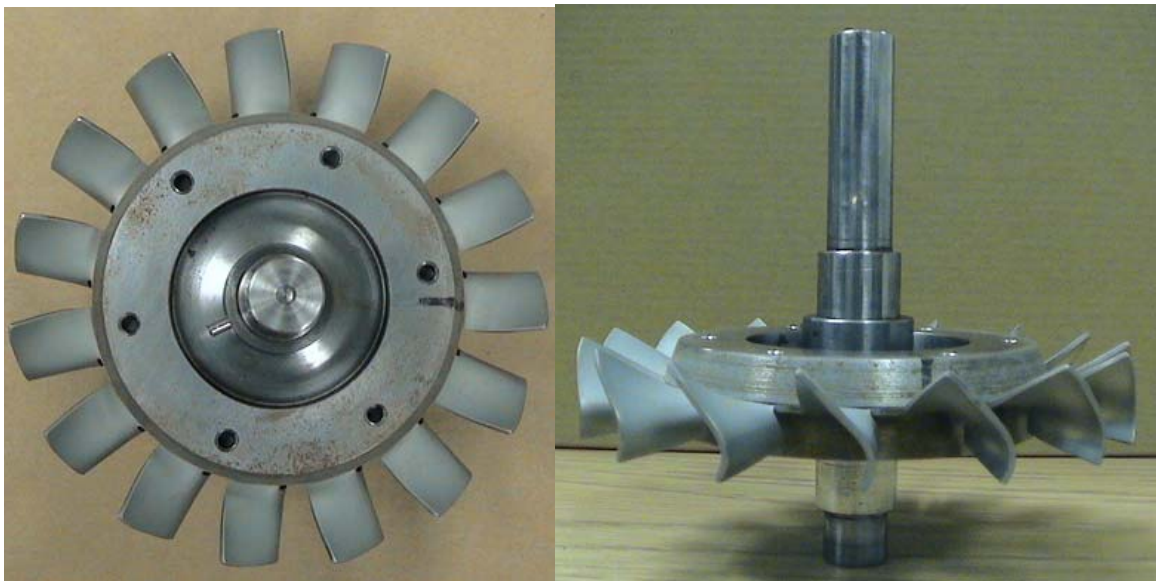

Figure 2.7: T-500 Impulse Turbine Rotor.

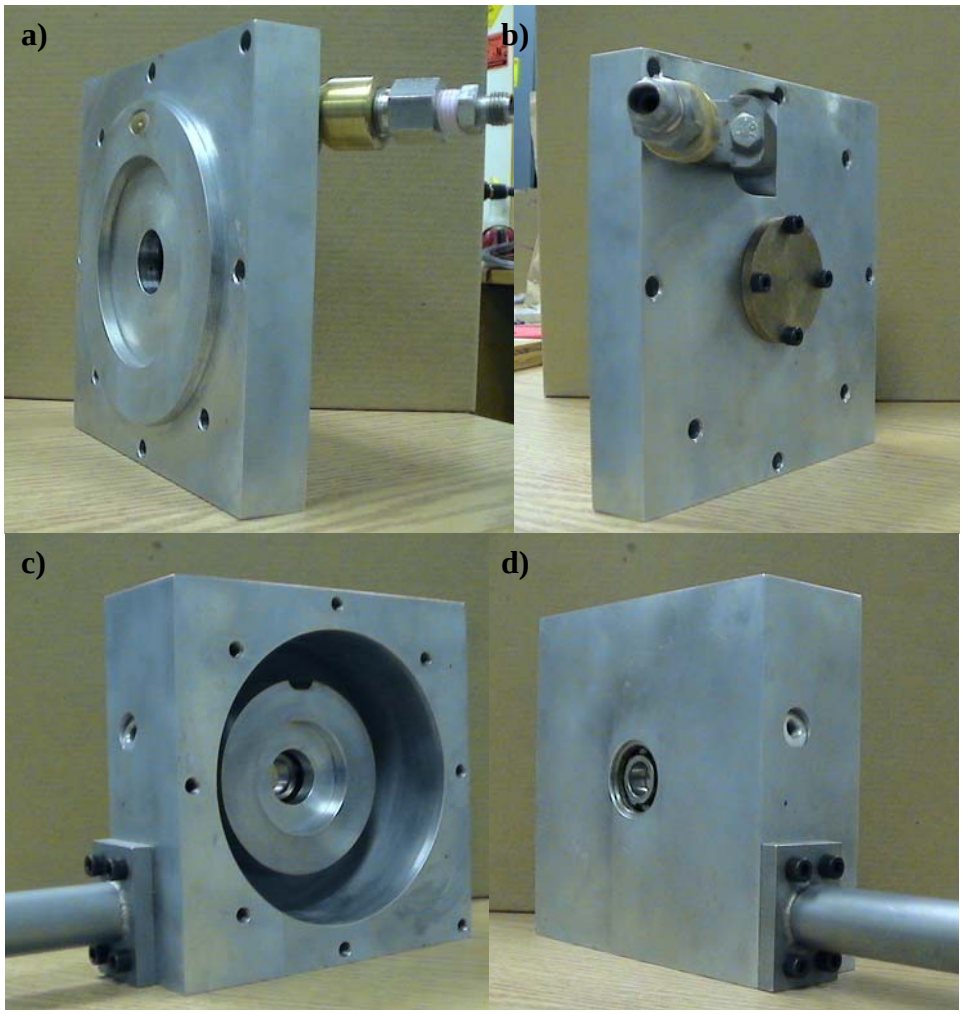

Figure 2.8: T-500 Steam Turbine Housing. a) Right housing plate, inside view, b) Right housing plate, outside view, c) Left housing body, inside view, d) Left housing body, outside view.

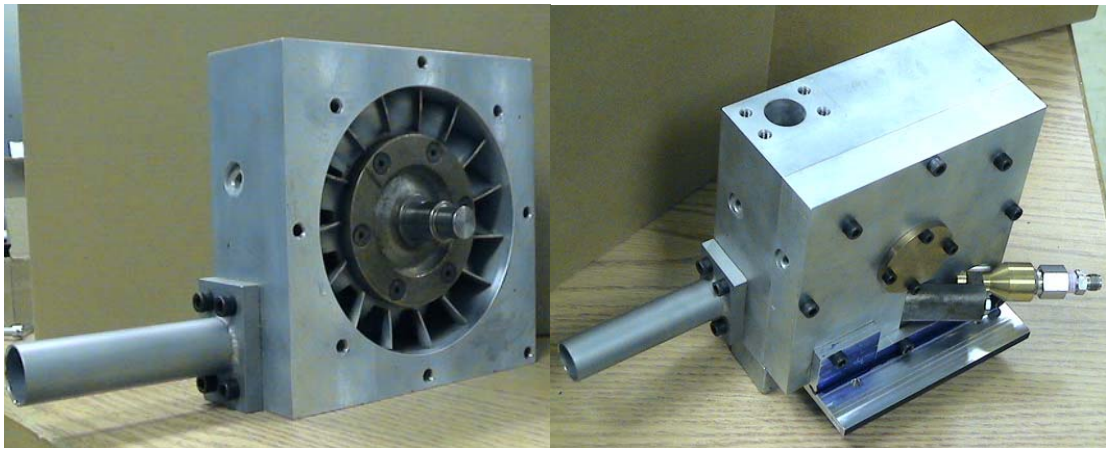

Figure 2.9: T-500 Steam Turbine. Image on the left shows the rotor installed in main part of housing. Image on the right shows fully assembled steam turbine.

2.5 Gear-Train

Although the steam turbine is capable of achieving high speeds, it is a very low torque device. Very high speed and low torque is a bad combination for use in a power generating system, although the higher speeds are needed to produce higher voltages; when a load is added to the generator, more torque is needed to overcome the load and produce the required current. Thus, for power production, it is ideal to have a shaft output that is more balanced, with a moderate rotational speed and torque. It is possible to achieve this by combining the steam turbine with a gear train.

Through the use of a gear train, the high speed and low torque of the steam turbine can be converted to low or moderate speeds with high to moderate torque. The gear train used here is a compound gear train consisting of two stages, with a total gear ratio of 12.5. The first stage (high speed stage) of the gear train consists of a high speed pinion spur gear with 22 teeth. The reduction gear in this first stage consists of 80 teeth, resulting in a 3.64 gear ratio. The second stage (intermediate speed stage) consists of an intermediate pinion gear of 21 teeth, and an intermediate gear with 72 teeth, for the resultant gear ratio of 12.5. This reduction slows the turbine shaft speed from a range of 3000 to 4000 rpm, to a more feasible range of 150 to 350 rpm. Figure 2.10 shows the assembly of the different stages of drive train and Figure 2.11 shows the fully assembled steam turbine and gear train. The CAD for the gear train can be found along with the CAD of the steam turbine in Appendix M.

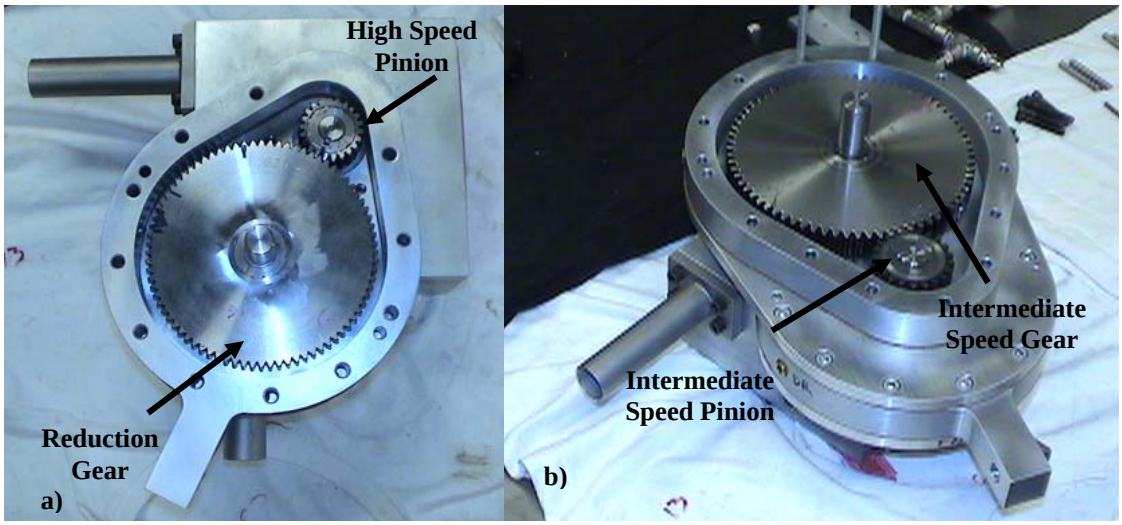

Figure 2.10: Pictures or the gear train assembly. a) Shows first stage assembly on top of steam turbine. High Speed Pinion and High Speed Gear. b) Second stage assembly atop of stage one. Intermediate Speed Pinion and Intermediate Speed Gear.

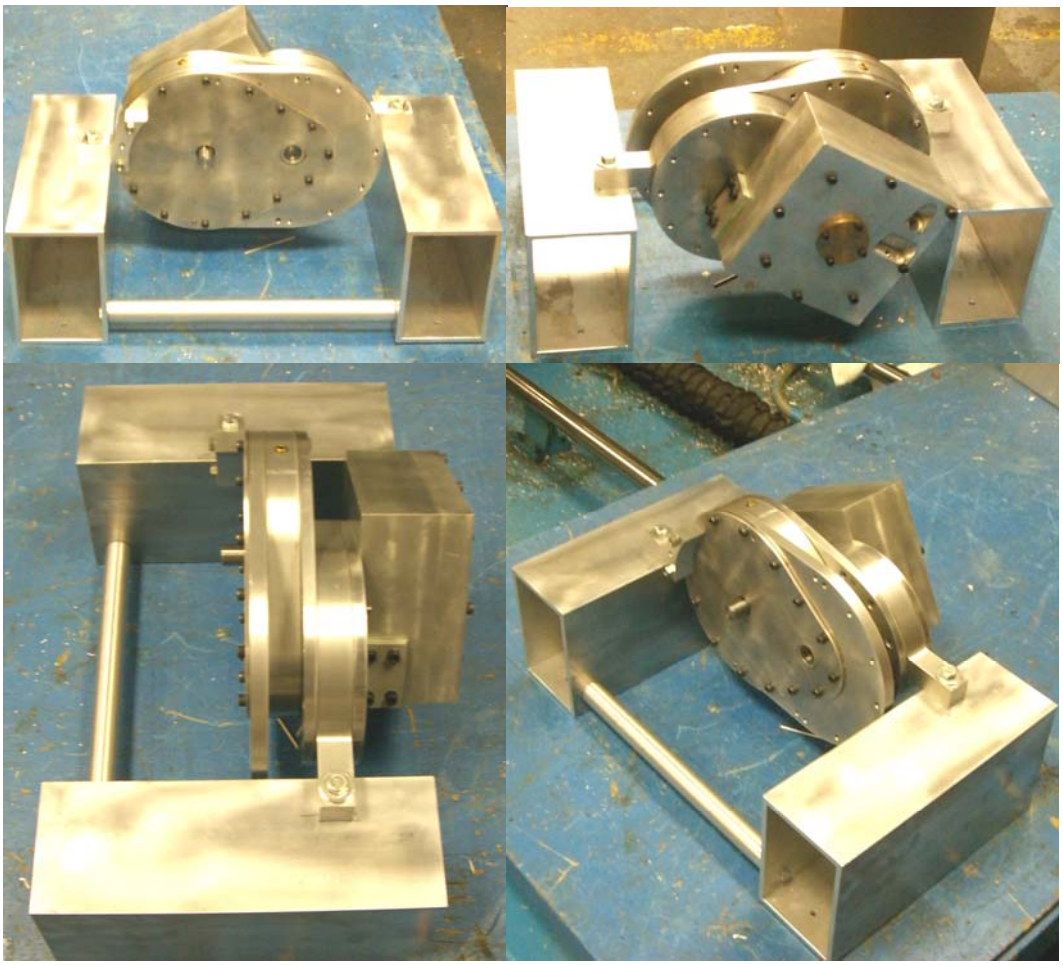

Figure 2.11: Completed assembly of steam turbine and drive train.

2.6 Working Fluid of Solar Thermal System

Since the design of this system was to be kept as simple as possible, water was chosen as the working fluid. If the system were set up off-grid in a field, then a well could be used to supply water for the solar thermal system. In the event that a water-well is unavailable, as was the case here, a reservoir for the water is needed. A steel constructed tank (Figure 2.12), with a capacity of 13 liters (~ 3.43 gallons) is used. Because of the conditions for which the system was designed, such as off-grid and emergency use, the water does not need filtered. However, if the water being used is full of debris, maintenance of the system will need to be performed more frequently, thus the use of a screen over the inlet supply line of the pump is suggested, but not necessary.

Figure 2.12: Water Tank used for supply water; wrapped in super wool insulation. a) Water line to pump, b) Return inlet from steam turbine, c) Thermocouple insert.

2.7 Pump

The water is supplied to the system from the tank by use of a Fluid-O-Tech pump located on the underside of the dish (Figure 2.13). The pump has a small foot print, with the motor having dimensions of 127 mm x 114 mm x 109 mm, and the controller, 93 mm x 115 mm x 83 mm. The pump has variable speed and power settings, ranging from speeds of 1000 rpm to 3500 rpm, and power settings from 30 percent to 85 percent. The pump runs off of 100 volt to 110 volt AC, with a maximum power usage of 250 Watts. The power setting on the pump has no affect on the flow rate; it affects the amount of pressure that the pump can overcome at a particular speed. The speeds of the pump, however, directly correspond to the flow rate, as shown in Table 2.2. The pump is designed for longevity by having an absence of moving parts within the motor, with only a short single shaft inside the pump. The control unit of the pump utilizes a double protection system on the circuit board, with a thermal 'cutout' to protect the pump and control unit from overheating and current protection for moments of high current peaks caused by overload or seizure of the pump. The original design of the pump was for espresso coffee machines, reverse osmosis systems, cooling systems, circuit washing, and/or solar heating systems, thus it was deemed ideal for use in the solar thermal system discussed in this work.

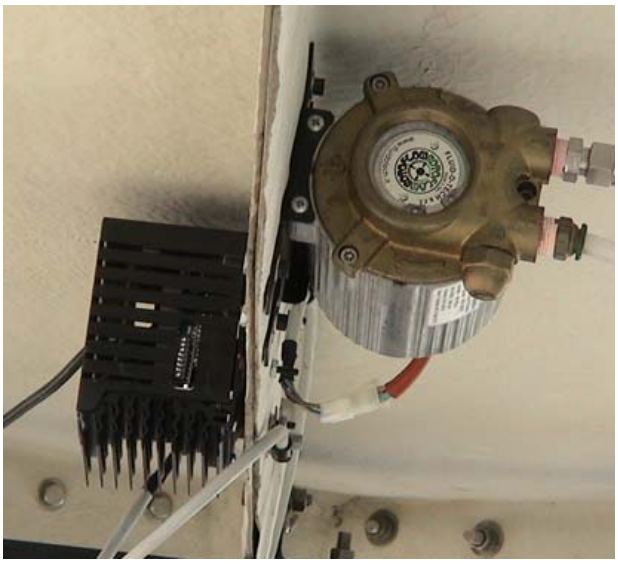

Figure 2.13: Pump and Controller located on underside of the dish.

Table 2.2: Correlation of Pump Speed to Flow Rate

RPM	Flow Rate (LPM)
1100	1
1500	1.14
1750	1.36
2000	1.58
2500	1.98
2750	2.18
3000	2.39
3500	2.79

2.8 Tracking

Tracking of the parabolic dish is done by a combination of satellite dish linear actuators and photo-sensing control units that are commercially available. Due to the need for two-axis tracking, two heavy duty linear actuators were used. The actuator for altitude tracking wass a SuperJack Pro Brand HARL3018, and the azimuth actuator is a SuperJack Pro Brand VBRL3024. The HARL3018 is a medium duty model, rated for a dynamic load of 600 lbs, with an 18 inch stroke length equipped with limit switches. The VBRL3024, a heavy duty actuator, is rated at a dynamic load of 1500 lbs, with a 24 inch stroke length and is also limit switch equipped. The heavy duty model was required for the azimuth tracking because of the East and West directional extremes required of the actuator. Each actuator requires 12 to 36 volts and up to 7.5 amps, depending on loading, for operation. Figure 2.14 shows images of the frame with the mentioned actuators.

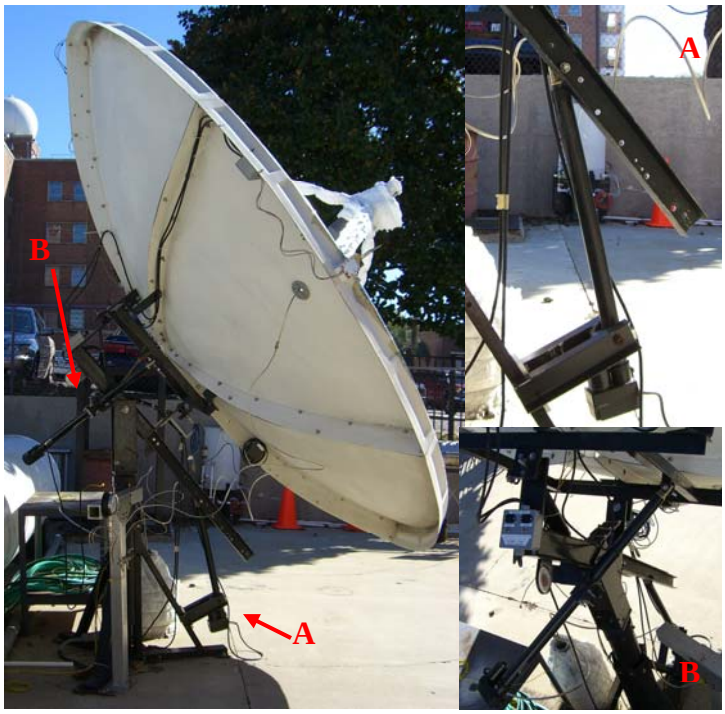

Figure 2.14: Images of the frame with attached actuators. A) Altitude (North/South) control actuator. B) Azimuth (East/West) control actuator.

Control of the actuators, and tracking of the dish, was done by a set of photo-sensing modules. The modules used are LED3s, designed and fabricated by Red Rock Energy (Figure 2.15). The LED3s were designed with the operation of satellite dish linear actuators in mind. The LED3s work by using two opposing green LEDs, in a comparative circuit setup, to track the sun. LEDs, like photovoltaic cells, produce voltage when in sunlight. Green LEDs produce from 1.65 to 1.74 volts, whereas silicon photovoltaic cells produce a mere 0.55 volts. The green LEDs produce such a high voltage because they are made of the Gallium Phosphide, which is a semiconductor that has a higher band-gap voltage, than silicon PV cells. The LED3 modules are capable of handling 10.5 to 44 volts, and can handle a current load of up to 20 amps. The modules can operate effectively in temperatures ranging from -40ºC to 85ºC before operating temperature becomes a subject of concern.

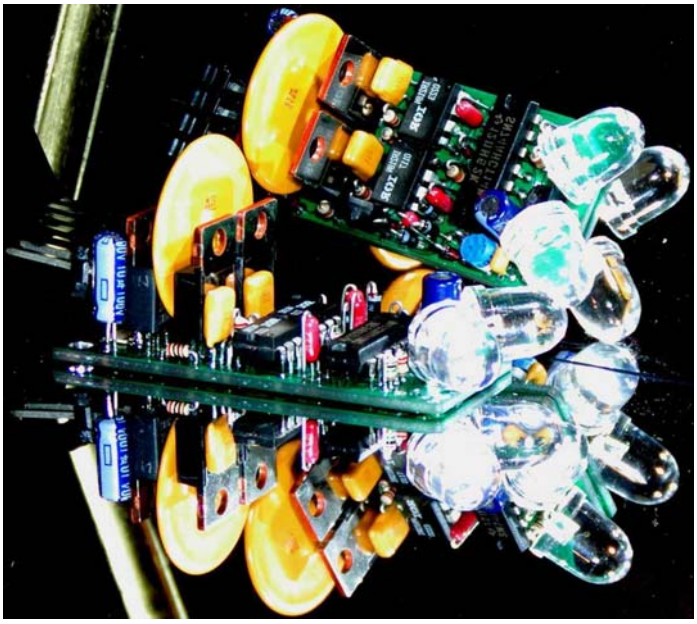

Figure 2.15: Image of the LED3 – Green LED Solar Tracker

The tracking module is not weatherproof and requires protection from the elements. A weatherproof housing was designed and used with the trackers, as shown in Figure 2.16. The housing is constructed of plexi-glass, so as not to block any incoming sun light and to keep reflections low. The housings were sealed with RTV silicone gasket maker by Permatex, shown in Figure 2.17. Once the modules and housings were mounted on the dish, they were mechanically adjusted for optimum tracking performance.

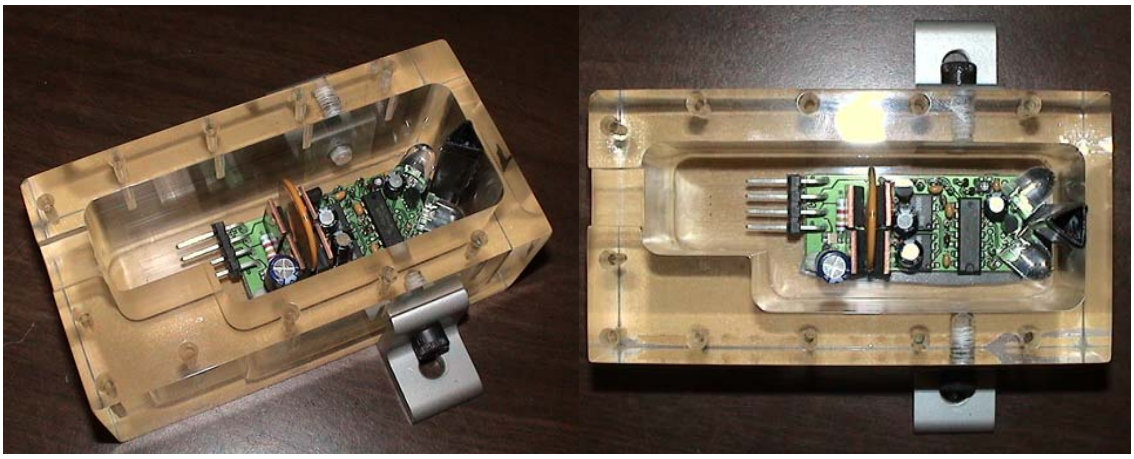

Figure 2.16: LED3 module inside of plexi-glass housing.

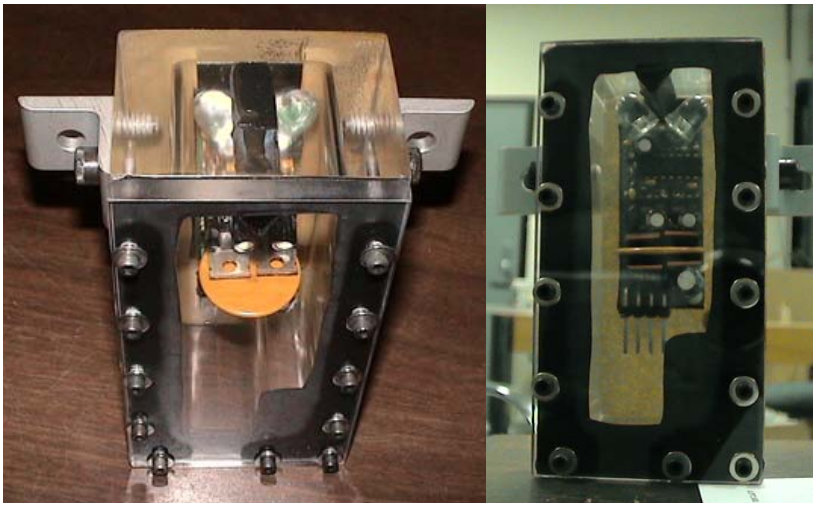

Figure 2.17: LED3 module sealed in plexi-glass housing.

To improve the accuracy, shading was later added to the trackers on the dish. The tracker module housings were also painted white to help reflect heat from the modules. This is shown in Figure 2.18 below.

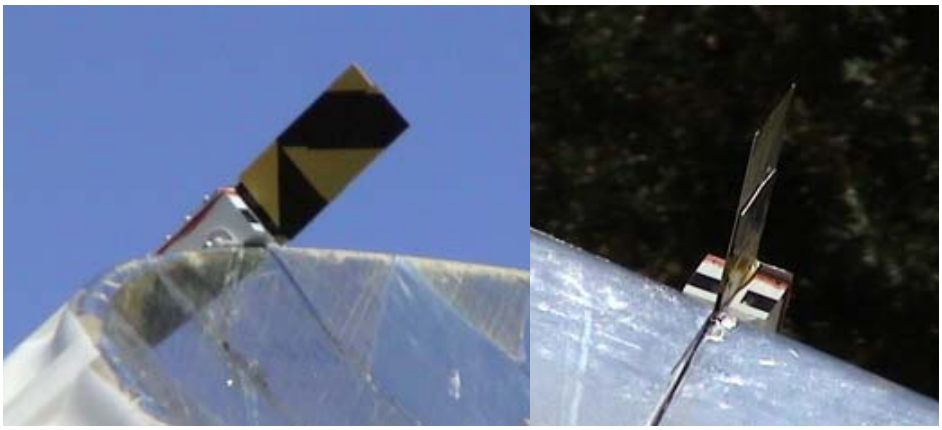

Figure 2.18: Tracker module housing painted white and shading added.

2.9 Data Acquisition

Temperature and pressure had to be constantly monitored and logged throughout the day for numerous days to be able to characterize the solar thermal system. A data acquisition system was implemented in order to avoid having to manually log these values by hand. The data acquisition system consisted of a Windows XP based personal computer (PC), and a National Instruments Signal Conditioning Board (SCB-68). The PC used a LabVIEW-based program named Surya after the Hindu Sun god, to acquire the temperatures of interest from the solar thermal system. An image of the GUI for this program is shown in Figure 2.19. The program monitored the inlet, outlet, and thermal bath temperatures of the receiver, along with the ambient, turbine inlet and outlet temperatures, and the working fluid reservoir temperature. The program displayed the data for quick reference of system operation throughout the day, and it logged all of the measurements with a time stamp of when the data was acquired.

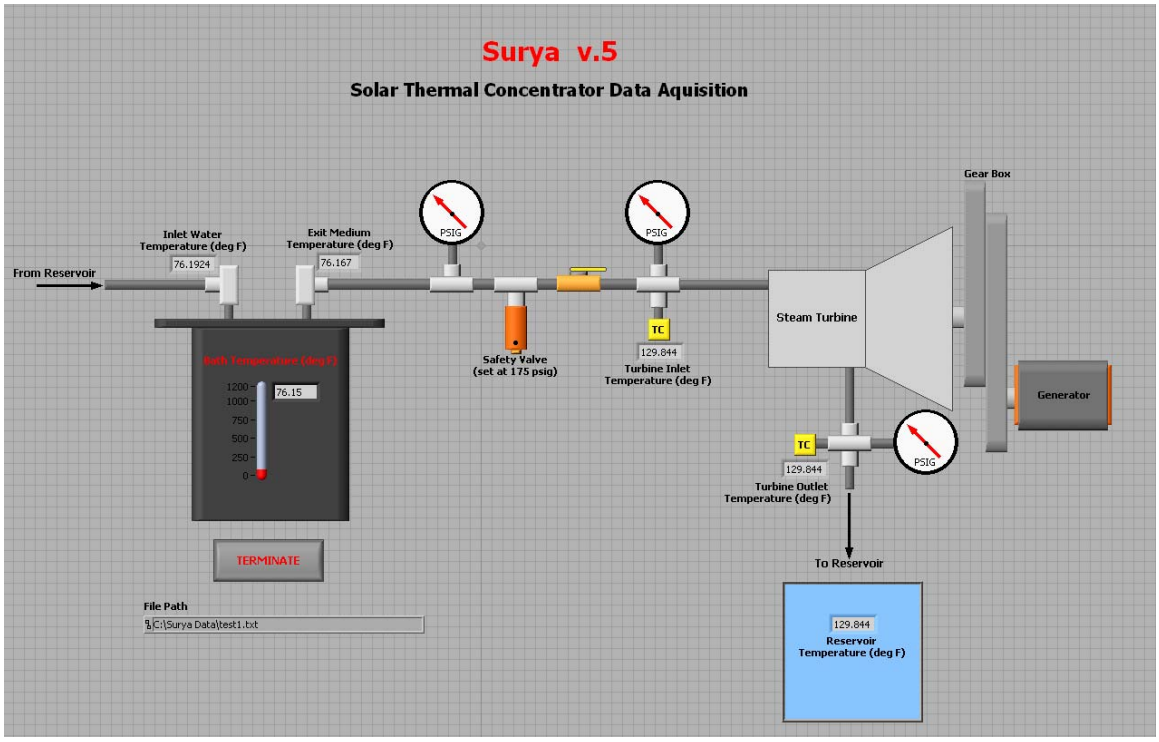

Figure 2.19: Image of Surya, the GUI used for Data Acquisition of the Solar Thermal System.

2.9.1 Instrumentation

The concentrating solar thermal system utilized a flow meter, high-temperature pressure gauges, and thermocouples. The thermocouples used were Omega K-type thermocouples (CASS-18U-6-NHX) with a protective outer sheath of stainless steel. The thermocouples were connected to the data acquisition hardware by use of K-type thermocouple extension wire. Three thermocouples were used in the receiver, two were used for measurement of the inlet and outlet temperatures of the steam turbine, and one was used for measurement of the water reservoir. Two of the thermocouples in the receiver were placed at the inlet and outlet of the water flow by use of compression fittings such that 3.175 mm of the thermocouple sheath was in the flow. The third thermocouple in the receiver was placed directly in the thermal draw salt bath at a depth of 76.2 mm. The thermocouples located at the inlet and outlet of the steam turbine also use compression fittings to position the tip of the sheath 3.175 mm into the steam flow.

High temperature pressure gauges, by Duro United Industries, were used to measure the pressure in the system as the water was flashed to steam. One gauge was used downstream of the boiler to measure the exiting steam pressure of the boiler, while two other gauges were used for measuring the inlet and outlet pressures of the steam turbine. The pressure gauges were designed to handle process steam above 422 K, and have a pressure range from 0 to 300 psig.

2.10 Power Supply

Although the system is designed to produce power, some power must be consumed in order to do so. Power was needed for the linear actuators for positioning of the dish, as well as for operation of the pump. This power was being provided by two 12-volt, valve regulated, deep cycle, AGM type Delco brand batteries, Figure 2.20. The batteries were wired in series to increase the voltage to 24 volts for control of the tracking.

Figure 2.20: Two 12-volt deep cycle batteries wired in series.

The batteries were kept constantly charged by use of two small, thin-filmed, photovoltaic panels wired in series. The panels were flexible and lightweight and had a plastic-type coating to protect the panel from the elements. The panels were mounted on a plexi-glass sheet for ease of mounting outdoors, shown in Figure 2.21a. The panels were purchased from Solar World, Inc, with each panel having a maximum output voltage of 15.7 volts and 100 milliamps. In order to supply the needed voltage for charging the batteries, the photovoltaic panels were wired in series, for a resultant voltage of 31.4 volts. In intense sunlight, the panels can generate a voltage slightly higher, as shown in Figure 2.21b.

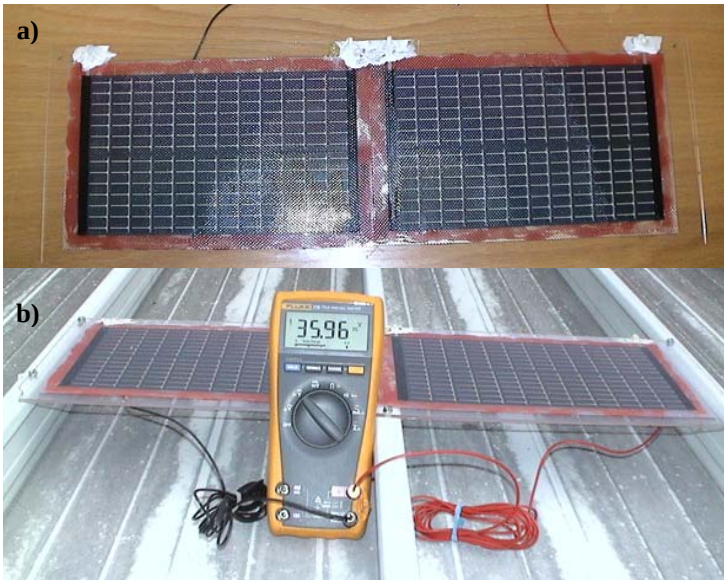

Figure 2.21: a) The thin-filmed solar panels assembled together in series on plexi-glass sheet. b) The solar panels mounted and producing 35.96 volts under intense sunlight.

In order to control the charging of the batteries, so as not to overcharge them, or to discharge to a point beyond use, a solar charging regulator was used, shown in Figure 2.22a. The solar charger was purchased as a kit; model K009C, from Oatley Electronics, and was assembled in house. For a 12 volt battery the solar charger will charge until 14.2 volts is reached, and then stop. Charging will resume when the battery voltage drops below 13.7 volts. For a 24 volt battery, the voltage of the battery needs to reach 28.4 volts before charging is stopped. Charging will subsequently resume when the battery voltages drops below 27.4 volts. Schematics of the solar charger can be found in Appendix O. The housing in which the charge controller is mounted is shown in Figure 2.22b.

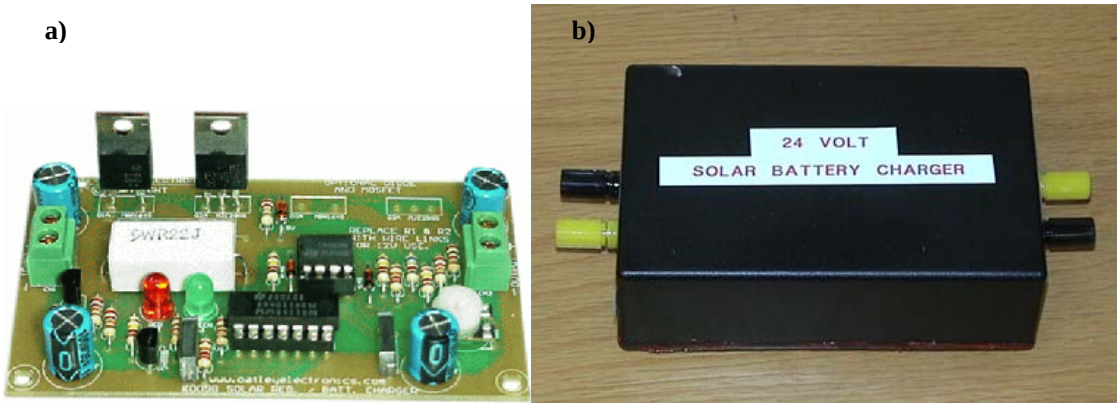

Figure 2.22: Image of Solar Charger Controller, Model K009C

Because the actuators and tracking modules operate on DC current, they were able to function directly from the battery bank. The pump, however, operated on AC power. In order to supply the type of current needed, a DC to AC power inverter was used. The power inverted used, shown in Figure 2.23, was capable of operating at 400 watts continuously, with intermittent peak power operation at 1000 watts.

Figure 2.23: 400 Watt DC to AC Power Inverter

2.11 Generator/Alternator

In order to produce electrical power from the system, a generator has to be coupled with the output shaft of the steam turbine, Figure 2.26. The generator used was a 443541-10Amp Permanent Magnet DC Generator from Windestream Power LLC. The generator is capable of producing power at speeds ranging from 0 to 5000 rpm at voltages between 12 and 48 volts. Maximum power production for this particular generator, for 12, 24, and 48 volts is 120, 240, and 480 watts, respectively. Figure 2.24 shows an image and Figure 2.25 shows the performance curves for the generator of mention. The schematics for the generator can be found in Appendix P.

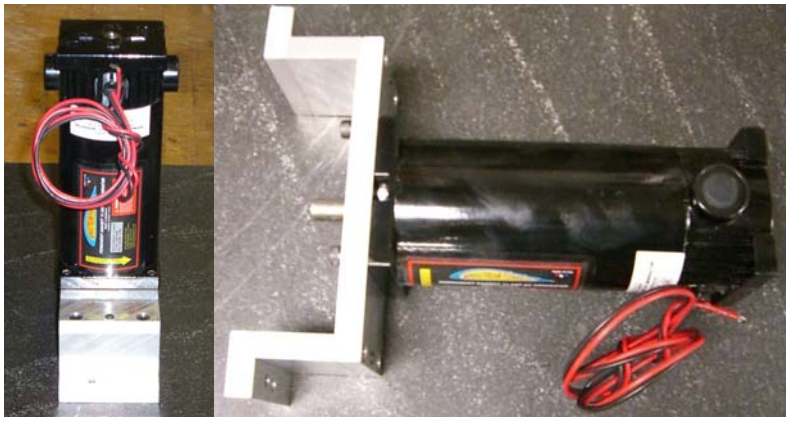

Figure 2.24: Windstream Power 10 Amp Permanent Magnet DC Generator.

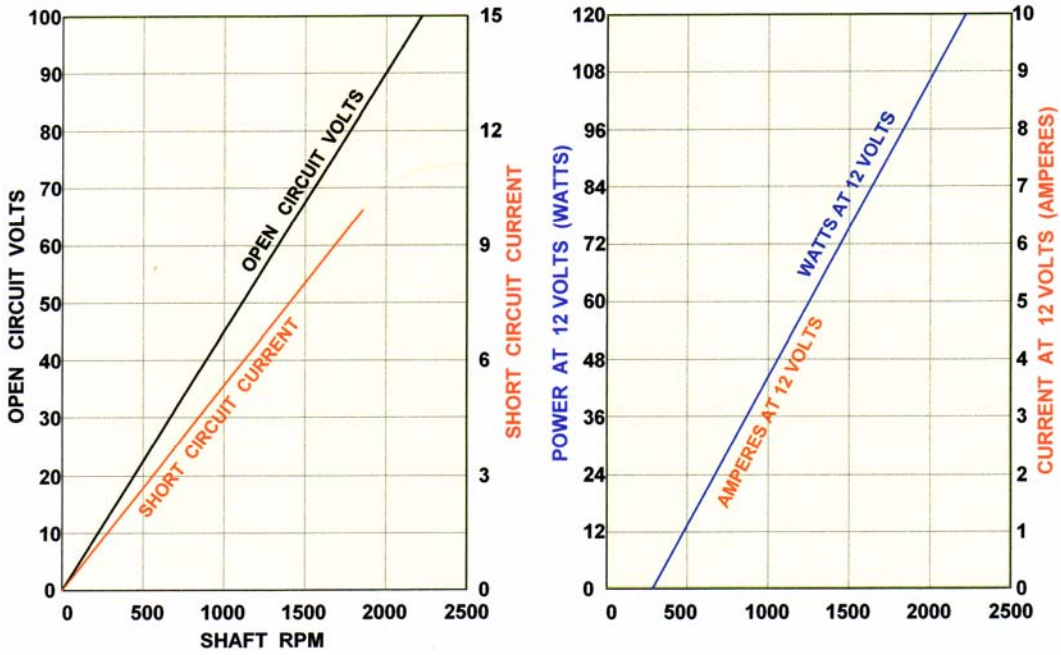

Figure 2.25: Performance curves for Windstream Power 10 Amp DC Permanent Magnet Generator.

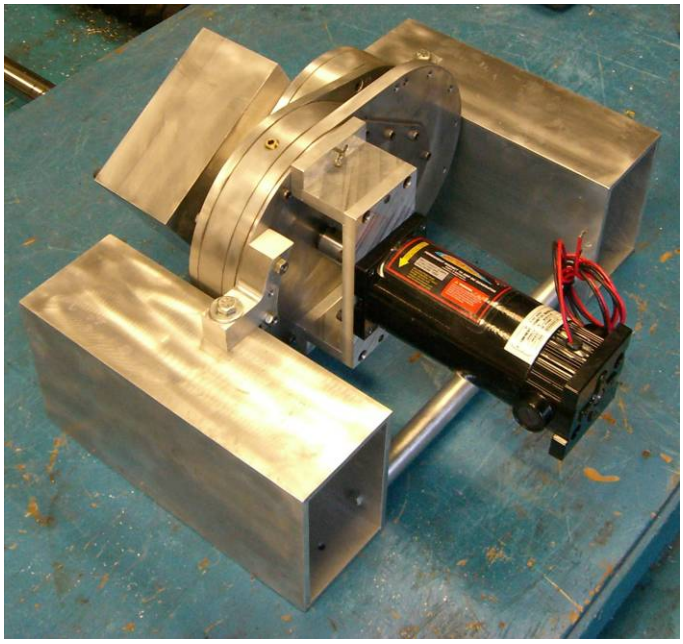

Figure 2.26: 10 Amp Windstream Power Permanent Magnet DC Generator coupled with steam turbine and gear-train for power production.

CHAPTER 3

ANALYSIS / RESULTS AND DISCUSSION

3.1 Introduction

This chapter contains a detailed description of the analysis and results which were obtained for the different components of the concentrating solar thermal system. The chapter starts with an overview of the solar calculations needed for the solar concentrator to track the sun. An analysis of the solar concentrator will then be discussed comparing the expected amount of collected solar radiation and achievable temperature to actual values. Following is a discussion on the remaining components of the system, including the receiver, the turbine, and the generator. The chapter is concluded by discussing the overall efficiency of the system.

3.2 Solar Calculations

For the solar concentrator to track the sun, and to determine the efficiency of the concentrator, the amount of solar radiation incident on the collector and the position of the sun 'relative' to the location of the collector (the Ptolemaic view) was needed. The location of the solar collector is Tallahassee, Florida with Latitude of 30.38° North, Longitude of 84.37° West, and a Standard Time Meridian of 75° West. For simplification, the calculations in this section are performed for a single day, October 12th (n is equal to 285), at solar noon, in which the hour angle is at 0 degrees. Full calculations for the particular day mentioned and for the range of the entire year are available in Appendicies B and C.

As was discussed in the section of Solar Geometry from Chapter 1, the solar declination angle, the angle between the earth-sun line and the plane through the equator (refer to Figure 1.6), is needed to perform calculations for the position of the sun. The

declination angle is found by using Equation 1-1, or by use of Figure 1.5. The declination angle for October 12th was found to be -8.482°.

By using the Ptolemaic view of the sun's motion, the position of the sun can be described at any time by two different angles, the solar altitude angle, α, and the solar azimuth angle, α_s for the date mentioned. The solar altitude angle is 51.138 degrees, and since the calculations are for solar noon, the solar azimuth angle is zero. Figure 3.1 below shows the solar altitude and azimuth for the entire day. However, since the solar altitude and azimuth angles are not fundamental angles, they need be related to the fundamental angular quantities, given previously as the sunrise and sunset hour angles, latitude, and declination angle. The hour angles for Tallahassee on October 12th were ±84.984 degrees; negative for morning and positive for evening and the time from solar noon was calculated to be 5 hours 39 minutes and 56 seconds. However, due to the irregularity of the earth's motion about the sun, a correction factor of 14.35 minutes is given by the Equation of Time. This correction factor is found by use of Equation 1-5 or by use of the graph shown in Figure 1.7 from Chapter 1. Applying the Equation of Time correction factor, the sunrise and sunset local standard times, were 7:43 AM and 7:03 PM, respectively, resulting in a day length of 11 hours and 20 minutes. The day length for Tallahassee can also be estimated by use of the plot in Figure 1.8.

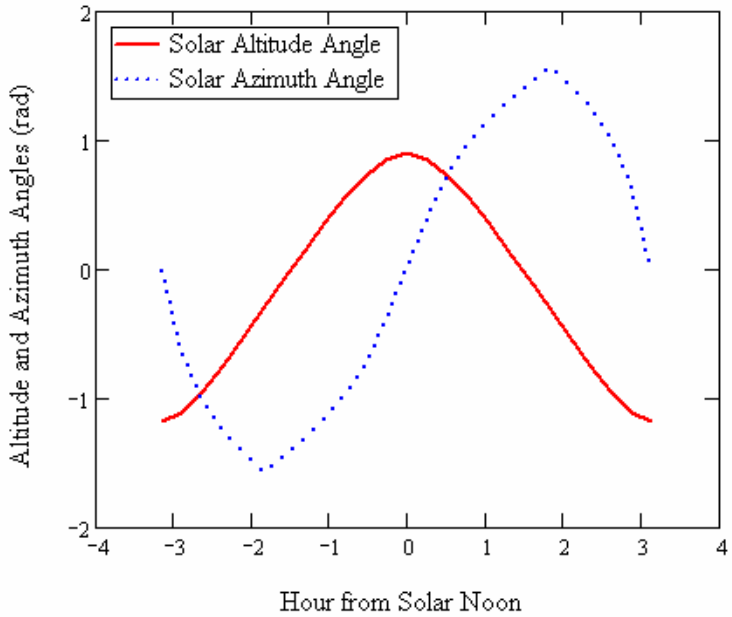

Figure 3.1: Solar Altitude and Azimuth angles for October 12th

By having a collector which follows the position of the sun, an optimum amount of solar radiation can be collected. At solar noon, the total instantaneous solar radiation falling on the parabolic concentrator was found to be approximately 1.15 kW/m^2. However, only beam (direct) insolation can be utilized due to the type of collector used. This results in approximately 1.064 kW/m^2 of solar radiation. The calculations for how these values were obtained are located in Appendix E. Figure 3.2, below, shows a comparison of the total instantaneous and beam solar insolation falling on the collector in Tallahassee, FL.

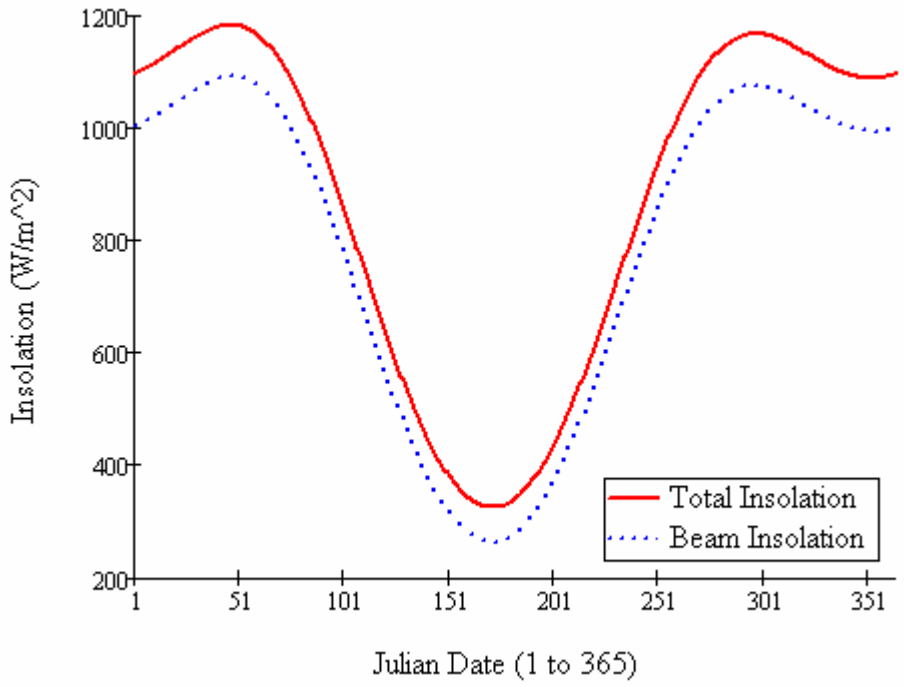

Figure 3.2: Comparison of the Total Insolation available to that of the Beam Insolation falling on the SESEC solar collector located in Tallahassee, FL.

3.2 Analysis of the Dish

Measurements of the dish were taken to calculate the equation to describe the shape of it. The dish is considered to be that of a parabolic concentrator with a diameter

of 3.66 *meters* (144 inches), and a depth of 0.648 *meters* (25.5 inches). The surface area of the dish is thus calculated by the following equation:

$$A_{concentrator} = \frac{2 \cdot \pi}{3 \cdot P} \cdot \left[\sqrt{\left(\frac{D^2}{4} + P^2 \right)^3} - P^3 \right] \qquad \textbf{(3-1)}$$

where

$$P = \frac{D^2}{8 \cdot H} \qquad \textbf{(3-2)}$$

The resulting surface area of the concentrator is 11.73 m^2 (126.28 ft^2). The cross-section of the concentrator can be viewed as a parabola, which is given by the equation

$$f(x) = a \cdot x^2 + b \qquad \textbf{(3-3)}$$

where *f(x)* is the function describing the shape of the parabola, *x* is the horizontal distance from the center, and the constants *a* and *b* describe the shape of the parabola. *b* can be made zero by placing the bottom center of the concentrator at the origin. From this constraint, the value of *f(x)* is equal to the depth when *x* is equal to the radius of the dish. Thus, the constant *a* can be calculated using the following equation:

$$a = \frac{Depth}{Radius^2} \qquad \textbf{(3-4)}$$

This constant is found to be 0.194 per meter (0.004919 per inch) and is used to determine the focal length of the collector. The focal length of the concentrator is defined as the distance from the bottom of the parabola to the concentration point (focal point). For a symmetric parabola, the focal point lies along the axis of symmetry where the distance above the intersection of the axis and curve gives the focal length by

$$\text{focal length} = \frac{1}{4 \cdot a} \qquad \textbf{(3-5)}$$

thus establishing where there focal point is located relative to the bottom of the concentrator.

The calculation of the focal length is useful for positioning of the receiver, however, due to the dynamics involving the sun, earth, and optics of the concentrator, the focal point will not be an exact point, but will actually be more of a focal area. The area in which the radiation is condensed determines the radiation intensity. The higher the intensity, the higher the temperature that the receiver can attain.

In order to calculate the maximum achievable temperature of the concentrator, the geometric concentration ratio needs to be determined. By convention, the receiver at the focal area would be considered as a flat plate absorber, thus the area that would be used for calculation of the concentration ratio would be the flat circular bottom region of the receiver. However, the receiver of the solar thermal system discussed here is 'submerged' in the focal region, thus more surface area of the absorber is receiving the concentrated solar radiation. The area of the receiver is calculated to be 0.109 m^2, with the aperture area of the concentrator being 10.507 m^2, resulting in a geometric concentration ratio of 96. By using the standard assumptions given by Rabb , the transmissivity,τ, is equal to 0.5, the absorptance of the receiver, α, is 0.7, and the emmittance of the receiver in the infrared region, ε, is 0.5; the radiation transfer from the sun to the receiver is calculated as follows:

$$Q_{sun \to receiver} = \tau \alpha A_{concentrator} \sin^2(\theta_{half}) \sigma T_{sun}^4 \qquad \textbf{(3-6)}$$

where the half-angle of the sun, θ_{half}, is found to be 0.266° by use of

$$\theta_{half} = \frac{r_{sun}}{R_{sun \to earth}} \qquad \textbf{(3-7)}$$

where $r_{sun} = 695500km$ and $R_{sun \to earth} = 1.4967 \times 10^8 km$. The ideal concentration ratio can then be determined using:

$$CR_{ideal} = \frac{1}{\sin^2(\theta_{half})} \quad \textbf{(3-8)}$$

which results in $CR_{ideal} = 46310$. These values can now be used in the following equation to calculate the maximum achievable temperature of the concentrator for the geometric concentration ratio of the system:

$$T_{receiver} = T_{sun}\left[(1-\eta)\tau\frac{\alpha}{\varepsilon}\frac{CR_{geometric}}{CR_{ideal}}\right]^{\frac{1}{4}} \quad \textbf{(3-9)}$$

From Equation 3-9, the maximum achievable temperature of the receiver, $T_{receiver}$, was found to be to be 984.732 K (1313°F). The calculations for the theoretical maximum temperature of the collector can be located in Appendix G. Experimentally, the maximum internal temperature of the receiver was approximately 834.15 K (1041°F) and the external temperature was 922 K (1200°F). It is assumed that this discrepancy is due to the assumed values for the transmissivity, absorbtivity, and emmittance of the dish, as well as the degradation of the reflective surface and the solar intensity of the day. In Figure 3.3, it is shown how the receiver temperature relates to the geometric concentration ratio of the system. The figure also shows how the concentrator discussed in this work is less efficient than ideal.

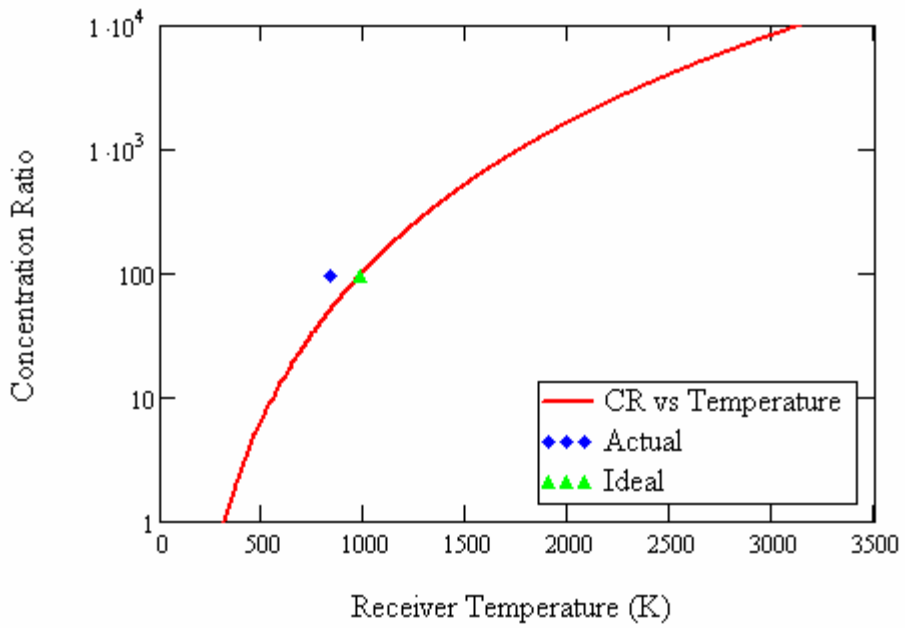

Figure 3.3: Relationship between the concentration ratio and the receiver operation temperature.

3.3.1 Efficiency of Collector

A solar concentrator is more efficient at high temperatures in that it reduces the area from which heat is lost. In order to calculate the efficiency of the concentrating collector, the absorbed radiation per unit area of aperture must be estimated from the radiation and the optical characteristics of the concentrator and receiver [2]. A simple energy balance equation yields the useful energy delivered by the collector to the receiver as

$$Q_{out} = \eta_o I_b A_a - U_L (T_r - T_{amb}) A_r \qquad \textbf{(3-10)}$$

The energy balance equation can be rearranged to yield the instantaneous efficiency of a solar thermal collector, which is defined as the ratio of the useful energy delivered to the total incoming solar energy. The following equation shows this relation

$$\eta_{collector} = \frac{Q_{out}}{A_a I_b} = \eta_o - \frac{A_r}{A_{amb}} \frac{U_L (T_r - T_a)}{I_b} \qquad \textbf{(3-11)}$$

In order to calculate the efficiency of the concentrating collector, the absorbed radiation per unit area of aperture must be estimated from the radiation and the optical characteristics of the concentrator and receiver. This is given by Q_{out}, which is defined as

$$Q_{out} = Q_{opt} - Q_{loss} \qquad \textbf{(3-12)}$$

where Q_{opt} is the rate of the optical energy absorbed by the receiver, and Q_{loss} is the rate of the energy lost from the receiver to the ambience. The optical energy that is absorbed by the receiver from the concentrating collector is defined by the following [2]

$$Q_{opt} = A_a \rho_{s\_m} \tau_g \alpha_\gamma S I_b \qquad \textbf{(3-13)}$$

The terms in this equation depend upon the geometry and parameters of the receiver and the collector. Where S is the receiver shading factor, α_r is the absorbtance of the receiver, ρ_{s_m} is the specular reflectance of the concentrator, and τ_g is the transmittance of the glass envelope over the receiver (if one is present), A_a is the aperture area of the collector, and I_b is the beam insolation incident on the collector aperture. The terms S, α_r, ρ_{s_m}, and τ_g are constants which are dependent on the materials used and the accuracy of the collector, and are nominally lumped into a single constant term, known as the optical efficiency of the collector, η_{opt}. The rate of optical energy absorbed by the receiver, Q_{opt}, was calculated to be 11.072 kW.

The thermal energy lost from the receiver, Q_{loss}, to the ambient surroundings is described by

$$Q_{loss} = A_r U_L (T_r - T_{amb}) \qquad \textbf{(3-14)}$$

where A_r is the surface area of the receiver, U_L is the overall heat loss coefficient, T_a is the ambient temperature, and T_r is the averaged receiver temperature. T_r is represented by the following equation

$$T_r = \frac{T_{out} + T_{in}}{2} \qquad \textbf{(3-15)}$$

where T_{out}, the temperature of the fluid exiting the receiver was 922 K, and T_{in}, the temperature of the fluid entering the receiver was 305 K. The resultant averaged receiver temperature was then calculated to be 613.5 K. The heat loss coefficient, U_L, however, is not a simple constant, but instead, varies as heat-loss mechanisms change with temperature. For example, as the temperature increases, the radiant heat loss from the receiver increases. For computation of the heat loss coefficient, it is assumed that there are no temperature gradients around the receiver and that there are no losses through conduction between the receiver and its supporting structure. The heat loss coefficient, U_L, for the receiver type discussed in this work is given as

$$U_L = \left[\frac{A_r}{(h_w + h_{r,c-a})A_c} + \frac{1}{h_{r,r-c}} \right]^{-1} \qquad \textbf{(3-16)}$$

where h_w is given as the convective coefficient, $h_{r,c\text{-}a}$ is the radiation coefficient between the receiver (or glass cover) and the ambient, $h_{r,r\text{-}c}$ is the radiation coefficient between the receiver and the glass cover (if there is a cover), A_r is the surface area of the receiver, and A_c is the surface area of the glass cover (if one is used). Since the receiver used in this work does not utilize a glass cover, Equation 3-16 is simplified to

$$U_L = \left[\frac{1}{h_w + h_r} \right]^{-1} \qquad \textbf{(3-17)}$$

The linearized radiation coefficient can thus be calculated by [2]

$$h_r = 4\sigma\varepsilon T_{mean}^3 \qquad \textbf{(3-18)}$$

where σ is the Stefan-Boltzmann constant, ε is the emittance of the absorbing surface, and T_{mean} is the mean temperature for radiation. The emittance had a value of 0.5 with the mean temperature being the same as the inlet water temperature, at 305 K. The radiation coefficient was calculated to be 3.218 W/m^2-K.

The convective heat loss coefficient, h_w, is modeled and solved as flow of air across a cylinder in an outdoor environment. The equations recommended by McAdams [2] have been modified to account for the outdoor conditions by increasing the original coefficients by 25 percent. The Nusselt number is thus given as

$$Nu = 0.40 + 0.54\,\mathrm{Re}^{0.52} \qquad \textbf{(3-19)}$$

for Reynolds numbers which fall between 0.1 and 1000, and as

$$Nu = 0.30\,\mathrm{Re}^{0.6} \qquad \textbf{(3-20)}$$

for Reynolds numbers between 1000 and 50000. For the calculations presented in this section, a wind speed of 0.5 m/s is assumed. The Reynolds number was calculated to be 1476 by use of Equation 3-21,

$$\mathrm{Re} = \frac{V \cdot D_{outer}}{\nu} \qquad \textbf{(3-21)}$$

where V is the wind speed, D_{outer} is the diameter of the receiver, and v is the viscosity, with a value of $5.15 \cdot 10^{-5}\ \frac{m^2}{\sec}$. The Reynolds number was then used in conjunction with Equation 3-20, yielding a Nusselt number of 23.907. The convection coefficient was then calculated by using Equation 3-22, to obtain a value of 7.172 W/m^2-K.

$$h_w = \frac{k_{air}}{D_{outer}} \cdot Nu \qquad \textbf{(3-22)}$$

The radiation coefficient and convection coefficient are then used with Equation 3-17, yielding a heat loss coefficient value of 10.39 W/m^2-K. The heat loss coefficient, U_L is then used in Equation 3-14 to solve for Q_{loss}, yielding a value of 384.42 *Watts* for the averaged receiver temperature. As was mentioned previously, the heat loss from the receiver increases as the operating temperature increases. Figure 3.4 illustrates the linear trend of the heat loss from the receiver along with the energy loss of the receiver at the averaged outlet temperature at steady-flow of 367 K.

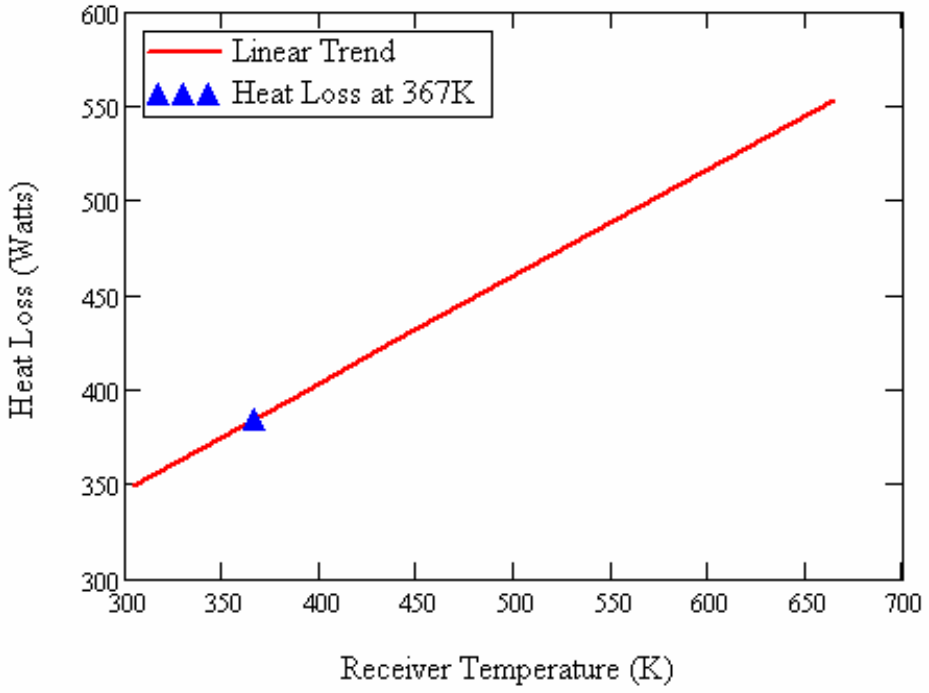

Figure 3.4: Heat loss from receiver as function of receiver temperature.

Substituting the obtained values of 11.072 *kW* and 384.42 *Watts*, for Q_{opt} and Q_{loss}, respectively, into Equation 3-12, the thermal output value of 10.68 *kW* was obtained. This is the amount of thermal energy that was being transferred from the concentrator to the receiver, which results in a collector efficiency of 95.56 percent. Figure 3.5 shows the collector efficiency for various receiver temperatures.

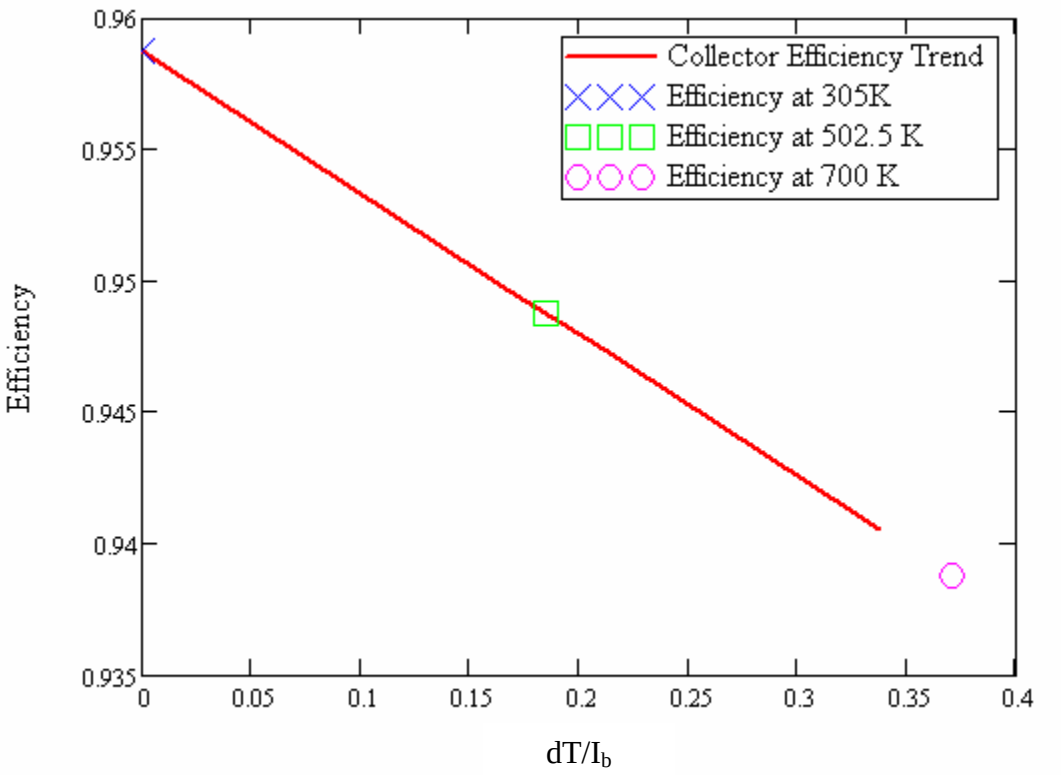

Figure 3.5: Experimental collector efficiency over a range of values of $(T_i - T_{amb})/I_b$.

3.4 Receiver

The next component of the solar thermal system to be characterized was the receiver, which acts as a boiler in a traditional Rankine cycle. Even though the receiver uses an integrated latent heat storage system, it was still subject to convective and radiation losses, as was described in the previous section. Two options were available to combat these losses; insulate the receiver or use an insulated cavity/cone allowing for the receiver to resemble that of a cavity type receiver. A comparison test was performed to determine which method of insulation would be optimal. For repeatability and consistency in the initial tests, a 1650 *Watt* electric burner was used for heating the receiver. As shown in Figure 3.6, it was found that an uninsulated receiver was only capable of achieving a temperature of 500 K, and would rapidly cool to 300 K in 40 minutes. The insulated cone allowed for a small increase in initial heating, up to 550 K,

and added longevity to the contained heat. Initially, with the insulated cone, the receiver would decrease by 100 K in the first four minutes, then slowly cool to 300 K in the following 90 minutes. When the receiver was insulated directly, it reached a maximum temperature of 700 K on the electric burner. Allowing the insulated receiver to cool, it reached 500 K in 18 minutes where it plateaued for five minutes, then began to cool again. From this plateau point, it took the insulated receiver 95 minutes to reach 300 K. In Figure 3.6 it can be seen that each of the three cases plateau around 500 K. This plateau is due to the draw salt mixture undergoing a phase change from a molten state back to a solid form.

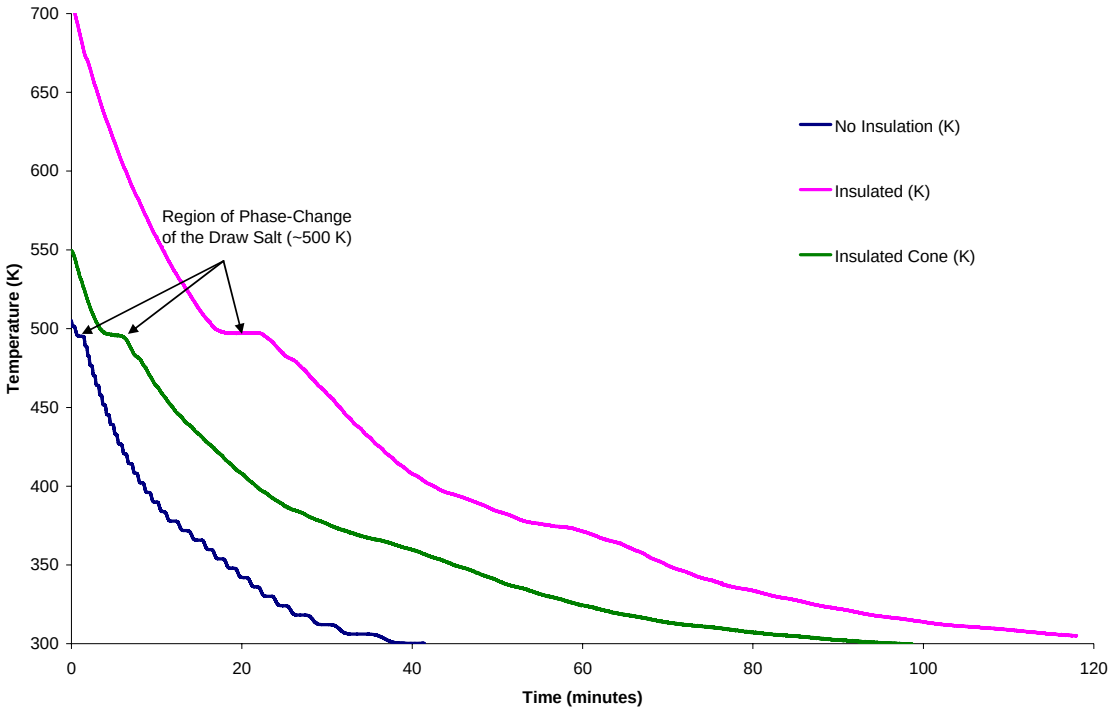

Figure 3.6: Transient Cooling of Thermal Bath at Room Temperature (~298 K)

Although the insulated cone allowed for a greater surface area of the receiver to attain the concentrated solar radiation, it permitted too great of heat transfer from the receiver to its surroundings. Thus, from these series of initial tests, it was concluded that it was best to insulate this particular receiver directly.

Once the method of insulation of the receiver was decided upon and the latent heat storage was characterized, the receiver was then placed at the focal point of the parabolic concentrator. The receiver was first subjected to a continuous heat addition test. This allowed for the experimental determination of the maximum possible temperature that the receiver could reach internally, thus giving a comparison to the theoretical maximum achievable temperature of the concentrator. As was mentioned earlier, the receiver was found to have reached a maximum temperature of 834.15 K (1041 °F), whereas the calculated maximum theoretical temperature was found to be 984.73 K (1313 °F).

In order to better characterize the receiver, a steady-flow experiment was performed. The receiver was left as an open system, and a flow-rate of 1.0 liter per minute of water, at an average inlet temperature of 300 K, was pumped through the receiver for five days. Figure 3.7 and Figure 3.8 show the thermal profiles for the receiver along with the inlet and outlet water temperatures, and the energy profile for the various days, respectively. Because of the heat transfer to the water, it was found that the receiver would only reach a fraction of the maximum achievable temperature. Also, in Figure 3.7, it shows that there is a maximum temperature that the water is capable of reaching in this steady-flow experiment, even as the temperature of the receiver increases, which is most likely due to the design of the receiver. Examination of the profiles reveals that the temperature of the system would vary due to the slightest cloud cover or variance in the tracking. The water exiting the receiver reached an average temperature of 310.6 K; which was insufficient for reaching the phase-change state of water. For this particular test, other flow rates were not utilized because of flow-rate limitations dictated by the pump being used, with 1.0 LPM being the lowest flow-rate of the particular pump, and since steam production was the goal of the system, a higher flow-rate would be of no use. Thus, for steady-flow characterization of the receiver, a flow-rate of 1.0 LPM was used.

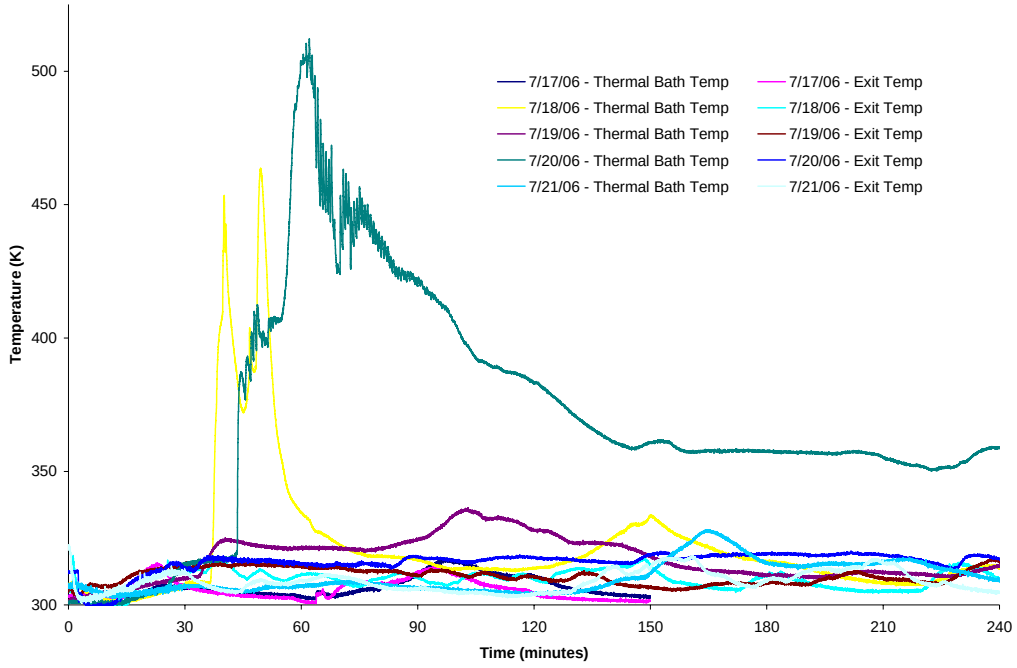

Figure 3.7: Temperature Profile for steady-flow tests at 1.0 LPM. Test performed for week of July 17 through July 21, 2006. Average inlet temperature of 300 K. Plot shows thermal draw salt bath temperature and exit water temperature.

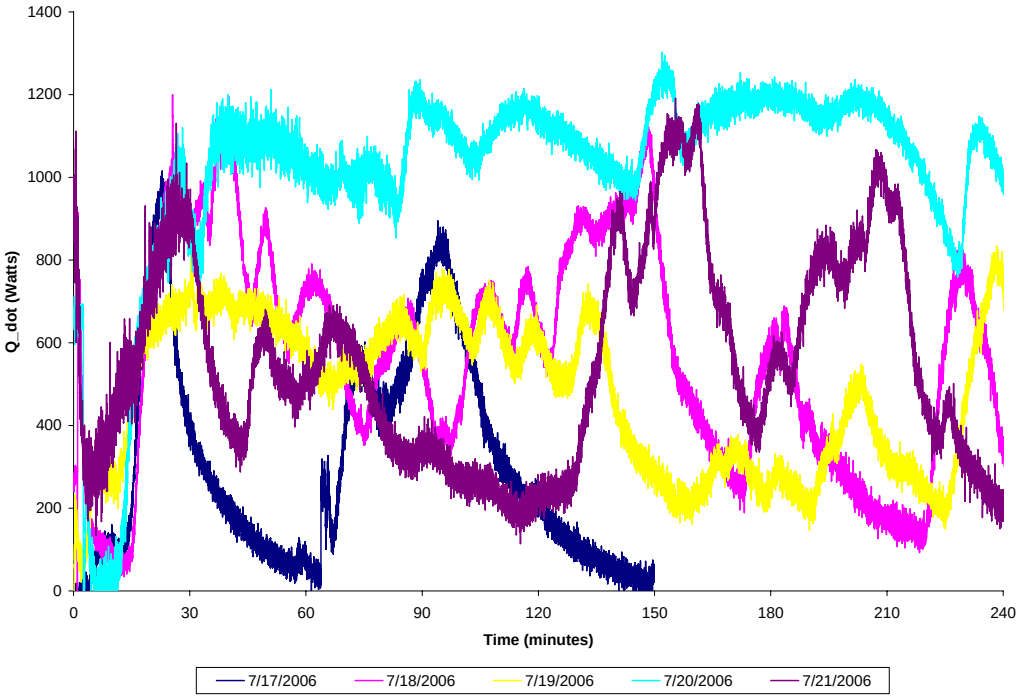

Figure 3.8: Usable energy (Q) in Watts for extended period of time over a period of five days. Date of 7/20/06 was perfectly clear skies. Other days had intermittent cloud cover, showers, or were overcast.

It was realized that an intense amount of energy would be required to generate a constant flow of steam from the receiver. As this system would be incapable of maintaining this amount of energy, it was decided to operate the system intermittently. The receiver was allowed to heat to a maximum temperature before water was pumped into the receiver where it would instantly flash to steam. The water flow would be terminated when the thermal bath of the receiver reached a minimum temperature. The system was then allowed to reheat to the maximum temperature and the cycle was repeated. The experiments performed for the intermitent system set the duty cycle, flow-rate, and maximum and minimum operating temperatures.

For the first set of tests, the receiver was heated by the concentrator to a temperature around 500 K. The pump was then turned on, and throttled back by use of a needle valve, to a flow-rate of 0.734 LPM. The water entering the receiver was at a temperature of 300 K before it was flashed to steam with an exit temperature of 450 K. In order to determine which flow rate would be best for overcoming the back pressure created by the steam, this test was repeated for the following flow rates: 1.36 LPM, 1.67 LPM, and 2.054 LPM. Figure 3.9 shows the comparison of the inlet, exit, and thermal bath temperatures for the flow-rates mentioned. It was found that a flow rate below 1.0 LPM was not enough to overcome the back pressure created by the steam to keep a flow of feed-water into the boiler, but a flow above 1.0 LPM was sufficient, as shown in Figures 3.10 and 3.11 for the flow rates of 0.734 LPM and 1.36 LPM, respectively. Figures 3.11 and 3.12 demonstrate repeatability of the experiments performed on different days. By comparison of the data between the various flow rates, and by hardware dictation, it was found that the minimum flow-rate of 1.0 LPM was optimum for steam production in our system because of the extended run time that it allowed. The system loop was closed with the addition of the steam turbine.

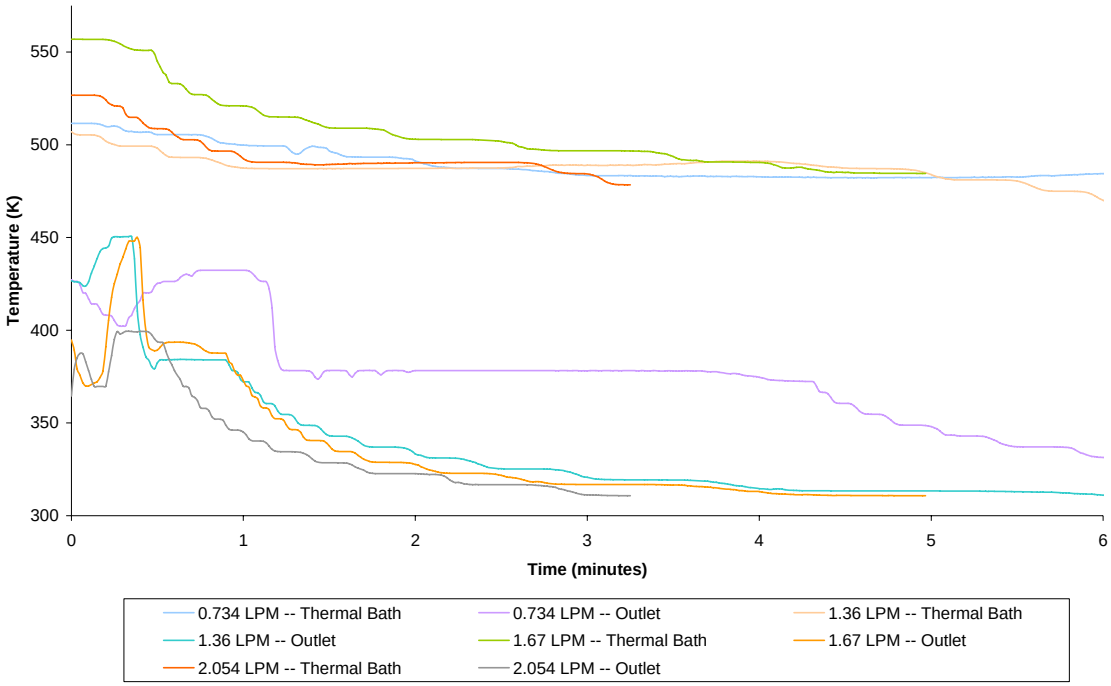

Figure 3.9: Various flow rate tests for steam flashing.

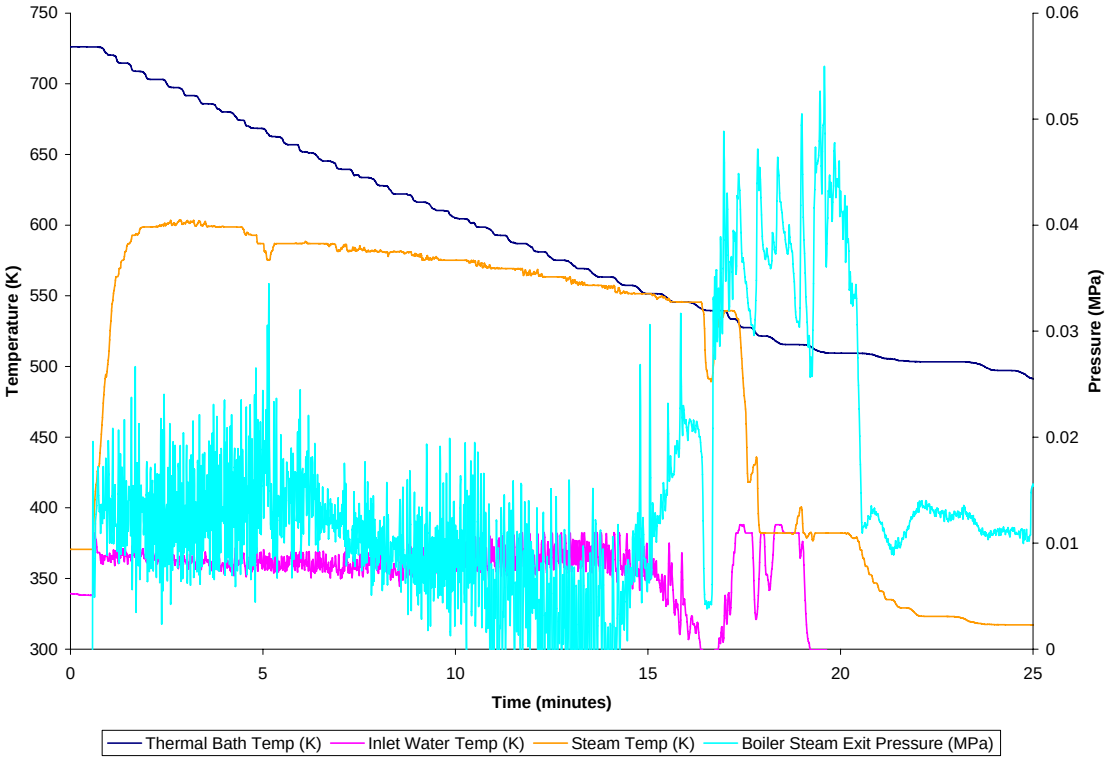

Figure 3.10: Temperature and Pressure profile for flash steam with feed water at flow rate of 0.734 LPM.

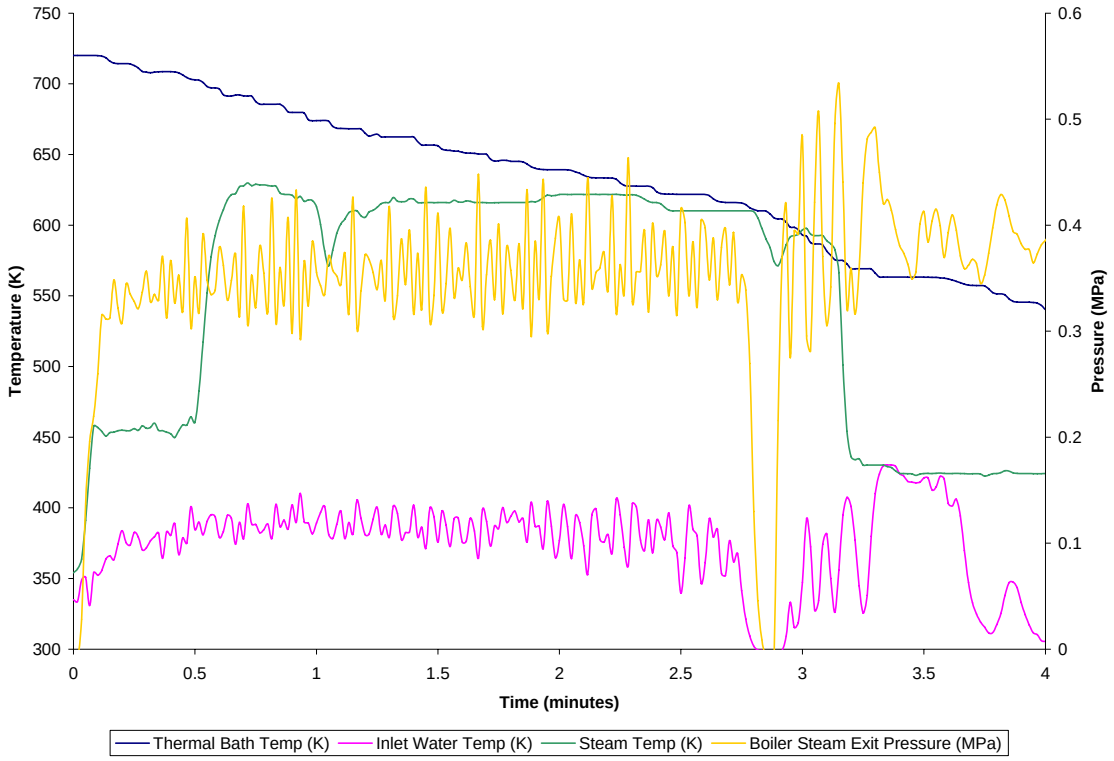

Figure 3.11: Temperature and Pressure profile for flash steam with feed water at flow rate of 1.36 LPM (Test 1)

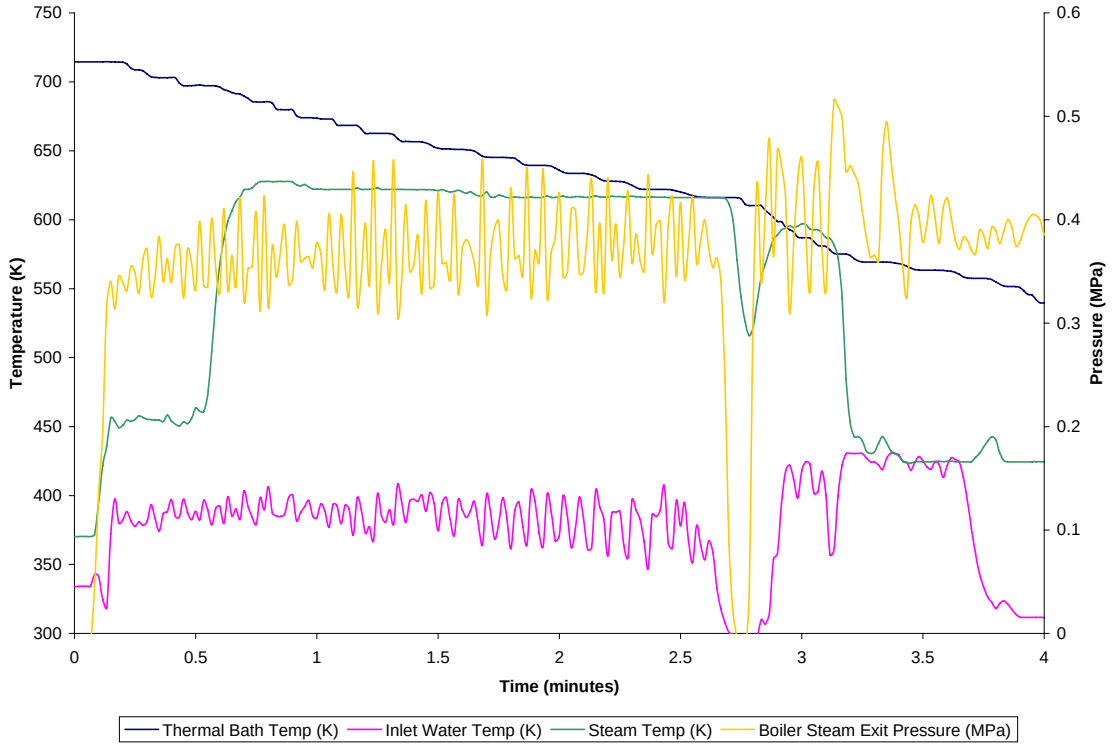

Figure 3.12: Temperature and Pressure profile for flash steam with feed water at flow rate of 1.36 LPM (Test 2). Comparable to Figure 3.11.

The first set of experiments performed with the system closed and turbine in place at a flow rate of 1.0 LPM was to determine the minimum and maximum operating temperature of the receiver. This was done to determine when to operate the pump. As was observed in previous tests, it was inadequate to operate the system while the thermal bath of the receiver was below a temperature of 533 K (500°F), which is the temperature at which the phase change of the salt occurs. Thus, the initial tests were run by heating the receiver to a temperature of 588.71 K (600°F). Once the operating temperature was reached, the pump was turned on and the water was flashed to steam, with the temperatures and pressures measured at strategic points in the system, as mentioned in section 8.2. The initial heating of the receiver took the longest due to the phase-change which the draw salt must undergo. Water was pumped into the receiver until the thermal bath reached a temperature of 533 K, at which point the pump was turned off. The receiver was then heated to a temperature of 644.26 K (700°F) and the process repeated. The experimental process was repeated at 100°F intervals until a maximum temperature of 810.93 K (1000°F) was achieved. Run time and receiver heating time was recorded along with the temperatures and pressures at the various points in the system.
Because the system is unable to generate enough energy to power a turbine continuously, the system is run intermittently. The previously mentioned tests determined the start up and shut down temperatures of 600 K and 700 K, for which the intermittent cycles will operate. Testing of the closed system was then continued to assure repeatability of results. Figure 3.13 shows a typical run cycle for 150 minutes, with a total of three runs. Figure 3.14 shows a closer inspection for the initial heating of this particular test. It clearly illustrates where the phase change of the draw salt occurs, between the 20 and 25 minute mark. This is the point where the draw salt changes from solid to a completely molten solution.

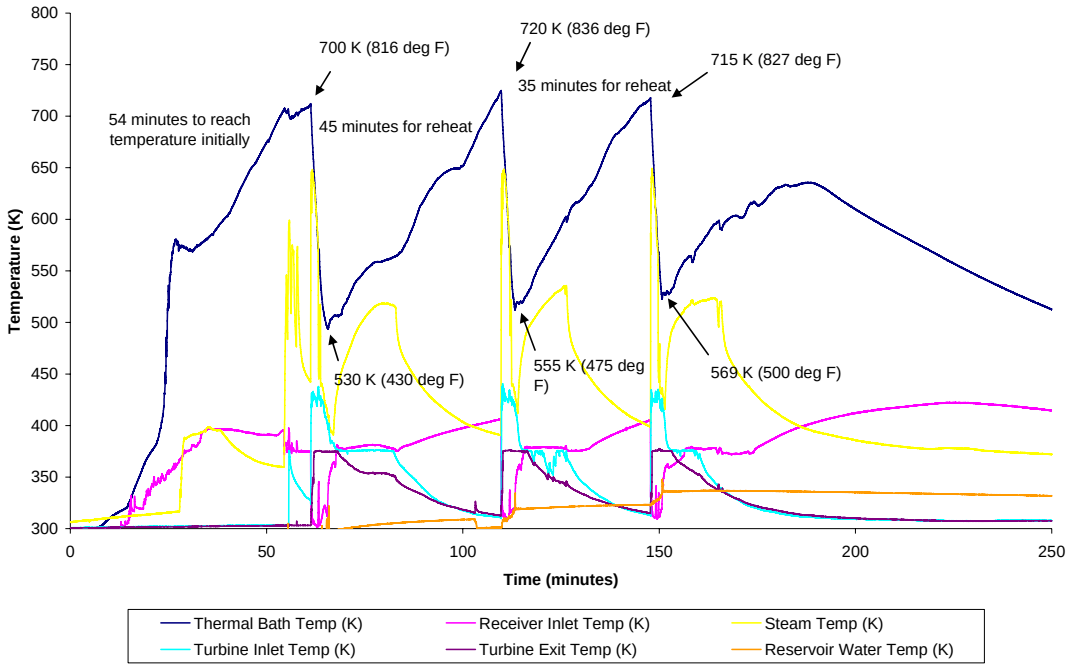

Figure 3.13: Plot of temperature profiles for the thermal bath, receiver inlet, receiver exit, turbine inlet, turbine exit, and the water supply/return reservoir. Shows repeatability of three runs in 150 minutes.

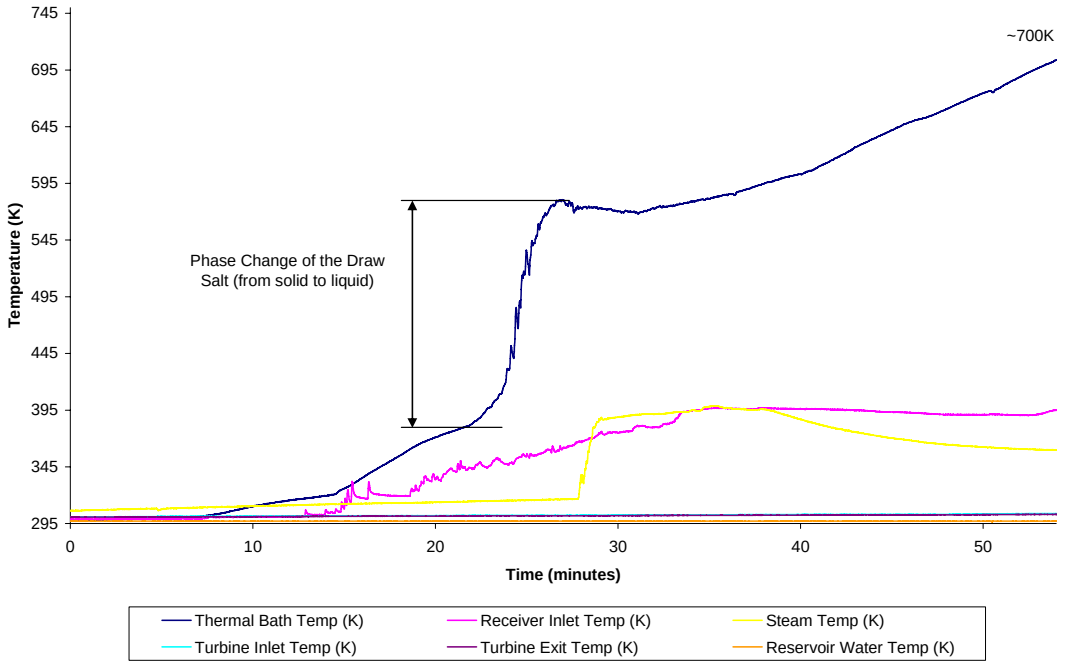

Figure 3.14: Initial heating of system from ambient to operating temperature of 700 K in 54 minutes. Shows phase change of the draw salt used in the thermal bath.

The following figure, Figure 3.15, shows a closer view of the thermal profile of the system further down the time line during the first run of the system. In this figure it is noticeable that there is a 175 K temperature drop of the steam between the exit of the receiver and the inlet of the turbine. This temperature drop is due to line losses from the long run from the boiler to the turbine and due to the line not being insulated, allowing for radiation of energy to the surroundings.

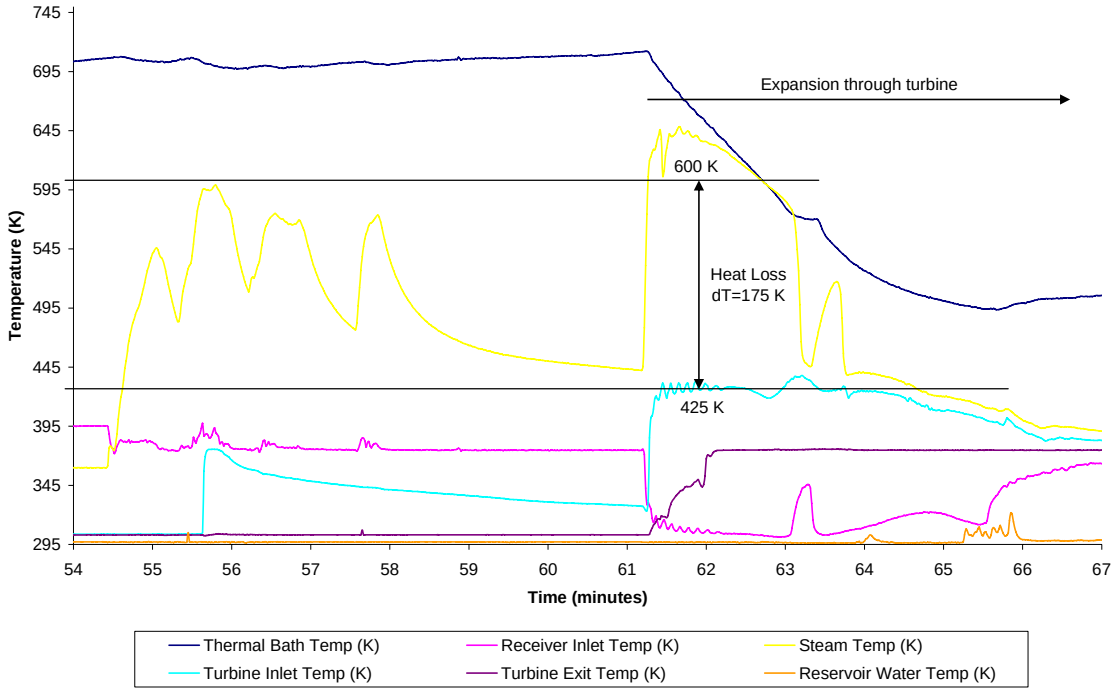

Figure 3.15: Run one of multiple tests for October 12th. Plot shows temperature drop in system as the steam is expanded through the turbine and the temperature drop of 175 K between the exit of the boiler and the inlet of the turbine.

Through the intermittent operation, the receiver is able to produce an average of 8.11 kW of usable thermal energy, with an instantaneous spike of 23.4 *kW* from when water first enters the boiler. This 23.4 *kW* spike of thermal energy is due to the instantaneous release of the stored energy from the latent heat storage of the receiver to the water, resulting in the production of superheated steam. Figure 3.16 shows the available thermal energy from the receiver for the set of three runs on October 12th. It was determined that the steam turbine had an average run time of 2.5 minutes for each of its

cycles, and for a given day of approximately 5 hours of useable sunlight, the system is capable of operating eight times. This was determined by use of the previous figures showing that the initial start-up of the system takes 60 minutes with the subsequent cycles taking only an average of 35 minutes to reach the operation temperature. By that which was shown in the experimental results, the system has a duty cycle of 6.67%, where the duty cycle is defined as the ratio of active time, 20 minutes, to the total time, 5 hours.

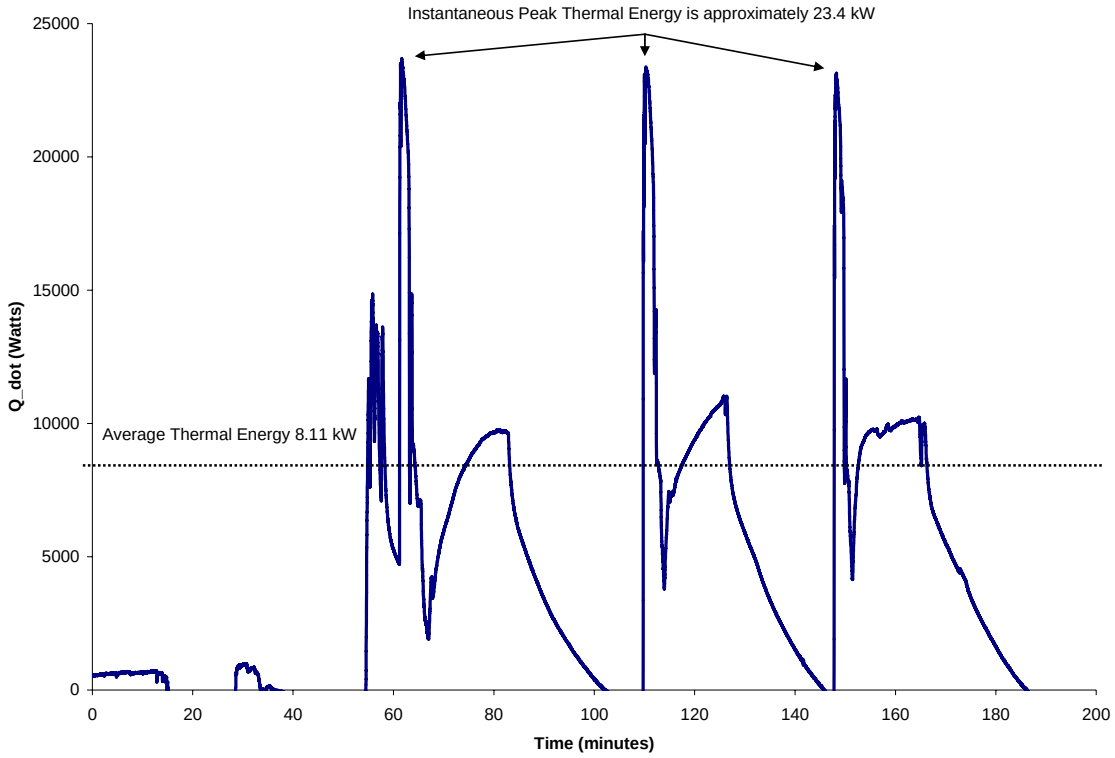

Figure 3.16: Available thermal energy during system operation on October 12th. Average thermal energy available is 8.11 kW with peaks at 23.4 kW for flash steam operation.

3.4.1 Boiler Efficiency

Since the receiver of the solar thermal system being presented in this work is designed to resemble and operate as a boiler, the efficiency of the receiver is calculated in the same fashion. In calculating boiler efficiency, there are two different methods; direct and indirect. The direct method for calculating boiler efficiency is defined as the usable heat from the boiler compared to the energy being put into the boiler.

$$\eta_{boiler} = \frac{Q_{output}}{Q_{input}} \qquad \textbf{(3-23)}$$

For steady flow through the boiler, Q_{output}, the usable heat output from the boiler, was found to be approximately 1 *kW*, and the power input of the boiler, Q_{input}, was 11.072 *kW*. By the direct method for determining boiler efficiency, the boiler was calculated to be 9.032 percent efficient. The indirect method, on the other hand, determines the boiler efficiency by the sum of the major losses from the boiler to the energy input of the boiler and is defined as

$$\eta_{boiler\_indirect} = 1 - \frac{Q_{losses}}{Q_{input}} \qquad \textbf{(3-24)}$$

where the sum of the major losses, Q_{losses}, was determined to be 349.37 *Watts*. This results in a boiler efficiency of about 96.85 percent. Although the indirect method for determining boiler efficiency provides a better understanding of how the losses effect the efficiency, it does not take in account other losses internally in the boiler. Thus, for this work, the boiler efficiency of 9.032 percent, calculated by the direct method, will be used because it is an actual comparison of the usable thermal energy to that of the energy input into the boiler. [32]

3.5 Turbine Efficiency

As the turbine that was used was an impulse turbine, it was already known that it would have a lower efficiency than the multistage turbines used in more advanced power systems. Short-term transient start-up or shutdown of the turbine will not be included for the calculations, only the steady operating period of time. In order to model the turbine for calculation purposes, it was assumed that the process through the turbine was a steady-state, steady-flow process.

The mass flow of steam into the turbine was first solved for by using the turbine inlet pressure and temperature of 480.537 *kPa* and 431.46 K, respectively. The steam turbine had a nozzle diameter of 0.229 *cm* and is modeled as that of a free jet. The flow was found to be choked, with $P_{exit} / P_{turbine}$ being equal to 0.211. The mass flow rate of steam through the nozzle into the turbine was then calculated to be $4.873 \times 10^{-3} kg / s$. The full calculations for the mass flow rate of the steam into the turbine are located in Appendix J.

The heat transfer from the turbine, $\dot{Q}$, was calculated to be 410.871 *Watts* with the work from the turbine being 650.818 *Watts* by use of Equation 1-44. In order to determine the efficiency of the turbine, however, it must be compared to the theoretical performance of the same turbine under ideal conditions. The ideal process for a steam turbine is considered to be a reversible adiabatic process between the inlet state of the turbine and its exhaust pressure. Thus, by comparing the turbine discussed in this work, under its actual operating conditions, to that of the same steam turbine under ideal conditions, we find that our steam turbine has a thermal efficiency of 31.56 percent. The full calculations for this are found in Appendix K.

3.6 Turbine/Gear-Train Analysis

With the gear-train attached to the steam turbine, tests were performed to determine the resulting shaft (mechanical) power of the gear train. The tests were performed by use of a Prony Brake with a 152.4 *mm* (6 in) diameter flywheel coupled to the output shaft of the gear-train with the turbine inlet at a steam pressure of 344.74 *kPa*. It was found that on average, the output shaft power of the turbine/gear-train was approximately 1.34 *kW* with an average shaft speed of 300 RPM. Table 3.1 shows the results from the tests, yielding shaft speed, torque, and shaft power.

Table 3.1: Test results for mechanical power determination of steam turbine/gear-train output shaft.

Force (ounces)	RPM	Torque (ounce-inch)	Torque (N-m)	Torque (in-lbs)	HP	Watts
8	20	24	0.1695	1.500	0.091	68.15
8	95	24	0.1695	1.500	0.434	323.72
8	110	24	0.1695	1.500	0.503	374.84
8	125	24	0.1695	1.500	0.571	425.95
8	300	24	0.1695	1.500	1.371	1022.28
8	450	24	0.1695	1.500	2.056	1533.43
12	200	36	0.2542	2.250	1.371	1022.28
12	325	36	0.2542	2.250	2.228	1661.21
12	350	36	0.2542	2.250	2.399	1789.00
12	200	36	0.2542	2.250	1.371	1022.28
16	50	48	0.3390	3.000	0.457	340.76
16	75	48	0.3390	3.000	0.685	511.14
16	95	48	0.3390	3.000	0.868	647.45

3.7 Analysis of the Rankine Cycle

The closed system discussed here is a Rankine Cycle, similar to that used in large scale power plants. In analyzing the Rankine cycle, the efficiency is dependent upon the average temperature at which heat is supplied and the average temperature at which heat is rejected. Any changes that increase the average temperature at which heat is supplied or decrease the average temperature at which heat is rejected will increase the overall Rankine cycle efficiency. For the calculations, changes in the kinetic and potential energies from one point in the cycle to another are neglected, which is a reasonable assumption for the actual cycle.

Temperature and pressure measurements were acquired from the inlet and outlet of each of the components of the cycle. Table 3.2 gives the values collected for the components, along with the entropy value for the given temperature and pressure.

Table 3.2: Inlet and Outlet temperature, pressure, and entropy values for the various components of the system.

Point	Pressures (kPa)	Temperatures (deg C)	Entropy (s) (kJ/kg-C)
Pump Inlet	101.325	23.84	0.3508
Pump Exit	963.17	23.84	0.3506
Boiler Inlet	790.801	35.72	0.5144
Boiler Exit	480.537	371.63	7.7238
Turbine Inlet	446.063	158.31	6.9149
Turbine Exit	101.325	101.85	7.3655

Figure 3.17 shows the temperature-entropy diagram for the concentrated solar thermal system discussed in this work. The point representing the exit of the boiler, 3_{boiler}, is high in the superheated region on the diagram. However, there is a large amount of heat which is lost between the boiler exit and the inlet of the turbine, depicted by point $3_{turbine}$. This loss of work is due to the temperature decrease (on average 200 K) between the boiler and the turbine, which results in the jump from the higher isobar to the lower isobar.

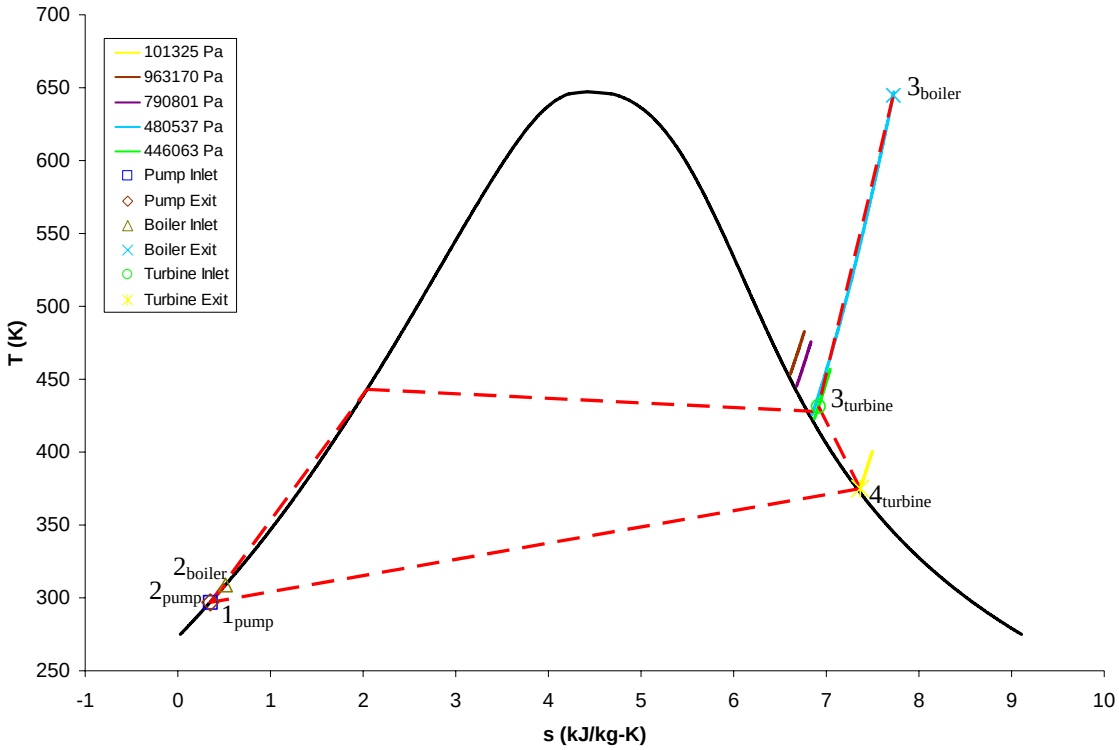

Figure 3.17: Temperature-Entropy diagram for the concentrated solar thermal system discussed in this work.

It is evident that the Rankine cycle has a lower efficiency than a Carnot cycle with the same maximum and minimum temperatures. For this system, with a maximum and minimum temperature of 297 K and 431.5 K, respectively, the Carnot efficiency is found to be 31.17 percent, which is the maximum achievable thermal efficiency. However, since this system operated on the Rankine cycle, the efficiency is much lower at an efficiency of about 3.195 percent, which is 10.252 percent of the Carnot efficiency. The full calculations for how these values were reached are located in Appendix L.

3.8 Generator and Energy Conversion Efficiency

As was mentioned in Chapter 2, the generator used in conjunction with the solar thermal system discussed in this work was a 443541-10Amp Permanent Magnet DC Generator from Windestream Power LLC. As is the case with most generators, the efficiency was found to increase as the generator speed increases. A sample of the load testing on the generator is shown in Table 3.3.

Table 3.3: Sample of loads tested on generator and the resulting voltage and power.

Resistance (Ohms)	Voltage	Current (Amps)	Power (Watts)
0.5	6.7	13.40	89.78
0.6	11.5	19.17	220.42
1.3	12	9.23	110.77

From the tests, it was found that the maximum electrical power generation, from the particular set-up is approximately 220 *Watts*, with an average electrical power generation of 100 *Watts*. By comparing these electrical power generation values with that of the shaft output power of the steam turbine, as discussed in section 3.6, for the maximum power generation of 220 *Watts*, being matched with the maximum shaft power, 1.34 *kW*, of the steam turbine, the generator was found to have an efficiency of 16.42%.

The total energy conversion efficiency of the system was also solved for. The total energy conversion efficiency was found by comparing the amount of electrical

power produced to that of the total amount of solar energy being collected. The total amount of solar energy being collected is equal to the amount of beam solar insolation incident on the concentrator, which is a total of 11.36 kW. By using Equation 3-25, it was found that the total energy conversion efficiency of the system, $\eta_{conversion}$, was 1.94 percent.

$$\eta_{conversion} = \frac{\text{Electric Power Output}}{\text{Solar Energy Input}} \qquad \textbf{(3-25)}$$

CHAPTER 4

CONCLUSIONS

4.1 Introduction

The main objective of the current work was to construct a concentrating solar thermal system which utilizes a Rankine cycle for electrical power generation, and evaluate the overall efficiency of the system. A brief summary of the results obtained from the work, along with recommendations for future work are given in the following sections of this chapter.

4.2 Solar Calculations

- When describing the position of the sun relative to that of the collector, it can be said that the sun moves along the azimuth at a rate of 15 degrees per hour with solar noon being based as the time that the sun is positioned exactly due south.

- Because of the characteristics of the concentrating solar collector, only beam radiation is usable, which on average, is 100 W/m^2 less than the total beam insolation available in Tallahassee, FL.

4.3 Trackers

- Photo-sensing tracking modules for controlling dish position does an efficient job at visually tracking the sun throughout the day, however, long periods of cloud cover become problematic for the trackers to keep the concentrator oriented properly.

4.4 Solar Concentrator

- Concentrator has an aperture area of 10.507 m^2 and a geometric concentration ratio of 96.

- Maximum theoretical temperature at focal region of concentrator is 984.732 K (1313ºF).

- Maximum achieved temperature in focal region of concentrator (internal temperature of receiver) was 834.15 K (1041ºF).

- Energy incident on collector for October 12th (date calculations where performed for) is approximately 1064 W/m^2 which is equivalent to a total of 11.18 kW.

- Collector (concentrator and receiver) is found to have an efficiency of approximately 95.56 percent.

4.5 Receiver / Boiler

- Optical energy absorbed by the receiver was found to be approximately 11.068 kW.

- Major losses from the boiler calculated to be 349.37 Watts.

- Direct method of calculating boiler efficiency yields an efficiency of 9.032 percent; indirect method yields 96.85 percent efficiency.

- Boiler not optimized to provide high pressure steam or continuous steam flow.

4.6 Steam Turbine

- Mass flow rate of steam through nozzle in to turbine is $4.873 \times 10^{-3} kg/s$.

- Efficiency of the steam turbine was calculated to be 49.98 percent for current operating conditions.

- Steam turbine/gear-train has a mechanical shaft output power of 1.34 *kW*.

4.7 Generator

- Maximum power production seen was 220 *Watts* with a load of 0.6-ohms.

- Average power production approximately 100 *Watts.*

- Turbine Efficiency (Electric Power Output / Mechanical Shaft Power) was 16.42% for the maximum power of 220 *Watts*.

4.8 Cycle

- Large temperature drop ($\Delta T = 175$ K) between boiler exit and turbine inlet.

- Carnot efficiency of the system calculated to be 31.17 percent.

- Rankine cycle efficiency of the system is 3.195 percent; 10.252 percent of the Carnot efficiency.

- Energy conversion efficiency from incoming solar energy to electric energy was 1.94%.

- Overall efficiency ($\eta_{collector} \times \eta_{pump} \times \eta_{turbine} \times \eta_{generator}$) was 7.30%.

4.9 Future Work

- Use a more optimized system for tracking, such as a program written in labVIEW to calculated the position of the sun along with potentiometers on each axis of the concentrator for live feed back as to where the system is located.

- Resurface the concentrator. Use a better material for the reflective coating than aluminized mylar.

- Redesign of the receiver to a cavity type receiver to optimize amount of energy absorbed and to minimize losses. Also, utilize a different type of internal boiler design to maximize heat transfer to the working fluid and to allow for extended periods of operation.

- Along with receiver redesign, optimize receiver support structure and collector to support weight of receiver with added weight of turbine and for ease of installation and maintenance of the receiver.

- Relocate turbine to receiver to minimize losses between the boiler and the receiver.

- Use a turbine with multiple stages to utilize more energy from the steam before returning to reservoir.

- Integrate in control and data acquisition program control for start-up / shut-down of pump.

- Investigate various steam engines/turbines for optimization for use with the system discussed in this work.

- Utilize the solar thermal system for tri-generation.

- Design and fabricate new concentrator, possibly out of composite materials, to make lighter and more durable.

APPENDIX A

RABL'S THEOREM

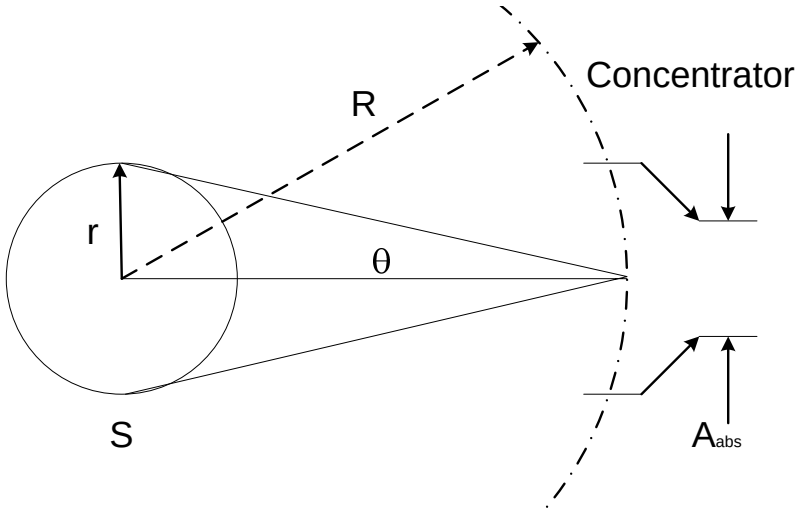

Figure A.1: Radiation Transfer from source S through aperture A of concentrator to absorber A_{abs}. [13]

In order to prove his theorem, Rabl set up a thought-experiment (shown in Figure A.1). The experiment is an isotropically radiating sphere of radius *r* surrounded by a sphere of radius *R* which has an aperture of area *A* that admits light to a concentrator behind *A*. The concentrator focuses the light entering through *A* onto a smaller area A_{abs}, corresponding to a theoretical concentration of

$$CR_{theoretical} = \frac{A}{A_{absorber}} \qquad \textbf{(A-1)}$$

It is assumed that the concentrator focuses all light entering *A* within the half-angle, θ, of the normal to *A*. If A/R^2 is small, the light from the source, *S*, incident on *A*, is uniformly distributed over all angles between 0 and θ, and there is no light from *S*, outside of θ. Extraneous radiation is eliminated by assuming black walls at absolute zero temperature. The procedure is now to calculate the rates of emission of radiant energy by the source

and the absorber, and then to note that the radiant transfer between the source and absorber must be equal if they are both at the same temperature. The source emits the radiant power

$$Q_s = 4\pi r^2 \sigma T_s^4 \qquad \textbf{(A-2)}$$

of which a fraction

$$F_{S\to A} = \frac{A}{4\pi R^2} \qquad \textbf{(A-3)}$$

hits the aperture. With the assumed perfect concentrator optics, no radiation is lost between the aperture and the absorber. Thus, the power radiated from the source to the absorber is

$$Q_{S\to abs} = Q_S F_{S\to A} = A\frac{r^2}{R^2}\sigma T_S^4 \qquad \textbf{(A-4)}$$

The absorber radiates an amount

$$Q_{abs} = A_{abs}\sigma T_{abs}^4 \qquad \textbf{(A-5)}$$

and the fraction of this radiation, $E_{abs\to S}$, which reaches the source cannot exceed unity. Hence, the radiative power transfer from the absorber to the source is

$$Q_{abs\to S} = E_{abs\to S} A_{abs}\sigma T_{abs}^4 \qquad \textbf{(A-6)}$$

with

$$E_{abs\to S} \le 1 \qquad \textbf{(A-7)}$$

If the source and the absorber are at the same temperature, the second law of thermodynamics requires that there cannot be any net heat transfer between these bodies. Thus, if we set $T_{abs} = T_S$, it follows that

$$Q_{S \to abs} = Q_{abs \to S} \qquad \textbf{(A-8)}$$

Therefore,

$$A\frac{r^2}{R^2} = E_{abs \to S} A_{abs} \qquad \textbf{(A-9)}$$

from which we deduce that the theoretical concentration satisfies

$$CR_{theoretical} = \frac{A}{A_{abs}} = \frac{R^2}{r^2} E_{abs \to S} = \frac{E_{abs \to S}}{\sin^2(\theta)} \qquad \textbf{(A-10)}$$

Since the maximum possible value of $E_{abs \to S}$ is unity, the concentration must satisfy

$$CR_{theoretical} \leq \frac{1}{\sin^2(\theta)} \qquad \textbf{(A-11)}$$

For collectors in which the equal sign holds are called ideal collectors.
[3]

APPENDIX B

SOLAR ANGLE AND INSOLATION CALCULATIONS

Solar Calculations

Calculations performed for Tallahassee, FL (located in Eastern Time Zone w/Daylight Savings) Where L is the local latitude, l_{local} is the local longitude, and L_{st} is the standard meridian for the local time zont.

$L := 30.38\,deg$ $\quad l_{local} := 84.37\,deg$ $\quad L_{st} := 75\,deg$

Julian Day (n): $n := 1, 2 .. 365$

Declination

$$\delta_s(n) := 23.45\,deg \cdot \sin\left[\left(360 \cdot \frac{284 + n}{365}\right) deg\right]$$

$\delta_s(n) =$

-23.012 deg

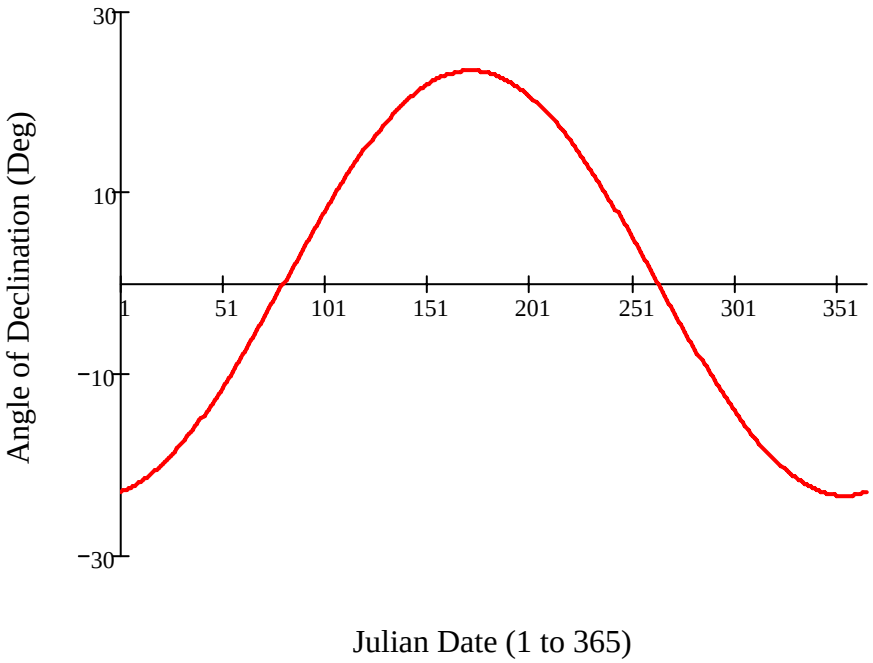

Figure B.1: Variation of solar declination dependant on time of year.

At solar noon, $h_s := 0$

The solar altitude is thus,

$$\sin(\alpha) = \cos(L)\cdot\cos(\delta_s)\cdot\cos(h_s) + \sin(L)\cdot\sin(\delta_s)$$

$$\alpha(n) := \operatorname{asin}\left(\cos(L)\cdot\cos(\delta_s(n))\cdot\cos(h_s) + \sin(L)\cdot\sin(\delta_s(n))\right)$$

$\alpha(n) =$

36.608 deg

And the solar azimuth angle is,

$$\alpha_s(n) := \operatorname{asin}\left(\cos(\delta_s(n))\cdot\frac{\sin(h_s)}{\cos(\alpha(n))}\right)$$

$\alpha_s(n) =$

0

At solar noon, the altitude can also be solved by an alternative method,

$$\alpha(n) := 90\text{deg} - (L - \delta_s(n))$$

$\alpha(n) =$

36.608 deg

Sunrise / Sunset Angle

$$h_{ss}(n) := \operatorname{acos}\left(-\tan(L)\cdot\tan(\delta_s(n))\right)$$

$h_{ss}(n) =$

75.583 deg

Note: Sunset and Sunrise angle are the same (+/-)

Time from Solar Noon

$$\text{time\_from\_solar\_noon}(n) := h_{ss}(n)\cdot 4\frac{\text{min}}{\text{deg}}$$

time_from_solar_noon(n)

302.332 min

time_from_solar_noon(n) =

	0
0	"5:2:19.891"

hhmmss

Sunrise will be 12:00 Solar Noon minus the 'time_from_solar_noon(n)' for the given day.
Sunset will be 12:00 Solar Noon plus the 'time_from_solar_noon(n)' for the given day.

Use Equation of Time to convert the Solar Times for sunrise and sunset to local times.

$$B(n) := 360\,deg \cdot \frac{n - 81}{364}$$

B(n) =
-79.121 deg

$$ET(n) := (9.87 \cdot \sin(2 \cdot B(n)) - 7.53 \cdot \cos(B(n)) - 1.5 \cdot \sin(B(n)))\,min$$

ET(n) =
-3.607 mir

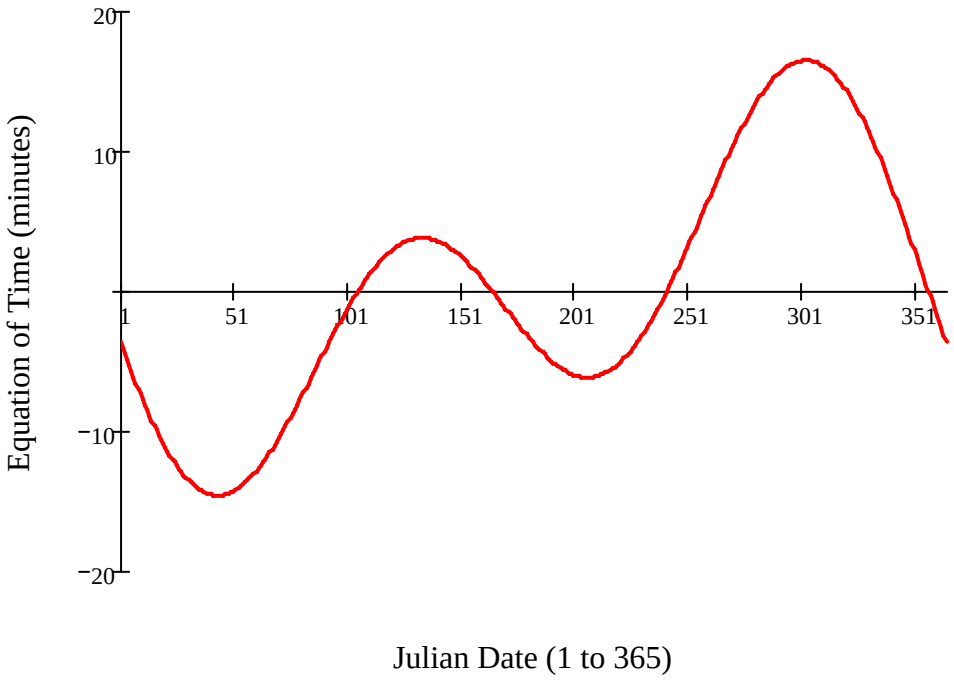

Figure B.2: Equation of Time, in minutes, as a function of the time of year.

Local Standard Time (LST)

$$LST = Solar\_Time - ET - 4\cdot\left(L_{st} - l_{local}\right)$$

$$\xi = -ET - 4\cdot\left(L_{st} - l_{local}\right)$$

$\xi(n) := -ET(n) - 4(75 - 84.37)$ mir

$\xi(n) =$

41.087 mir

$$LST = Solar\_Time + \xi(n)$$

Note: The sunrise and sunset times are calculted when the center of the sun is at the horizon, thus to the naked eye, the sunrise and sunset appears to differ from the apparent times.

The length of the day can also be calculated by the following method:

$$day\_length(n) := \frac{2\cdot h_{ss}(n)}{15\,\frac{deg}{hr}}$$

$day\_length(n) =$ "10:4:39.782" hhmmss

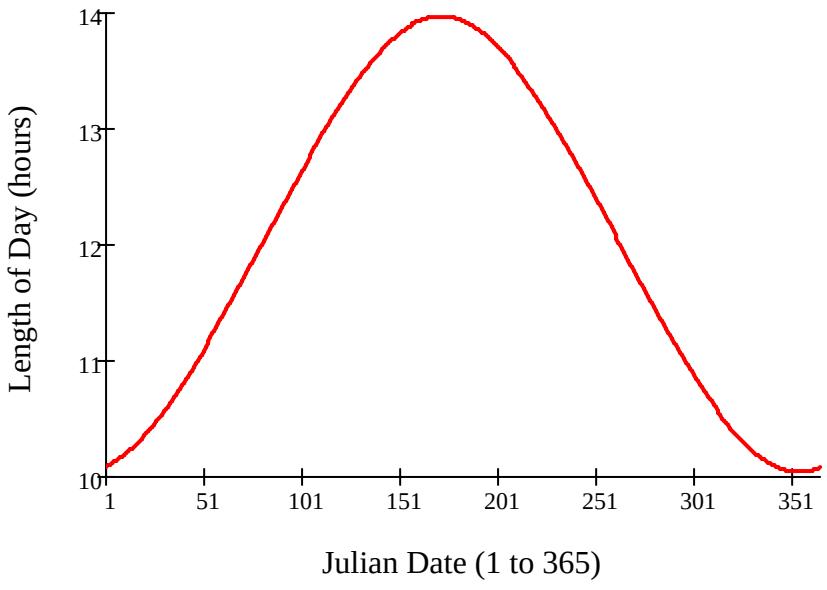

Figure B.3: Lenght of the day, in hours, as a function of the date.

The instantaneous solar radiation on an object in Tallahassee at 12:00 noon.

The angle of incidence, *i*, of the beam radiation on a tilted surface, the panel azimuth angle, α_W, and the panel tilt angle, β:

Panel tilt angle is same as the solar altitude angle: $\beta(n) := \alpha(n)$

Panel azimuth angle is same as solar azimuth angle: $\alpha_W(n) := \alpha_S(n)$

$$\cos(i) = \cos(\alpha(n))\cdot\cos(\alpha_S(n) - \alpha_W(n))\cdot\sin(\beta(n)) + \sin(\alpha(n))\cdot\cos(\beta(n))$$

$$i(n) := \operatorname{acos}(\cos(\alpha(n))\cdot\cos(\alpha_S(n) - \alpha_W(n))\cdot\sin(\beta(n)) + \sin(\alpha(n))\cdot\cos(\beta(n)))$$

$i(n) =$

16.783 deg

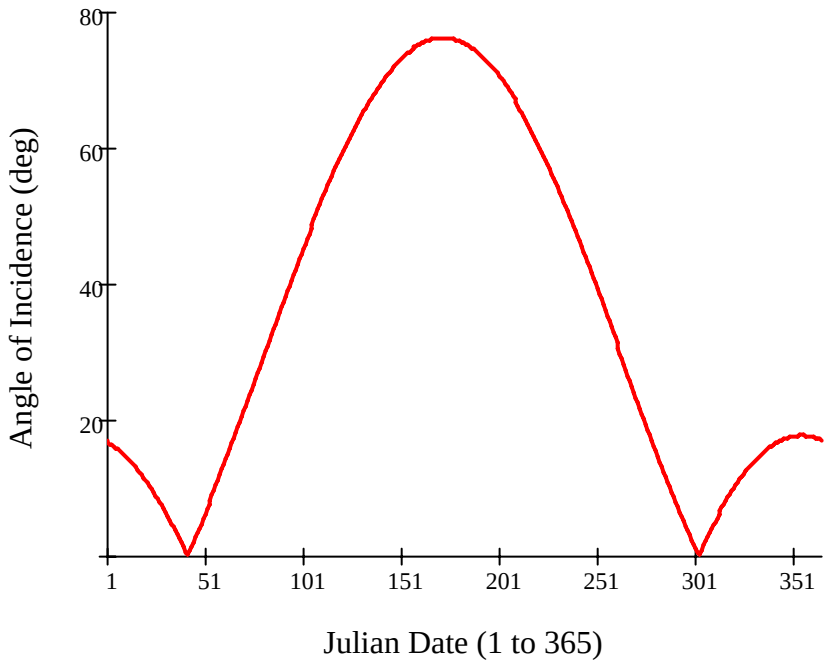

Figure B.4: Variation of the angle of incidence as a function of the date.

Extraterrestrail Solar Radiation

D -- The distance between the sun and the earth
D_0 -- The mean earth-sun distance (1.496×10^{11}m)
I_0 -- The solar constant as given by NASA (1353 W/m^2)

$I_0 := 1353 \frac{W}{m^2}$ $D_0 := 1.496 \cdot 10^{11} m$

The extraterrestrial solar radiation varies by the inverse square law: $I = I_0 \cdot \left(\frac{D_0}{D} \right)^2$

Where $(D_0/D)^2$ is approximated by:

$$\left(\frac{D_0}{D} \right)^2 = 1.00011 + 0.034221 \cos(x) + 0.00128 \sin(x) + 0.000719 \cos(2 \cdot x) + 0.000077 \sin(2 \cdot x)$$

where $x = 360 \cdot \frac{n - 1}{365} deg$

Thus, solving for the extraterrstrial solar radiation:

$x(n) := 360 \cdot \frac{n - 1}{365} deg$

for calculation purposes, set $(D_0/D)^2$ equal to D_{factor}

$$D_{factor}(n) := 1.00011 + 0.034221 \cos(x(n)) + 0.00128 \sin(x(n)) + 0.000719 \cos(2 \cdot x(n)) + 0.000077 \sin(2 \cdot x(n))$$

The extraterrestrial radiation is thus:

$I(n) := I_0 \cdot D_{factor}(n)$ $I(n) =$ $1.4 \cdot 10^3$ $\frac{W}{m^2}$

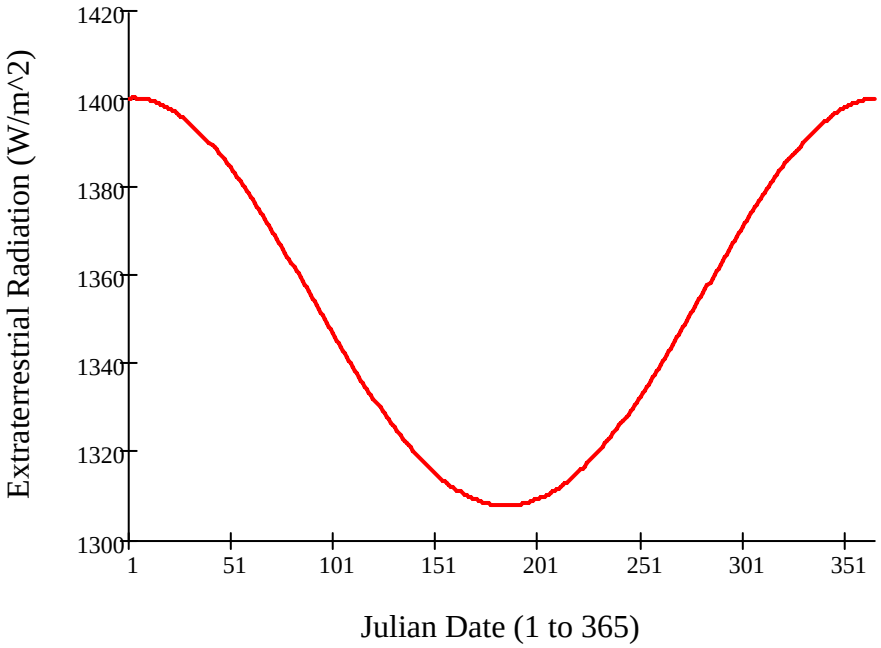

Figure B.5: Variation of extraterrestrial solar radiation with time of year.

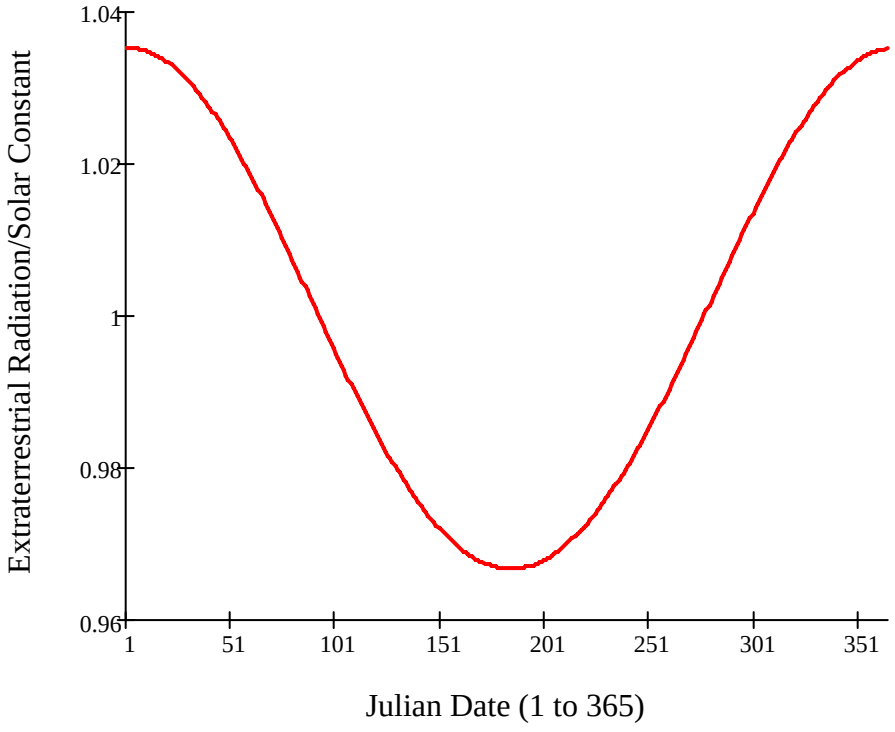

Figure B.6: Effect of the time of year of extraterrestraial radiation to the nominal solar constant

Graph above shows the effect of the time of year on the radio of extraterrestrial radiation to the nominal solar constant.

Terrestrial Solar Radiation

The Atmospheric Extinction of Solar Radiation

Clearness number is assumed as: $C_n := 1$

k value is averaged from values found in Table 1.1 (from Chapter 1). $k := 0.172$

$$I_{b\_N}(n) := C_n \cdot I(n) \cdot e^{\frac{-k}{\sin(\alpha(n))}}$$

$I_{b\_N}(n) =$ 1.05·10³ $\frac{W}{m^2}$

Beam Radiation on the Collector

$$I_{b\_c}(n) := I_{b\_N}(n) \cdot \cos(i(n))$$

$I_{b\_c}(n) =$ 1.005·10³ $\frac{W}{m^2}$

Sky Diffuse Radiation on the Collector

C_{month_avg} is found in Table 1.1 (from Chapter 1), the average is used for these calculations.

$C_{month\_avg} := 0.1$

$$I_{d\_c}(n) := C_{month\_avg} \cdot I_{b\_N}(n) \cos\left(\frac{\beta(n)}{2}\right)^2$$

$I_{d\_c}(n) =$ 94.602 $\frac{W}{m^2}$

Ground reflected radiation is neglected because the system is a concentrating collector located 6 feet off the ground. Therefore, the total insolation on the collector is:

$$I_c(n) := I_{b\_c}(n) + I_{d\_c}(n)$$

$I_c(n) =$ 1.099·10³ $\frac{W}{m^2}$

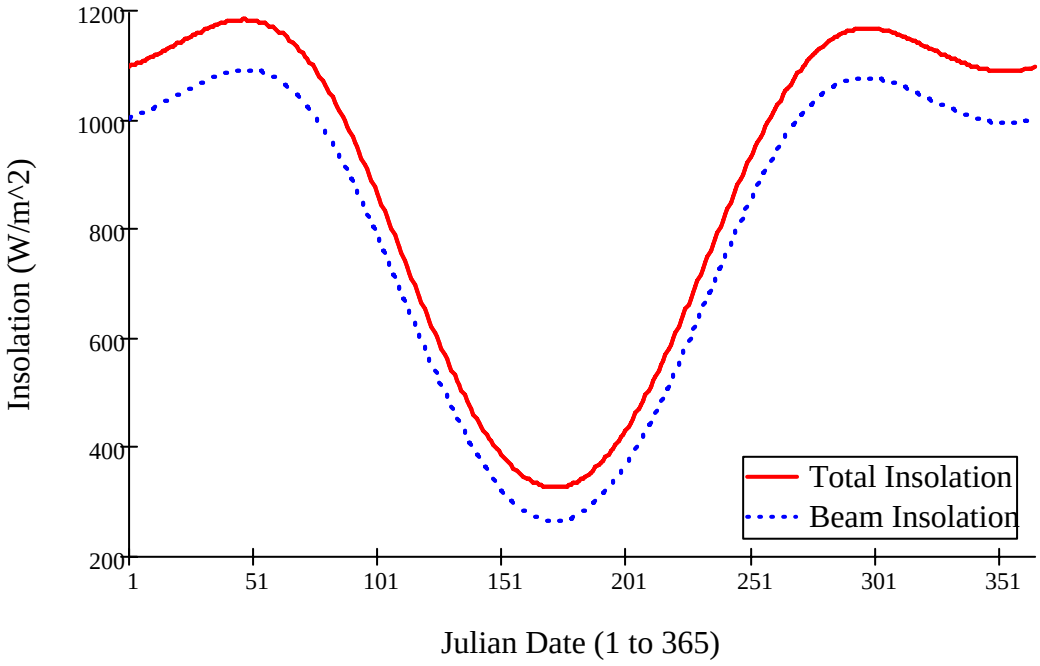

Figure B.7: Total Insolation compared to the Beam Insolation incident on the collector.

APPENDIX C

SOLAR CALCULATIONS FOR OCTOBER 12th

Solar Calculations (for Particular Day of October 12th)

Calculations performed for Tallahassee, FL (located in Eastern Time Zone w/Daylight Savings) Where L is the local latitude, l_{local} is the local longitude, and L_{st} is the standard meridian for the local time zont.

$L := 30.38\,deg$ $\quad l_{local} := 84.37\,deg$ $\quad L_{st} := 75\,deg$

Julian Day (n): $n := 285$

Angle of Declination

$$\delta_s(n) := 23.45\,deg \cdot \sin\left[\left(360 \cdot \frac{284 + n}{365}\right) deg\right]$$

$$\delta_s(n) = -8.482\,deg$$

At solar noon, $h_s := 0$

The solar altitude is thus,

$$\sin(\alpha) = \cos(L)\cdot\cos(\delta_s)\cdot\cos(h_s) + \sin(L)\cdot\sin(\delta_s)$$

$$\alpha(n) := \operatorname{asin}\left(\cos(L)\cdot\cos(\delta_s(n))\cdot\cos(h_s) + \sin(L)\cdot\sin(\delta_s(n))\right)$$

$$\alpha(n) = 51.138\,deg$$

And the solar azimuth angle is,

$$\alpha_s(n) := \operatorname{asin}\left(\cos(\delta_s(n))\cdot\frac{\sin(h_s)}{\cos(\alpha(n))}\right)$$

$$\alpha_s(n) = 0$$

Sunrise / Sunset Angle

$$h_{ss}(n) := \operatorname{acos}\left(-\tan(L)\cdot\tan\left(\delta_s(n)\right)\right)$$

$$h_{ss}(n) = 84.984\,\text{deg}$$

Note: Sunset and Sunrise angle are the same (+/-)

Time from Solar Noon

$$\text{time\_from\_solar\_noon}(n) := h_{ss}(n)\cdot 4\,\frac{\text{min}}{\text{deg}}$$

$$\text{time\_from\_solar\_noon}(n) = 339.938\,\text{min}$$

$$\text{time\_from\_solar\_noon}(n) = \text{"5:39:56.27"}\,\text{hhmmss}$$

Sunrise will be 12:00 Solar Noon minus the 'time_from_solar_noon(n)' for the given day.
Sunset will be 12:00 Solar Noon plus the 'time_from_solar_noon(n)' for the given day.

Use Equation of Time to convert the Solar Times for sunrise and sunset to local times.

$$B(n) := 360\,\text{deg}\cdot\frac{n-81}{364} \qquad B(n) = 201.758\,\text{deg}$$

$$ET(n) := (9.87\cdot\sin(2\cdot B(n)) - 7.53\cdot\cos(B(n)) - 1.5\cdot\sin(B(n)))\,\text{min}$$

$$ET(n) = 14.346\,\text{min}$$

Local Standard Time (LST)

$$LST = \text{Solar\_Time} - ET - 4\cdot\left(L_{st} - l_{local}\right)$$

$$\xi = -ET - 4\cdot\left(L_{st} - l_{local}\right)$$

$$\xi(n) := -ET(n) - 4(75 - 84.37)\,\text{min}$$

$$\xi(n) = 23.134\,\text{min}$$

Note: The sunrise and sunset times are calculted when the center of the sun is at the horizon, thus to the naked eye, the sunrise and sunset appears to differ from the apparent times.

The length of the day can also be calculated by the following method:

$$\text{day\_length}(n) := \frac{2 \cdot h_{ss}(n)}{15 \frac{\text{deg}}{\text{hr}}} \qquad \text{day\_length}(n) = \text{"11:19:52.54"hhmmss}$$

The instantaneous solar radiation on an object in Tallahassee at 12:00 noon.

The angle of incidence, *i*, of the beam radiation on a tilted surface, the panel azimuth angle, α_W, and the panel tilt angle, β:

Panel tilt angle is same as the solar altitude angle: $\beta(n) := \alpha(n)$

Panel azimuth angle is same as solar azimuth angle: $\alpha_w(n) := \alpha_s(n)$

$$\cos(i) = \cos(\alpha(n)) \cdot \cos(\alpha_s(n) - \alpha_w(n)) \cdot \sin(\beta(n)) + \sin(\alpha(n)) \cdot \cos(\beta(n))$$

$$i(n) := \text{acos}(\cos(\alpha(n)) \cdot \cos(\alpha_s(n) - \alpha_w(n)) \cdot \sin(\beta(n)) + \sin(\alpha(n)) \cdot \cos(\beta(n)))$$

Angle of Incidence

$i(n) = 12.276\text{deg}$

Extraterrestrail Solar Radiation

D -- The distance between the sun and the earth

D_0 -- The mean earth-sun distance (1.496×10^{11}m)

I_0 -- The solar constant as given by NASA (1353 W/m^2)

$$I_0 := 1353 \frac{W}{m^2} \qquad D_0 := 1.496\,10^{11}\text{m}$$

The extraterrestrial solar radiation varies by the inverse square law: $I = I_0 \cdot \left(\frac{D_0}{D}\right)^2$

Where $(D_0/D)^2$ is approximated by:

$$\left(\frac{D_0}{D}\right)^2 = 1.00011 + 0.034221\cos(x) + 0.00128\sin(x) + 0.000719\cos(2 \cdot x) + 0.000077\sin(2 \cdot x)$$

where $x = 360 \cdot \frac{n - 1}{365} \text{deg}$

Thus, solving for the extraterrstrial solar radiation:

$$x(n) := 360 \cdot \frac{n - 1}{365} \text{deg}$$

for calculation purposes, set $(D_0/D)^2$ equal to D_{factor}

$$D_{factor}(n) := 1.00011 + 0.034221\cos(x(n)) + 0.00128\sin(x(n)) + 0.000719\cos(2 \cdot x(n)) + 0.000077\sin(2 \cdot x(n))$$

The extraterrestrial radiation is thus:

$$I(n) := I_0 \cdot D_{factor}(n) \qquad I(n) = 1.359 \times 10^3 \frac{W}{m^2}$$

Terrestrial Solar Radiation

The Atmospheric Extinction of Solar Radiation

Clearness number is assumed as: $C_n := 1$

k value is averaged from values found in Table 1.1 (Chapter 1). $k := 0.160$

$$I_{b\_N}(n) := C_n \cdot I(n) \cdot e^{\frac{-k}{\sin(\alpha(n))}} \qquad I_{b\_N}(n) = 1.106 \times 10^3 \frac{W}{m^2}$$

Beam Radiation on the Collector

$$I_{b\_c}(n) := I_{b\_N}(n) \cdot \cos(i(n)) \qquad I_{b\_c}(n) = 1.081 \times 10^3 \frac{W}{m^2}$$

Sky Diffuse Radiation on the Collector

C_{month_avg} is found in Table 1.1 (Chapter 1), the average is used for these calculations.

$$C_{month\_avg} := 0.073$$

$$I_{d\_c}(n) := C_{month\_avg} \cdot I_{b\_N}(n) \cos\left(\frac{\beta(n)}{2}\right)^2 \qquad I_{d\_c}(n) = 65.714 \frac{W}{m^2}$$

Ground reflected radiation is neglected because the system is a concentrating collector located 6 feet off the ground. Therefore, the total insolation on the collector is:

$$I_c(n) := I_{b\_c}(n) + I_{d\_c}(n) \qquad I_c(n) = 1.147 \times 10^3 \frac{W}{m^2}$$

APPENDIX D

COLLECTOR EFFICIENCY FOR VARIED WIND SPEEDS

Overall Loss Coefficient (UL)

$D_{inner} := 0.146m$ $D_{outer} := 0.152m$ $L := 0.191m$

$T_{outer} := 922K$ $T_{inner} := 700K$ $T_{air} := 305K$

$V_1 := 0\frac{m}{s}, 0.025\frac{m}{s} .. 0.339\frac{m}{s}$ $V_2 := 0.339\frac{m}{s}, 0.5\frac{m}{s} .. 8\frac{m}{s}$ $0.339\frac{m}{s} = 0.758mph$

$T_{film} := 0.5(T_{air} + T_{outer})$ $T_{film} = 613.5K$

$k_{air} := 0.0456\frac{W}{m \cdot K}$ $\nu := 5.15 \cdot 10^{-5}\frac{m^2}{s}$ $Pr := 0.698$

$Re_1(V_1) := \frac{V_1 \cdot D_{outer}}{\nu}$ $Re_1(V_1) =$ 0

$Re_2(V_2) := \frac{V_2 \cdot D_{outer}}{\nu}$ $Re_2(V_2) =$ $1.001 \cdot 10^3$

For wind speeds of 0 m/s to 0.339 m/s, 0.1 < Re < 1000

For wind speeds of 0.339 m/s to 8 m/s, 1000 < Re < 50000

$Nu_1(V_1) := 0.40 + 0.54 \cdot Re_1(V_1)^{0.52}$

$Nu_1(V_1) =$ 0.4

$h_1(V_1) := \frac{k_{air}}{D_{outer}} \cdot Nu_1(V_1)$

$h_1(V_1) =$ 0.12 $\frac{W}{m^2 \cdot K}$

$Nu_2(V_2) := 0.30 Re_2(V_2)^{0.6}$

$Nu_2(V_2) =$ 18.935

$h_2(V_2) := \frac{k_{air}}{D_{outer}} \cdot Nu_2(V_2)$

$h_2(V_2) =$ 5.68 $\frac{W}{m^2 \cdot K}$

Linearized Radiation Coefficient

Stefan-Boltzmann constant (σ): $\sigma := 5.670410^{-8}\,kg\cdot s^{-3}\cdot K^{-4}$

Emmittance of the surface (ε): $\varepsilon := 0.5$

$h_r := 4\cdot\sigma\cdot\varepsilon\cdot T_{air}^{3}$ $\quad h_r = 3.218\,\frac{W}{m^2\cdot K}$

For wind speeds below 0.339 m/2

$U_{L1}(V_1) := \left(\frac{1}{h_1(V_1) + h_r}\right)^{-1}$ $\quad U_{L1}(V_1) =$ 3.338 $\frac{W}{m^2\cdot K}$

For wind speeds between 0.339 m/s and 8.0 m/s

$U_{L2}(V_2) := \left(\frac{1}{h_2(V_2) + h_r}\right)^{-1}$ $\quad U_{L2}(V_2) =$ 8.898 $\frac{W}{m^2\cdot K}$

Therefore, the Thermal Energy Lost from the Reciever is as follows:

$A_r := 0.109m^2$ $\quad T_r := \frac{T_{outer} + T_{inner}}{2}$ $\quad T_r = 811\,K$

$Q_{loss\_1}(V_1) := A_r\cdot U_{L1}(V_1)\cdot(T_r - T_{air})$ $\quad Q_{loss\_1}(V_1) =$ 184.087 W

$Q_{loss\_2}(V_2) := A_r\cdot U_{L2}(V_2)\cdot(T_r - T_{air})$ $\quad Q_{loss\_2}(V_2) =$ 490.769 W

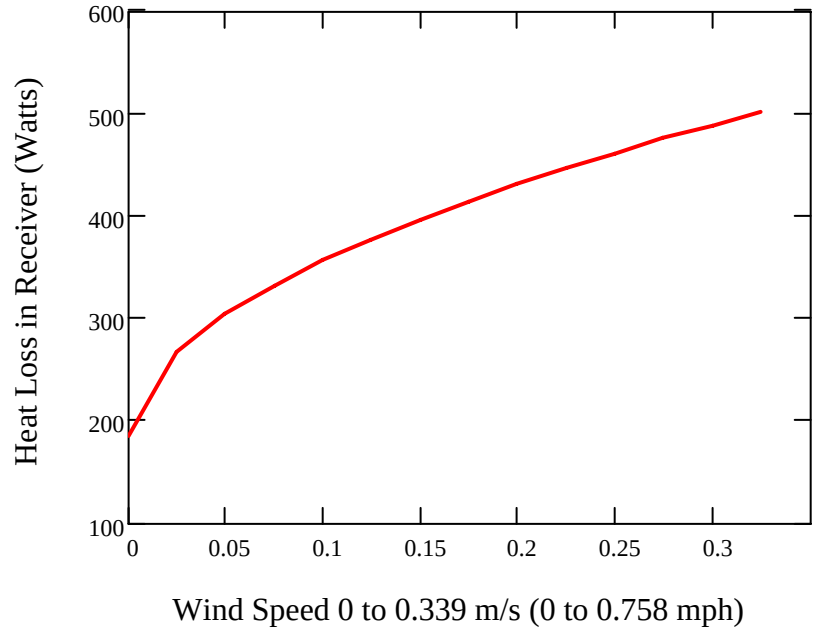

Figure D.1: Heat loss from receiver for wind speeds less than 0.339 m/s.

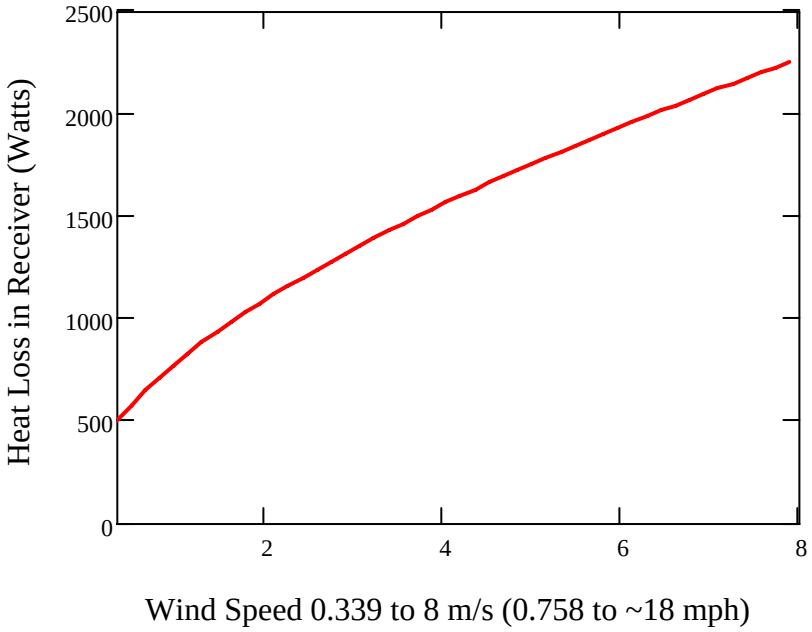

Figure D.2: Heat loss from receiver for wind speeds greater than 0.339 m/s.

Optical Energy Absorbed by the Receiver

$Q_{opt} = A_a \cdot \rho_{s\_m} \cdot \tau_g \cdot \alpha_r \cdot R \cdot S \cdot I_a$

ρ_{s_m} -- specular reflectance of concentrating mirror

τ_g -- transmittance of any glass envelope covering the receiver

A_a -- aperture area of the collector

S -- receiver shading factor (fraction of collector aperture not shadowed by the recevier)

I_a -- insolation incident on the collector aperture

α_r -- absorbtance of the receiver

S, **α_r**, **ρ_{s_m}**, and **τ_g** are constants dependent only on the materials used and the structure accuracy of the collector. These constants are nominally lumped into a single constant term, **η_{opt}**, the optical efficiency of the collector.

$S := 1 \qquad \alpha_r := 0.9 \qquad \rho_{s\_m} := 1 \qquad \tau_g := 1 \qquad A_a := 10.507\,m^2$

$I_a := 1064 \frac{W}{m^2} \qquad k := 10^3$

$Q_{opt} := A_a \cdot \rho_{s\_m} \cdot \tau_g \cdot \alpha_r \cdot S \cdot I_a \qquad Q_{opt} = 11.068\,k \cdot W$

Thus, the quantity of thermal energy produced by the solar collector is described by:

$Q_{out\_1}(V_1) := Q_{opt} - Q_{loss\_1}(V_1)$ $\qquad Q_{out\_1}(V_1) =$ $1.088 \cdot 10^4$ W

$Q_{out\_2}(V_2) := Q_{opt} - Q_{loss\_2}(V_2)$ $\qquad Q_{out\_2}(V_2) =$ $1.058 \cdot 10^4$ W

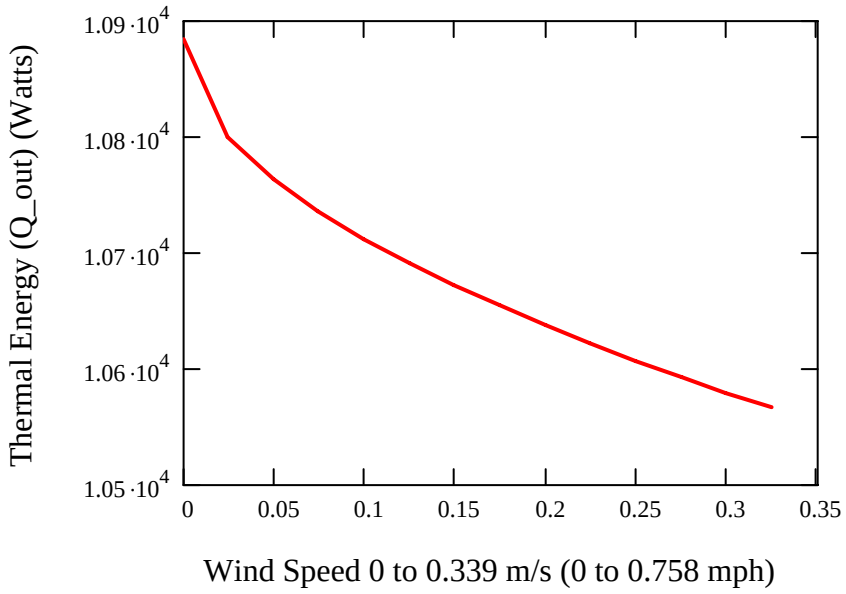

Figure D.2: Thermal energy produced by collector taking winds less than 0.339 m/s into account.

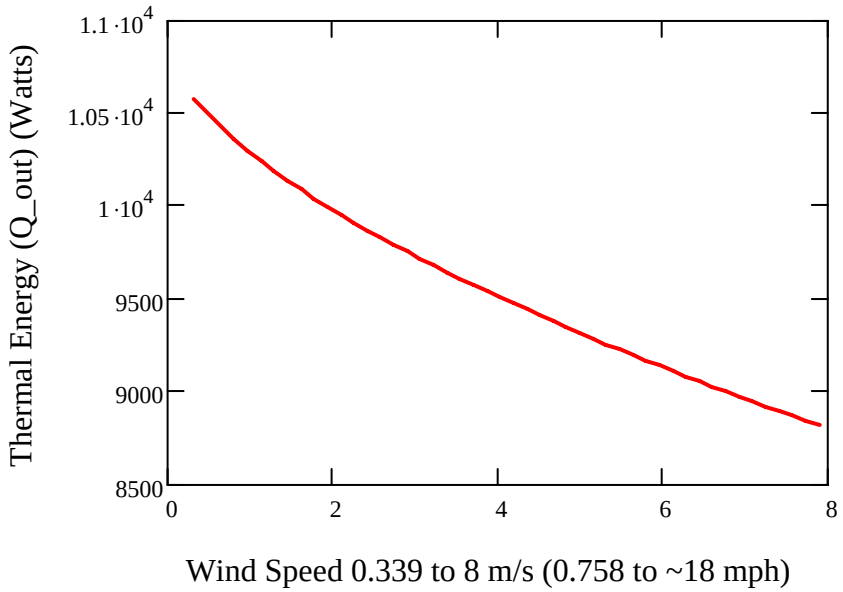

Figure D.3: Thermal energy produced by collector taking winds greater than 0.339 m/s into account.

Collector Efficiency

$$\eta_{collector\_1}(V_1) := \frac{Q_{out\_1}(V_1)}{A_a \cdot I_a}$$

$\eta_{collector\_1}(V_1)$ = 97.353 %

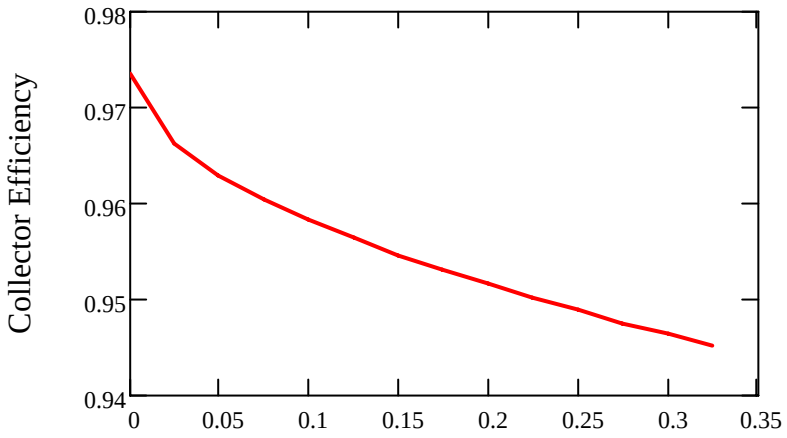

Figure D.4: Effects of collector efficiency for wind speeds less than 0.339 m/s.

$$\eta_{collector\_2}(V_2) := \frac{Q_{out\_2}(V_2)}{A_a \cdot I_a}$$

$\eta_{collector\_2}(V_2)$ = 94.61 %

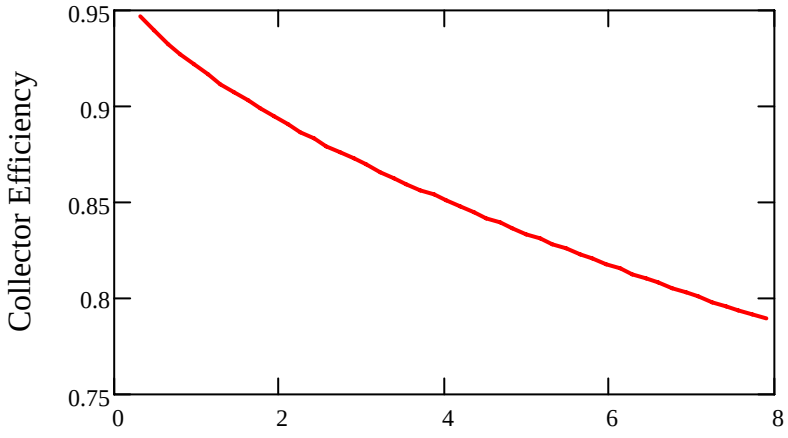

Figure D.5: Effects of collector efficiency for wind speeds greater than 0.339 m/s.

APPENDIX E

CALCULATIONS FOR COLLECTOR EFFICIENCY ON OCTOBER 21st FOR VARIED BEAM INSOLATION THROUGHOUT THE DAY

Collector Efficiency for Varied Beam Insolation on Particular Day

$L := 30.38\,deg$ $\quad l_{local} := 84.37\,deg$ $\quad L_{st} := 75\,deg$

Julian Day (n): $n := 285$

Angle of Declination

$$\delta_s := 23.45\,deg \cdot \sin\left[\left(360 \cdot \frac{284 + n}{365}\right) deg\right]$$

$$\delta_s = -8.482\,deg$$

Hour angle of a oit on the earths surface is defined as the angle through which the earth would turn to bring the meridian of the point directly under the sun. The hour angle at soalr noon is zero, with each 360/24 or 15 degrees of longitude equivalent to 1 hour, with afternoon hours being designated as positive. (i.e. -- h is -30deg for 10 AM and h is +30deg for 2 PM)

$$h_s := -180\,deg, -165\,deg .. 180\,deg$$

The **solar altitude** is thus,

$$\sin(\alpha) = \cos(L)\cdot\cos(\delta_s)\cdot\cos(h_s) + \sin(L)\cdot\sin(\delta_s)$$

$$\alpha(h_s) := \operatorname{asin}\left(\cos(L)\cdot\cos(\delta_s)\cdot\cos(h_s) + \sin(L)\cdot\sin(\delta_s)\right)$$

$\alpha(h_s) =$

-68.102 deg

And the **solar azimuth angle** is,

$$\alpha_s(h_s) := \operatorname{asin}\left(\cos(\delta_s)\cdot\frac{\sin(h_s)}{\cos(\alpha(h_s))}\right)$$

$\alpha_s(h_s) =$

-1.861·10-14 deg

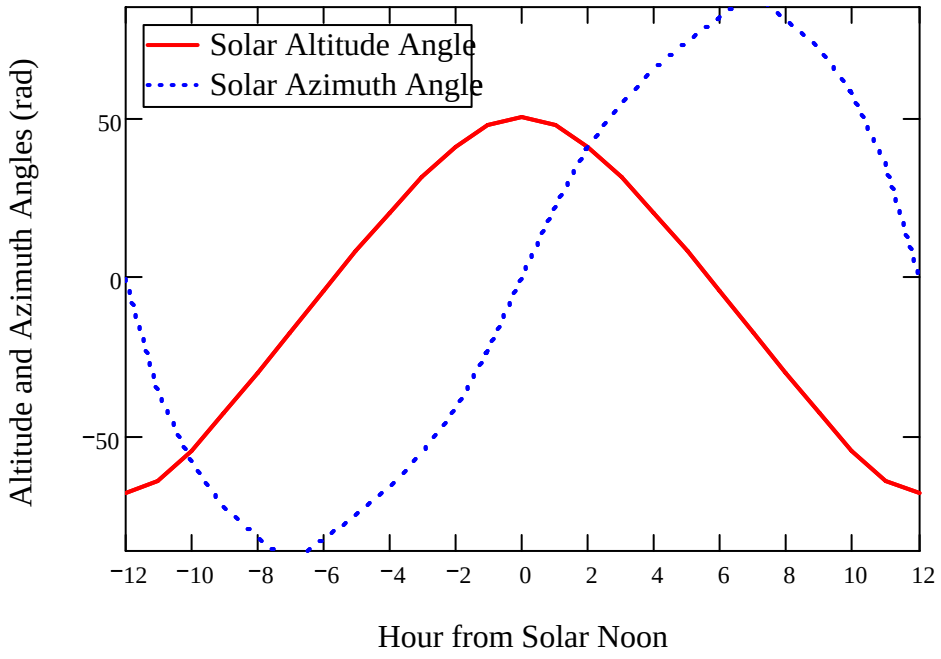

Figure E.1: Solar Altitude and Azimuth angles for October 21st (given in radians)

The angle of incidence, *i*, of the beam radiation on a tilted surface, the panel azimuth angle, α_W, and the panel tilt angle, β:

Panel tilt angle is same as the solar altitude angle: $\beta(h_s) := \alpha(h_s)$

Panel azimuth angle is same as solar azimuth angle: $\alpha_w(h_s) := \alpha_s(h_s)$

$$\cos(i) = \cos(\alpha(h_s))\cdot\cos(\alpha_s(h_s) - \alpha_w(h_s))\cdot\sin(\beta(h_s)) + \sin(\alpha(h_s))\cdot\cos(\beta(h_s))$$

$$i(h_s) := \operatorname{acos}\left(\cos(\alpha(h_s))\cdot\cos(\alpha_s(h_s) - \alpha_w(h_s))\cdot\sin(\beta(h_s)) + \sin(\alpha(h_s))\cdot\cos(\beta(h_s))\right)$$

$i(h_s) =$

133.796 deg

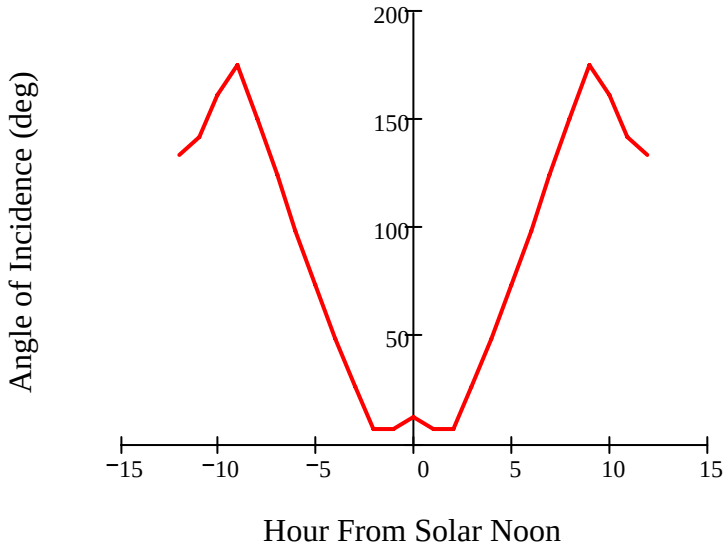

Figure E.2: Angle of incidence on October 21st for time from solar noon.

Extraterrestrail Solar Radiation

D -- The distance between the sun and the earth
D_0 -- The mean earth-sun distance (1.496×10^{11}m)
I_0 -- The solar constant as given by NASA (1353 W/m^2)

$$I_0 := 1353\frac{W}{m^2} \qquad D_0 := 1.496\cdot 10^{11}m$$

The extraterrestrial solar radiation varies by the inverse square law: $$I = I_0\cdot\left(\frac{D_0}{D}\right)^2$$

Where $(D_0/D)^2$ is approximated by:

$$\left(\frac{D_0}{D}\right)^2 = 1.00011 + 0.034221\cos(x) + 0.00128\sin(x) + 0.000719\cos(2\cdot x) + 0.000077\sin(2\cdot x)$$

where $$x = 360\cdot\frac{n-1}{365\,deg}$$

Thus, solving for the extraterrstrial solar radiation:

$$x := 360 \cdot \frac{n - 1}{365} \text{ deg}$$

for calculation purposes, set $(D_0/D)^2$ equal to D_{factor}

$$D_{factor} := 1.00011 + 0.034221 \cos(x) + 0.00128 \sin(x) + 0.000719 \cos(2 \cdot x) + 0.000077 \sin(2 \cdot x)$$

The extraterrestrial radiation is thus:

$$I := I_0 \cdot D_{factor} \qquad I = 1.359 \times 10^3 \frac{W}{m^2}$$

Terrestrial Solar Radiation

The Atmospheric Extinction of Solar Radiation

Clearness number is assumed as: $C_n := 1$

k value is averaged from values found in Table ##. $k := 0.172$

$$I_{b\_N}(h_s) := C_n \cdot I \cdot e^{\frac{-k}{\sin(\alpha(h_s))}} \qquad I_{b\_N}(h_s) = 1.635 \cdot 10^3 \ \frac{W}{m^2}$$

Beam Radiation on the Collector

$$I_{b\_c}(h_s) := I_{b\_N}(h_s) \cdot \cos(i(h_s)) \qquad I_{b\_c}(h_s) = -1.132 \cdot 10^3 \ \frac{W}{m^2}$$

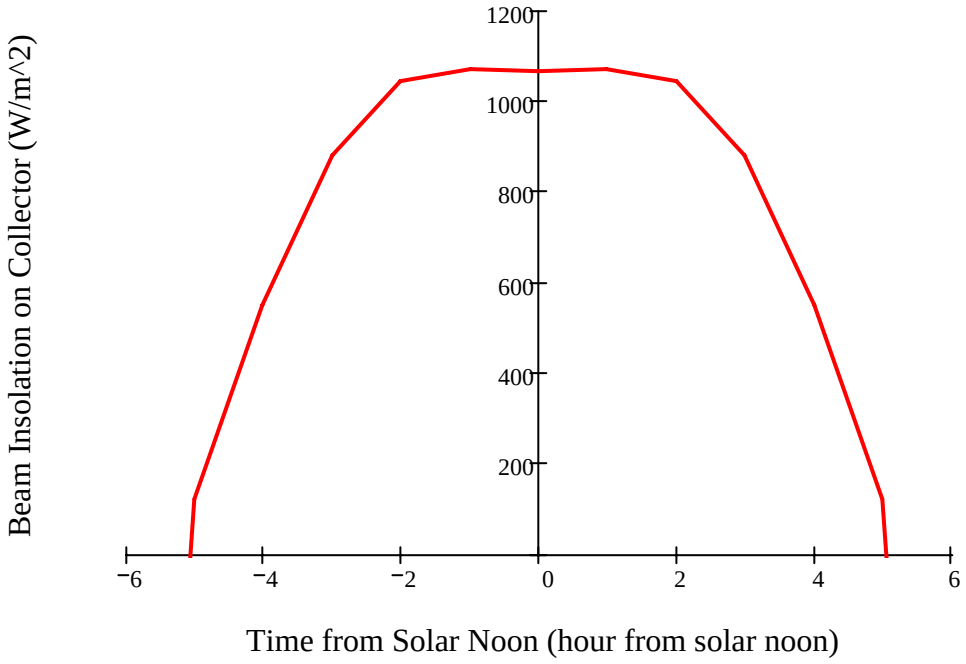

Figure E.3: Beam insolation incident on collector throughout the day on October 21st.

Collector Efficiency Variation for October 21st

Values for Receiver to solve for Collector Efficiency

$D_{inner} := 0.146m$ $D_{outer} := 0.152m$ $L := 0.191m$

$T_{outer} := 922K$ $T_{inner} := 305K$ $T_{air} := 305K$

$V := 0.5\frac{m}{s}$

$T_{film} := 0.5(T_{air} + T_{outer})$ $T_{film} = 613.5K$

$k_{air} := 0.0456\frac{W}{m \cdot K}$ $\nu := 5.15 \cdot 10^{-5}\frac{m^2}{s}$ $Pr := 0.698$

$Re := \frac{V \cdot D_{outer}}{\nu}$ $Re = 1.476 \times 10^3$

$Nu := 0.30 Re^{0.6}$ $Nu = 23.907$

$h := \frac{k_{air}}{D_{outer}} \cdot Nu$ $h = 7.172 \frac{W}{m^2 \cdot K}$

Linearized Radiation Coefficient

Stefan-Boltzmann constant (σ): $\sigma := 5.6704 10^{-8} kg \cdot s^{-3} \cdot K^{-4}$

Emmittance of the surface (ε): $\varepsilon := 0.5$

$h_r := 4 \cdot \sigma \cdot \varepsilon \cdot T_{air}^{3}$ $h_r = 3.218 \frac{W}{m^2 \cdot K}$

$U_L := \left(\frac{1}{h + h_r} \right)^{-1}$ $U_L = 10.39 \frac{W}{m^2 \cdot K}$

Thus, the Thermal Energy Lost from the Receiver is:

$A_r := 0.109 m^2$ $T_r(T_{inner}) := \frac{T_{outer} + T_{inner}}{2}$ $T_r(T_{inner}) = 613.5 K$

$Q_{loss}(T_{inner}) := A_r \cdot U_L \cdot (T_r(T_{inner}) - T_{air})$ $Q_{loss}(T_{inner}) = 349.372 W$

Optical Energy Absorbed by the Receiver

$S := 1$ $\alpha_r := 0.95$ $\rho_{s\_m} := 1$ $\tau_g := 1$ $A_a := 10.507 m^2$

$I_a(h_s) := I_{b\_c}(h_s)$ $k := 10^3$

$Q_{opt}(h_s) := A_a \cdot \rho_{s\_m} \cdot \tau_g \cdot \alpha_r \cdot S \cdot I_a(h_s)$ $Q_{opt}(h_s) =$ -11.773 $k \cdot W$

Thus, the quantity of thermal energy produced by the solar collector is described by:

$$Q_{out}(h_s, T_{inner}) := Q_{opt}(h_s) - Q_{loss}(T_{inner})$$

$Q_{out}(h_s, T_{inner})$ = -1.212·10^4 W

Collector Efficiency

$$\eta_{collector}(h_s, T_{inner}) := \frac{Q_{out}(h_s, T_{inner})}{A_a \cdot I_a(h_s)}$$

$\eta_{collector}(h_s, T_{inner})$ = 101.938 %

$$H_T(h_s, T_{inner}) := \frac{T_{inner} - T_{air}}{I_a(h_s)}$$

$H_T(h_s, T_{inner})$ = 0 $\frac{m^2 \cdot K}{W}$

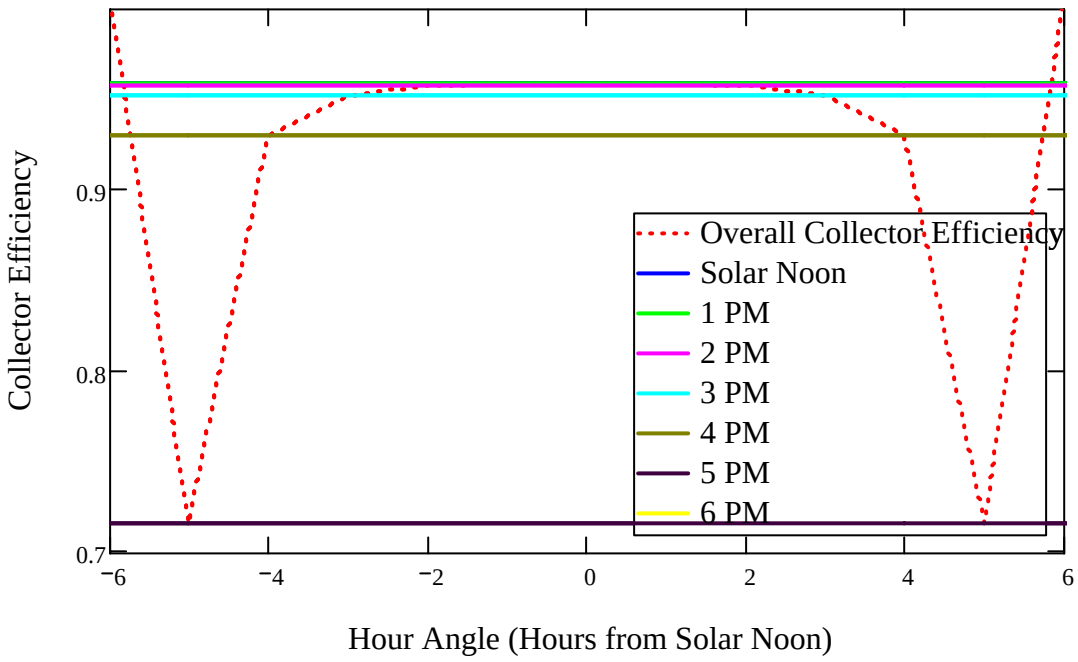

Figure E.4: Collector efficiency due to beam insolation variation for October 21st.

APPENDIX F

COLLECTOR EFFICIENCY AS RECEIVER TEMPERATURE INCREASES

Collector Efficiency Plot vs. dT/l_b

$D_{inner} := 0.146m$ $D_{outer} := 0.152m$ $L := 0.191m$

$T_{outer} := 922K$ $T_{inner} := 305K, 350K .. 700K$ $T_{air} := 305K$

$V := 0.5\frac{m}{s}$

$T_{film}(T_{outer}) := 0.5(T_{air} + T_{outer})$ $T_{film}(T_{outer}) = 613.5\,K$

$k_{air} := 0.0456\frac{W}{m \cdot K}$ $\nu := 5.15 \cdot 10^{-5}\frac{m^2}{s}$ $Pr := 0.698$

$Re := \frac{V \cdot D_{outer}}{\nu}$ $Re = 1.476 \times 10^3$

$Nu := 0.30Re^{0.6}$ $Nu = 23.907$

$h := \frac{k_{air}}{D_{outer}} \cdot Nu$ $h = 7.172\frac{W}{m^2 \cdot K}$

Linearized Radiation Coefficient

Stefan-Boltzmann constant (σ): $\sigma := 5.6704 10^{-8} kg \cdot s^{-3} \cdot K^{-4}$

Emmittance of the surface (ε): $\varepsilon := 0.5$

$h_r := 4 \cdot \sigma \cdot \varepsilon \cdot T_{air}^{3}$ $\quad h_r = 3.218 \frac{W}{m^2 \cdot K}$

$U_L := \left(\frac{1}{h + h_r} \right)^{-1}$ $\quad U_L = 10.39 \frac{W}{m^2 \cdot K}$

Thus, the **Thermal Energy Lost from the Receiver** is:

$A_r := 0.109 m^2$ $\quad T_r(T_{inner}) := \frac{T_{outer} + T_{inner}}{2}$ $\quad T_r(T_{inner}) =$ 613.5 K

$Q_{loss}(T_{inner}) := A_r \cdot U_L \cdot (T_r(T_{inner}) - T_{air})$ $\quad Q_{loss}(T_{inner}) =$ 349.372 W

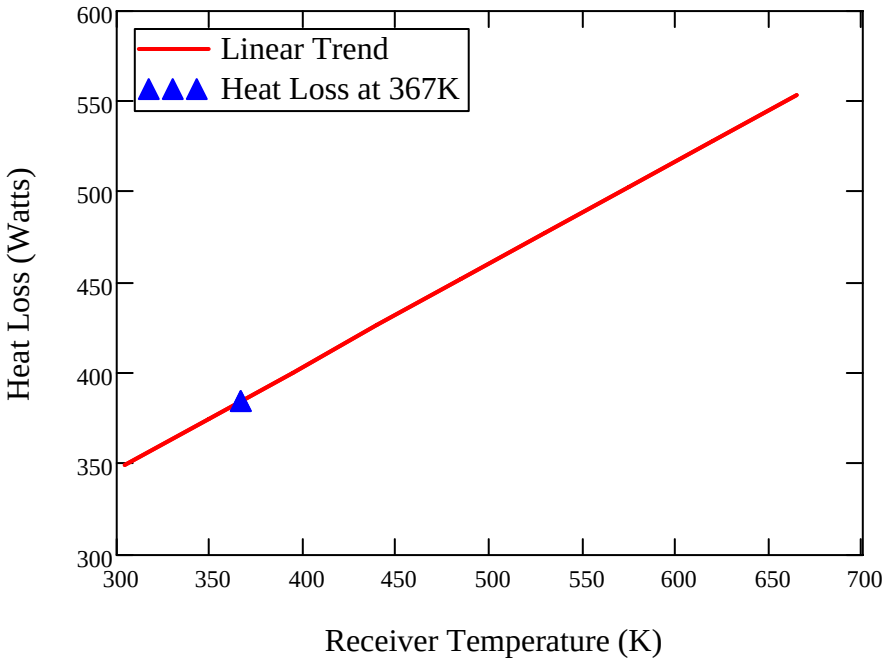

Figure F.1: Heat loss from the receiver as the temperature increases.

Optical Energy Absorbed by the Receiver

$S := 1 \qquad \alpha_r := 0.9$ $\qquad \rho_{s\_m} := 1 \qquad \tau_g := 1 \qquad A_a := 10.507\,m^2$

$I_a := 1064\,\frac{W}{m^2} \qquad k := 10^3$

$Q_{opt} := A_a \cdot \rho_{s\_m} \cdot \tau_g \cdot \alpha_r \cdot S \cdot I_a \qquad Q_{opt} = 11.068k \cdot W$

Thus, the quantity of thermal energy produced by the solar collector is described by:

$Q_{out}(T_{inner}) := Q_{opt} - Q_{loss}(T_{inner}) \qquad Q_{out}(T_{inner}) =$ 1.072·10^4 W

Collector Efficiency

$\eta_{collector}(T_{inner}) := \frac{Q_{out}(T_{inner})}{A_a \cdot I_a} \qquad \eta_{collector}(T_{inner})$ 95.875 %

$H_T(T_{inner}) := \frac{T_{inner} - T_{air}}{I_a} \qquad H_T(T_{inner}) =$ 0 $\frac{m^2 \cdot K}{W}$

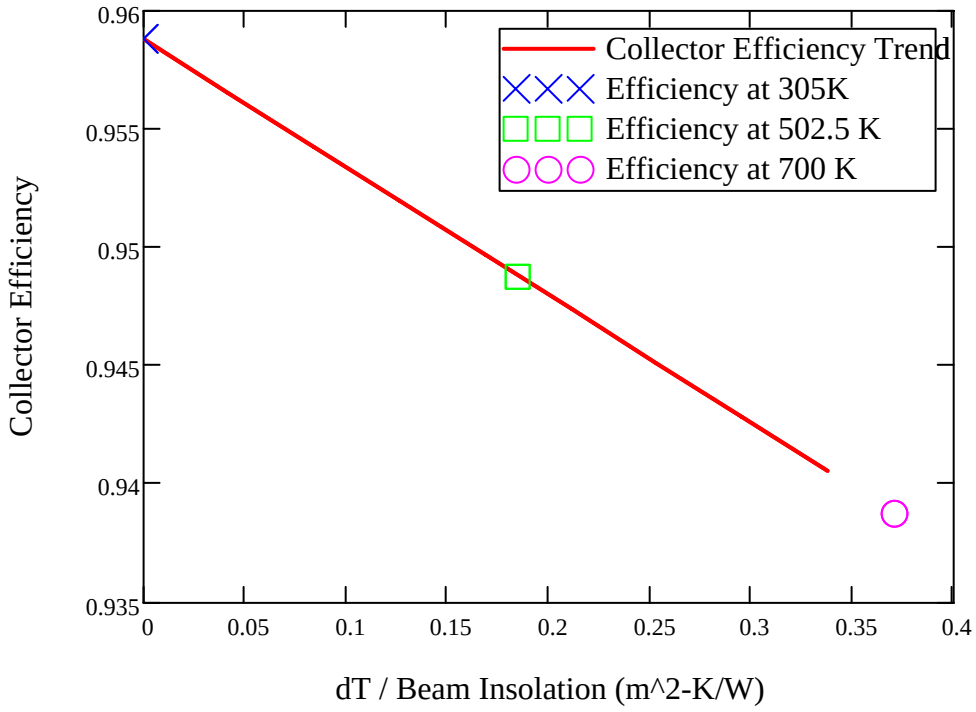

Figure F.2: Collector performance efficiency as receiver temperature increases.

APPENDIX G

GEOMETRIC CONCENTRATION RATIO AND MAXIMUM THEORETICAL TEMPERATURE

Operating Temperature as a Function of Concentration

Assume the sun and the rest of the universe to be blackbodies. The sun is at a surface temperature of T_{sun}; the rest of the universe (other than the sun and the receiver/absorber) is at T_{amb}, which is equal to zero.

$T_{sun} := 6000K$ $T_{sun} = 5726.85°C$ $k := 10^3$

$T_{amb} := 0K$

Radius of the sun (r): $r_{sun} := 695500km$

Stefan-Boltzmann constant (σ): $\sigma := 5.6704 10^{-8} kg \cdot s^{-3} \cdot K^{-4}$

Radiation emitted by the sun:

$Q_{sun} := 4 \cdot \pi \cdot r_{sun}^2 \cdot \sigma \cdot T_{sun}^4$ $Q_{sun} = 4.467 \times 10^{23} kW$

Radiation incident on a collector of aperture area ($A_{concentrator}$):

Dimensions of the Concentrator

H: Depth
D: Diameter

$D := 12ft$ $H := 25.5in$

$P := \frac{D^2}{8 \cdot H}$ $P = 2.582m$

Area of Solar Concentrator:

$$A_{concentrator\_surface\_area} := \frac{2\cdot\pi}{3\cdot P}\cdot\left[\sqrt{\left(\frac{D^2}{4}+P^2\right)^3}-P^3\right]$$

$A_{concentrator\_surface\_area} = 11.732\,m^2$

$A_{concentrator\_surface\_area} = 126.277\,ft^2$

Aperture Area of Solar Concentrator

$$A_{concentrator} := \pi\cdot\left(\frac{D}{2}\right)^2$$

$A_{concentrator} = 10.507\,m^2$

$A_{concentrator} = 113.097\,ft^2$

Sun-Earth distance (R_{sun_earth}): $R_{sun\_earth} := 93000000\,m$

$$Q_{sun\_concentrator} := \frac{A_{concentrator}}{4\cdot\pi\cdot R_{sun\_earth}^2}\cdot Q_{sun}$$

$Q_{sun\_concentrator} = 16.674\,kW$

Half-angle of the sun: $\theta_{half} := \frac{r_{sun}}{R_{sun\_earth}}$

$\theta_{half} = 4.647\times 10^{-3}$

$\theta_{half} = 0.266\,deg$

$\tau = (1-\eta) = (1 - optical\_losses\_in\_atmosphere\_and\_in\_collector\ )$

Assume: $\tau := 0.5$

Absorbtance of receiver/absorber for solar radiation (α): $\alpha := 0.7$

Therefore, the radiation transfer from sun to receiver is as follows:

$$Q_{sun\_receiver} := \tau\cdot\alpha\cdot A_{concentrator}\cdot\sin(\theta_{half})^2\cdot\sigma\cdot T_{sun}^4$$

$Q_{sun\_receiver} = 5.836\,kW$

Emittance of the absorber in infrared region (ε): $\varepsilon := 0.5$

Dimensions of Receiver

h: Height
d: Diameter

$h := 7.5in$ $d := 6in$

$A_{base} := \pi \cdot \left(\frac{d}{2}\right)^2$ $A_{base} = 0.018\,m^2$

$A_{sides} := d \cdot \pi \cdot h$ $A_{sides} = 0.091\,m^2$

$A_{receiver} := A_{base} + A_{sides}$ $A_{receiver} = 0.109\,m^2$

The radiation losses from the receiver are thus:

$Q_{receiver\_radiation} = \varepsilon \cdot A_{receiver} \cdot \sigma \cdot T_{receiver}$

A fraction (η) of the incoming solar radiation $Q_{sun\_receiver}$ is used in the useful heat transfer to the working fluid and/or is lost by convection/conduction. Thus, the energy balance equation for the receiver is:

$Q_{sun\_receiver} = Q_{receiver\_radiation} + \eta \cdot Q_{sun\_receiver}$

This equation can also be presented as:

$(1 - \eta) \cdot \tau \cdot \alpha \cdot A_{concentrator} \cdot \sin(\theta_{half})^2 \cdot T_{sun}^{\ 4} = \varepsilon \cdot A_{receiver} \cdot T_{receiver}^{\ 4}$

Assume that: $\eta := 0.5$

Geometric Concentration Ratio

$CR_{geometric} := \frac{A_{concentrator}}{A_{receiver}}$ $CR_{geometric} = 96$

Ideal Concentration Ratio

$$CR_{ideal} := \frac{1}{\sin\left(\theta_{half}\right)^2} \qquad CR_{ideal} = 4.631 \times 10^4$$

The operating temperature of the receiver can now be found:

$$T_{receiver} := T_{sun} \cdot \left[(1 - \eta) \cdot \tau \cdot \frac{\alpha}{\varepsilon} \cdot \frac{CR_{geometric}}{CR_{ideal}} \right]^{\frac{1}{4}}$$

$$T_{receiver} = 984.732K$$

$$T_{receiver} = 711.582°C$$

$$T_{receiver} = 1.313 \times 10^3 °F$$

Note: As $T_{receiver}$ approaches T_{sun}, the highest possible absorber temperature, $T_{receiver\_max}$, is equal to T_{sun}, which is approximately 6000K. This temperature is only in theory and could only ever be achieved if no heat is extracted and the concentration ration was equal to 45300.

APPENDIX H

GEOMETRIC CONCENTRATION RATIO AS FUNTION OF RECEIVER TEMPERATURE

Concentration Ration as a Function of Receiver Temperature

$T_{sun} := 6000K$ $T_{sun} = 5726.85°C$

$T_{amb} := 0K$

Radius of the sun (r): $r_{sun} := 695500km$

Stefan-Boltzmann constant (σ): $\sigma := 5.6704 10^{-8} kg \cdot s^{-3} \cdot K^{-4}$

Radiation emitted by the sun:

$Q_{sun} := 4 \cdot \pi \cdot r_{sun}^{2} \cdot \sigma \cdot T_{sun}^{4}$ $Q_{sun} = 4.467 \times 10^{23} kW$

Radiation incident on a collector of aperture area ($A_{concentrator}$):

Dimensions of the Concentrator

H: Depth
D: Diameter

$D := 12ft$ $H := 25.5in$

Aperture Area of Solar Concentrator:

$A_{concentrator} := \pi \cdot \left(\frac{D}{2}\right)^{2}$ $A_{concentrator} = 10.507 m^{2}$

$A_{concentrator} = 113.097 ft^{2}$

Concentration Ratio Range

$CR := 0, 1 .. 1000$

Sun-Earth distance (R_{sun_earth}): $R_{sun\_earth} := 93000000m$

$$Q_{sun\_concentrator} := \frac{A_{concentrator}}{4 \cdot \pi \cdot R_{sun\_earth}^{2}} \cdot Q_{sun} \qquad Q_{sun\_concentrator} = 16.674kW$$

Half-angle of the sun: $\theta_{half} := \frac{r_{sun}}{R_{sun\_earth}}$ $\theta_{half} = 4.647 \times 10^{-3}$

$\theta_{half} = 0.266deg$

Assume: $\tau := 0.5$

Absorbtance of receiver/absorber for solar radiation (α): $\alpha := 0.7$

Therefore, the radiation transfer from sun to receiver is as follows:

$$Q_{sun\_receiver} := \tau \cdot \alpha \cdot A_{concentrator} \cdot \sin\left(\theta_{half}\right)^{2} \cdot \sigma \cdot T_{sun}^{4} \qquad Q_{sun\_receiver} = 5.836kW$$

Emittance of the absorber in infared region (ε): $\varepsilon := 0.5$

Assume that: $\eta := 0.5$

Ideal Concentration Ratio

$$CR_{ideal} := \frac{1}{\sin\left(\theta_{half}\right)^{2}} \qquad CR_{ideal} = 4.631 \times 10^{4}$$

The operating temperature of the receiver can now be found:

$$T_{receiver}(CR) := T_{sun} \cdot \left[(1 - \eta) \cdot \tau \cdot \frac{\alpha}{\varepsilon} \cdot \frac{CR}{CR_{ideal}} \right]^{\frac{1}{4}} \qquad T_{receiver}(CR) = \boxed{0}\ K$$

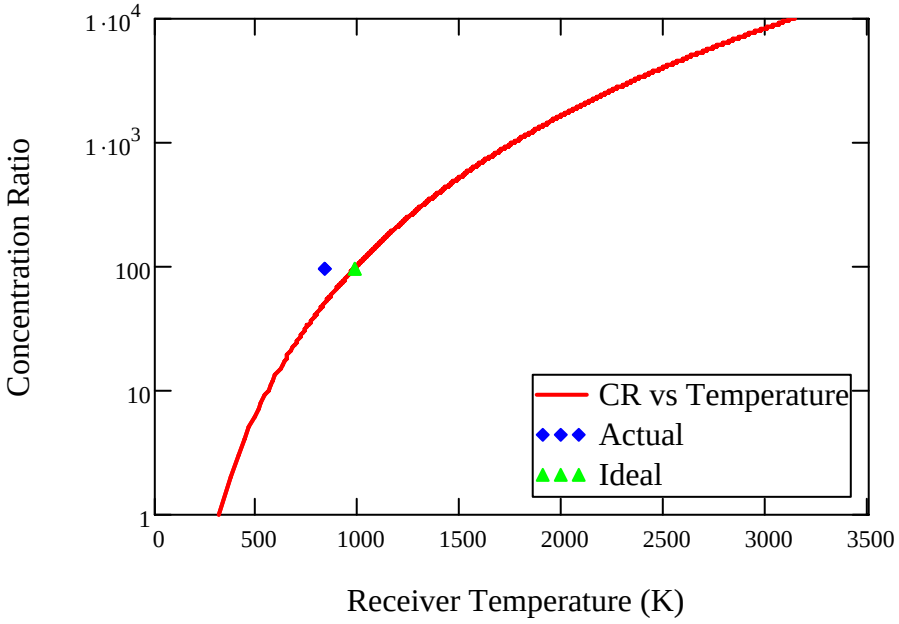

Figure H.1: Concentration given as a function of the operating temperature. For our system, the ideal concentration ratio of 96 is given at the point which falls on the curve. In reality, our system falls slightly behind the curve.

APPENDIX I

RECEIVER / BOILER EFFICIENCY CALCULATIONS

Boiler Efficiency $k := 10^3$

Direct Method

Directly defined by the exploitable heat output from the boiler and bythe fuel power input of the boiler.

$$\eta_{boiler\_direct} = \frac{Q_{output}}{Q_{input}}$$

Indirect Method

Determines efficiency by the sum of the major losses and by the fuel power of the boiler. The indirect method provides a better understanding of the individual losses on the boiler efficiency.

$$\eta_{boiler\_indirect} = 1 - \frac{Q_{losses}}{Q_{input}}$$

$Q_{losses} := 349.372 W$ $Q_{input} := 11.072 k \cdot W$ $Q_{output} := 1 k \cdot W$

$$\eta_{boiler\_direct} := \frac{Q_{output}}{Q_{input}} \qquad \eta_{boiler\_direct} = 9.032\%$$

$$\eta_{boiler\_indirect} := 1 - \frac{Q_{losses}}{Q_{input}} \qquad \eta_{boiler\_indirect} = 96.845\%$$

APPENDIX J

MASS FLOW RATE CALCULATIONS FOR STEAM INTO TURBINE

Mass Flow Rate through Steam Turbine Nozzle

Area of the Steam Turbine Nozzle

$d := 0.09\,in$ $A := \pi \cdot \left(\frac{d}{2}\right)^2$ $A = 4.104 \times 10^{-6}\,m^2$

Speed of Sound Properties for Steam

$T_{steam} := 373.15\,K$ $R := 461.4\,\frac{N \cdot m}{kg \cdot K}$ $\rho := 0.60\,\frac{kg}{m^3}$ $\gamma := 1.324$

Turbine Inlet Steam Temperature Turbine Inlet Steam Pressure $k := 10^3$

$T := 470\,K$ $P_t := 0.480537\,MPa$

From the Steam Tables for the given pressure and temperature

$t_s := 448.51\,K$ $\nu := 0.4394\,\frac{m^3}{kg}$ $s := 7.0648\,\frac{k \cdot J}{kg \cdot K}$

Since the inlet temperature is higher than the saturation temperature, the steam is superheated.

Speed of Sound

$a := \sqrt{\frac{\gamma \cdot P_t}{\rho}}$ $a = 1.03 \times 10^3\,\frac{m}{s}$

Check for choked flow

$\frac{P_{exit}}{P_t} = 0.528$

$P_{exit} := 101.325 \cdot kPa$

$\frac{P_{exit}}{P_t} = 0.211$ Value is less than 0.5283, thus the flow is choked.

Mach Number
(assuming M=1 because of geometry)

$M := 1$ $M = \frac{V}{a}$

The velocity of the flow is:

$V := M \cdot a$ $V = 1.03 \times 10^{3} \frac{m}{s}$

The mass flow rate is thus:

$m_{dot} := P_t \cdot A \cdot M \cdot \sqrt{\frac{\gamma}{R \cdot T}}$ $m_{dot} = 4.873 \times 10^{-3} \frac{kg}{s}$

APPENDIX K

STEAM TURBINE EFFICIENCY CALCULATIONS

Steam Turbine Calculations

$k := 10^3$

Mass Flow Rate into the turbine: $m_{dot} := 4.873 \cdot 10^{-3} \frac{kg}{s}$

Enthalpy Values for Turbine Inlet (h_3) and Outlet (h_4): $h_3 := 2764.0848 \frac{k \cdot J}{kg}$ $h_4 := 2679.7689 \frac{k \cdot J}{kg}$

Heat Transfer from the Turbine: $Q_{dot} := m_{dot} \cdot (h_4 - h_3)$

$Q_{dot} = -410.871 W$

$P_{inlet} := 480.537 k \cdot Pa$ $P_{outlet} := 101.325 k \cdot Pa$

$T_{inlet} := 431.46 K$

$m_{dot} = \rho_{in} \cdot V_{inlet} \cdot A_{nozzle}$ $m_{dot} = \rho_{out} \cdot V_{out} \cdot A_{nozzle}$

$A_{nozzle} := 4.104 \cdot 10^{-6} m^2$ $A_{exit} := 1.267 \cdot 10^{-4} m^2$ $\rho_{in} := 2.2760 \frac{kg}{m^3}$ $\rho_{out} := 0.5409 \frac{kg}{m^3}$

$V_{inlet} := \frac{m_{dot}}{\rho_{in} \cdot A_{nozzle}}$ $V_{outlet} := \frac{m_{dot}}{\rho_{out} \cdot A_{exit}}$

$V_{inlet} = 521.695 \frac{m}{s}$ $V_{outlet} = 71.105 \frac{m}{s}$

Elevation of turbine inlet and outlet above reference plane:

$Z_{inlet} := 10in$ $Z_{outlet} := 6in$

From the Steam Tables:

$h_{inlet} := h_3$ $h_{outlet} := h_4$

$$Q_{dot} + m_{dot}\cdot\left(h_{inlet} + \frac{V_{inlet}^{2}}{2} + g\cdot Z_{inlet}\right) = m_{dot}\cdot\left(h_{outlet} + \frac{V_{outlet}^{2}}{2} + g\cdot Z_{outlet}\right) + W_{dot\_CV}$$

$$W_{dot\_CV} := Q_{dot} + m_{dot}\cdot\left(h_{inlet} + \frac{V_{inlet}^{2}}{2} + g\cdot Z_{inlet}\right) - m_{dot}\cdot\left(h_{outlet} + \frac{V_{outlet}^{2}}{2} + g\cdot Z_{outlet}\right)$$

$W_{dot\_CV} = 650.818W$ Power Output of the Turbine

Work Output of the Turbine is solved by:

$$w_a := \frac{W_{dot\_CV}}{m_{dot}} \qquad w_a = 133.556\frac{k\cdot J}{kg}$$

To determine the efficiency of the turbine (or any machine in that matter), we compare the actual performacne of the machine under given conditions to the performance that would have been achieved in an ideal process. A steam turbine is inteded to be an adiabatic machine. The only heat transfer which takes place is the unavoidable heat transfer between the turbine and its surroundings. Also, we consider the turbine to be running at steady-state, steady-flow, thus, the state of the steam entering the turbine and the exhaust pressure are fixed. Thsu, the ideal process is considered to be a reversible adiabatic process (which is also an isentropic process), between the turbine inlet state and the turbine exhaust pressure. Thus, if we denote the actual work done per unit mass of steam flow thorugh the turbine as w_a and the work that would be done in an ideal cycle as w_s, the efficiency fo the turbine is thus defined as:

$$\eta_{turbine} = \frac{w_a}{w_s}$$

$T_{turbine\_inlet} := T_{inlet}$ $P_{turbine\_inlet} := P_{inlet}$ $P_{turbine\_outlet} := 101.325\,k \cdot Pa$

$T_{turbine\_inlet} = 158.31°C$ $P_{turbine\_inlet} = 0.481MPa$

$h_i := h_{inlet}$

$h_i = 2.764 \times 10^3 \frac{k \cdot J}{kg}$

Ideal value by use of table calculation program: $h_e := 2496.9084 \frac{k \cdot J}{kg}$

Calculate the work, w_S, that would be done in an isentropic process between the given inlet state and the final pressure.

$w_s := h_i - h_e$ $w_s = 267.176 \frac{k \cdot J}{kg}$

Turbine Efficiency is thus:

$\eta_{turbine} := \frac{w_a}{w_s}$ $\eta_{turbine} = 0.5$ $\eta_{turbine} = 49.988\%$

APPENDIX L

RANKINE CYCLE CALCULATIONS

Rankine Cycle Calculations

$k := 10^3$

Pump Inlet / Reservoir

$P_1 := 101.325 k \cdot Pa$ $h_1 := 100.0097 \frac{k \cdot J}{kg}$ $s_1 := 0.3508 \frac{k \cdot J}{kg \cdot K}$ $v_1 := 0.001 \frac{m^3}{kg}$

Pump Exit (actual)

$P_{2ap} := 963.17 k \cdot Pa$ $h_{2ap} := 100.8108 \frac{k \cdot J}{kg}$ $s_{2ap} := 0.3506 \frac{k \cdot J}{kg \cdot K}$ $v_{2ap} := 0.001 \frac{m^3}{kg}$

Pump Exit (ideal)

$P_{2a} := 963.17 k \cdot Pa$ $h_{2a} := 100.8708 \frac{k \cdot J}{kg}$ $s_{2a} := 0.3508 \frac{k \cdot J}{kg \cdot K}$ $v_{2a} := 0.001 \frac{m^3}{kg}$

Boiler Inlet (actual)

$P_{2p} := 963.17 k \cdot Pa$ $h_{2p} := 150.4245 \frac{k \cdot J}{kg}$ $s_{2p} := 0.5144 \frac{k \cdot J}{kg \cdot K}$ $v_{2p} := 0.001 \frac{m^3}{kg}$

Boiler Inlet (ideal)

$P_2 := 963.17 k \cdot Pa$ $h_2 := 100.9302 \frac{k \cdot J}{kg}$ $s_2 := 0.3508 \frac{k \cdot J}{kg \cdot K}$ $v_2 := 0.001 \frac{m^3}{kg}$

Boiler Exit

$P_{3b} := 480.537 k \cdot Pa$ $h_{3b} := 3213.334 \frac{k \cdot J}{kg}$ $s_{3b} := 7.7238 \frac{k \cdot J}{kg \cdot K}$ $v_{3b} := 0.6146 \frac{m^3}{kg}$

Turbine Inlet

$P_{3t} := 480.537 k \cdot Pa$ $h_{3t} := 2764.0848 \frac{k \cdot J}{kg}$ $s_{3t} := 6.8754 \frac{k \cdot J}{kg \cdot K}$ $v_{3t} := 0.3979 \frac{m^3}{kg}$

Turbine Exit (actual -- for using turbine inlet values)

$P_{4p\_t} := 101.325\,k\cdot Pa$ $h_{4p\_t} := 2679.7689\,\frac{k\cdot J}{kg}$ $s_{4p\_t} := 7.3655\,\frac{k\cdot J}{kg\cdot K}$ $v_{4p\_t} := 0.001\,\frac{m^3}{kg}$

Turbine Exit (ideal -- for using turbine inlet values)

$P_{4\_t} := 101.325\,k\cdot Pa$ $h_{4\_t} := 2496.9084\,\frac{k\cdot J}{kg}$ $s_{4\_t} := 6.8754\,\frac{k\cdot J}{kg\cdot K}$ $v_{4\_t} := 1.5403\,\frac{m^3}{kg}$

Turbine Exit (theoretical / actual -- for using boiler exit values and dT)

$P_{4p\_b} := 101.325\,k\cdot Pa$ $h_{4p\_b} := 3105.0094\,\frac{k\cdot J}{kg}$ $s_{4p\_b} := 8.2632\,\frac{k\cdot J}{kg\cdot K}$ $v_{4p\_b} := 2.6737\,\frac{m^3}{kg}$

Turbine Exit (theoretical / ideal -- for using boiler exit values and dT)

$P_{4\_b} := 101.325\,k\cdot Pa$ $h_{4\_b} := 2826.9198\,\frac{k\cdot J}{kg}$ $s_{4\_b} := 7.7238\,\frac{k\cdot J}{kg\cdot K}$ $v_{4\_b} := 2.0303\,\frac{m^3}{kg}$

Pump Efficiency

$w_{pump\_in\_actual} := h_{2ap} - h_1$ $w_{pump\_in\_actual} = 0.801\,\frac{k\cdot J}{kg}$

$w_{pump\_in\_ideal} := h_{2a} - h_1$ $w_{pump\_in\_ideal} = 0.861\,\frac{k\cdot J}{kg}$

$\eta_{pump} := \frac{w_{pump\_in\_actual}}{w_{pump\_in\_ideal}}$ $\eta_{pump} = 93.032\%$

$\eta_{pump\_alt} := \frac{h_{2ap} - h_1}{h_{2a} - h_1}$ $\eta_{pump\_alt} = 93.032\%$

Turbine Efficiency

$w_{turbine\_out\_actual} := h_{3t} - h_{4p\_t}$ $\quad w_{turbine\_out\_actual} = 84.316 \frac{k \cdot J}{kg}$

$w_{turbine\_out\_ideal} := h_{3t} - h_{4\_t}$ $\quad w_{turbine\_out\_ideal} = 267.176 \frac{k \cdot J}{kg}$

$\eta_{turbine} := \frac{w_{turbine\_out\_actual}}{w_{turbine\_out\_ideal}}$ $\quad \eta_{turbine} = 31.558\%$

$\eta_{turbine\_alt} := \frac{h_{3t} - h_{4p\_t}}{h_{3t} - h_{4\_t}}$ $\quad \eta_{turbine\_alt} = 31.558\%$

Theoretical Turbine Efficiency using Exit of Boiler for Turbine Inlet

$w_{turbine\_out\_theoretical} := h_{3b} - h_{4p\_b}$ $\quad w_{turbine\_out\_theoretical} = 108.325 \frac{k \cdot J}{kg}$

$w_{turbine\_out\_ideal\_theoretical} := h_{3b} - h_{4\_b}$ $\quad w_{turbine\_out\_ideal\_theoretical} = 386.414 \frac{k \cdot J}{kg}$

$\eta_{turbine\_theoretical} := \frac{w_{turbine\_out\_theoretical}}{w_{turbine\_out\_ideal\_theoretical}}$ $\quad \eta_{turbine\_theoretical} = 28.033\%$

Boiler Efficiency *(Using Turbine Inlet Temp as Point 3)*

$q_{boiler\_in\_actual} := h_{3t} - h_{2p}$ $\quad q_{boiler\_in\_actual} = 2.614 \times 10^3 \frac{k \cdot J}{kg}$

$q_{boiler\_in\_ideal} := h_{3t} - h_{2}$ $\quad q_{boiler\_in\_ideal} = 2.663 \times 10^3 \frac{k \cdot J}{kg}$

$\eta_{boiler} := \frac{q_{boiler\_in\_actual}}{q_{boiler\_in\_ideal}}$ $\quad \eta_{boiler} = 98.142\%$

Boiler Efficiency *(Using Boiler Exit Temp as Point 3)*

$q_{boiler\_in\_theoretical} := h_{3b} - h_{2p}$ $\quad q_{boiler\_in\_theoretical} = 3.063\times 10^{3}\ \frac{k\cdot J}{kg}$

$q_{boiler\_in\_ideal\_theoretical} := h_{3b} - h_{2}$ $\quad q_{boiler\_in\_ideal\_theoretical} = 3.112\times 10^{3}\ \frac{k\cdot J}{kg}$

$\eta_{boiler\_theoretical} := \frac{q_{boiler\_in\_theoretical}}{q_{boiler\_in\_ideal\_theoretical}}$ $\quad \eta_{boiler\_theoretical} = 98.41\%$

Condenser / Reservoir *(for using turbine inlet values)*

$q_{reservoir\_out\_actual} := h_{4p\_t} - h_{1}$ $\quad q_{reservoir\_out\_actual} = 2.58\times 10^{3}\ \frac{k\cdot J}{kg}$

$q_{reservoir\_out\_ideal} := h_{4\_t} - h_{1}$ $\quad q_{reservoir\_out\_ideal} = 2.397\times 10^{3}\ \frac{k\cdot J}{kg}$

$\eta_{reservoir} := \frac{q_{reservoir\_out\_ideal}}{q_{reservoir\_out\_actual}}$ $\quad \eta_{reservoir} = 92.912\%$

Condenser / Reservoir *(for using boiler exit values)*

$q_{reservoir\_out\_actual\_b} := h_{4p\_b} - h_{1}$ $\quad q_{reservoir\_out\_actual\_b} = 3.005\times 10^{3}\ \frac{k\cdot J}{kg}$

$q_{reservoir\_out\_ideal\_b} := h_{4\_b} - h_{1}$ $\quad q_{reservoir\_out\_ideal\_b} = 2.727\times 10^{3}\ \frac{k\cdot J}{kg}$

$\eta_{reservoir\_b} := \frac{q_{reservoir\_out\_ideal\_b}}{q_{reservoir\_out\_actual\_b}}$ $\quad \eta_{reservoir\_b} = 90.746\%$

Net Work Output

$w_{net\_out} := \left(h_{3t} - h_{4p\_t}\right) - \left(h_{2ap} - h_1\right)$ $w_{net\_out} = 83.515 \frac{k \cdot J}{kg}$

$w_{net} := w_{turbine\_out\_actual} - w_{pump\_in\_actual}$ $w_{net} = 83.515 \frac{k \cdot J}{kg}$

Net Work Output *(theoretical using boiler exit values)*

$w_{net\_theoretical} := w_{turbine\_out\_theoretical} - w_{pump\_in\_actual}$ $w_{net\_theoretical} = 107.524 \frac{k \cdot J}{kg}$

Heat Input

$q_{in} := q_{boiler\_in\_actual}$ $q_{in} = 2.614 \times 10^3 \frac{k \cdot J}{kg}$

Heat Input *(theoretical)*

$q_{in\_theoretical} := q_{boiler\_in\_theoretical}$ $q_{in\_theoretical} = 3.063 \times 10^3 \frac{k \cdot J}{kg}$

Rankine Cycle Efficiency

$\eta_{cycle} := \frac{w_{net\_out}}{q_{in}}$ $\eta_{cycle} = 3.195\%$

$\eta_{cycle\_alt} := \frac{\left(h_{3t} - h_{4p\_t}\right) - \left(h_{2ap} - h_1\right)}{h_{3t} - h_{2p}}$ $\eta_{cycle\_alt} = 3.195\%$

Rankine Cycle Efficiency *(theoretical)*

$$\eta_{cycle\_theoretical} := \frac{w_{net\_theoretical}}{q_{in\_theoretical}} \qquad \eta_{cycle\_theoretical} = 3.511\%$$

$$\eta_{cycle\_theoretical\_alt} := \frac{\left(h_{3b} - h_{4p\_b}\right) - \left(h_{2ap} - h_1\right)}{h_{3b} - h_{2p}} \qquad \eta_{cycle\_theoretical\_alt} = 3.511\%$$

Ideal Rankine Cycle Efficiency

$$w_{net\_ideal} := w_{turbine\_out\_ideal} - w_{pump\_in\_ideal} \qquad w_{net\_ideal} = 266.315\frac{k{\cdot}J}{kg}$$

$$w_{net\_out\_ideal} := \left(h_{3t} - h_{4\_t}\right) - \left(h_{2a} - h_1\right) \qquad w_{net\_out\_ideal} = 266.315\frac{k{\cdot}J}{kg}$$

$$q_{in\_ideal} := q_{boiler\_in\_ideal} \qquad q_{in\_ideal} = 2.663\times 10^3\,\frac{k{\cdot}J}{kg}$$

$$\eta_{cycle\_ideal} := \frac{w_{net\_ideal}}{q_{in\_ideal}} \qquad \eta_{cycle\_ideal} = 10\%$$

$$\eta_{cycle\_ideal\_alt} := \frac{\left(h_{3t} - h_{4\_t}\right) - \left(h_{2a} - h_1\right)}{h_{3t} - h_2} \qquad \eta_{cycle\_ideal\_alt} = 10\%$$

***Ideal Rankine Cycle Efficiency** (theoretical)*

$w_{net\_ideal\_theoretical} := w_{turbine\_out\_ideal\_theoretical} - w_{pump\_in\_ideal}$

$w_{net\_ideal\_theoretical} = 385.553 \frac{k \cdot J}{kg}$

$w_{net\_out\_ideal\_theoretical} := (h_{3b} - h_{4\_b}) - (h_{2a} - h_1)$ $w_{net\_out\_ideal\_theoretical} = 385.553 \frac{k \cdot J}{kg}$

$q_{in\_ideal\_theoretical} := q_{boiler\_in\_ideal\_theoretical}$ $q_{in\_ideal\_theoretical} = 3.112 \times 10^3 \frac{k \cdot J}{kg}$

$\eta_{cycle\_ideal\_theoretical} := \frac{w_{net\_ideal\_theoretical}}{q_{in\_ideal\_theoretical}}$ $\eta_{cycle\_ideal\_theoretical} = 12.388\%$

$\eta_{cycle\_ideal\_theoretical\_alt} := \frac{(h_{3b} - h_{4\_b}) - (h_{2a} - h_1)}{h_{3b} - h_2}$ $\eta_{cycle\_ideal\_theoretical\_alt} = 12.388\%$

Comparison of Actual to Ideal

$\eta_{actual\_to\_ideal} := \frac{\eta_{cycle}}{\eta_{cycle\_ideal}}$ $\eta_{actual\_to\_ideal} = 31.953\%$

***Comparison of Actual to Ideal** (theoretical)*

$\eta_{actual\_to\_ideal\_theoretical} := \frac{\eta_{cycle\_theoretical}}{\eta_{cycle\_ideal\_theoretical}}$ $\eta_{actual\_to\_ideal\_theoretical} = 28.339\%$

Carnot Efficiency

$T_C := 296.99K$ $T_{H\_t} := 431.46K$ $T_{H\_b} := 644.78K$

$$\eta_{carnot\_t} := 1 - \frac{T_C}{T_{H\_t}} \qquad \eta_{carnot\_t} = 31.166\%$$

$$\eta_{carnot\_b} := 1 - \frac{T_C}{T_{H\_b}} \qquad \eta_{carnot\_b} = 53.939\%$$

System Efficiency Compared to Carnot

$$\eta_{rankine\_to\_carnot\_t} := \frac{\eta_{cycle}}{\eta_{carnot\_t}} \qquad \eta_{rankine\_to\_carnot\_t} = 10.252\%$$

$$\eta_{rankine\_to\_carnot\_b} := \frac{\eta_{cycle}}{\eta_{carnot\_b}} \qquad \eta_{rankine\_to\_carnot\_b} = 5.924\%$$

System Efficiency Compared to Carnot *(theoretical)*

$$\eta_{rankine\_to\_carnot\_theoretical} := \frac{\eta_{cycle\_theoretical}}{\eta_{carnot\_b}} \qquad \eta_{rankine\_to\_carnot\_theoretical} = 6.508\%$$

APPENDIX M

AUTOCAD DRAWINGS AND DIMENSIONING

OF

T-500

IMPULSE STEAM TURBINE

AND

GEAR TRAIN

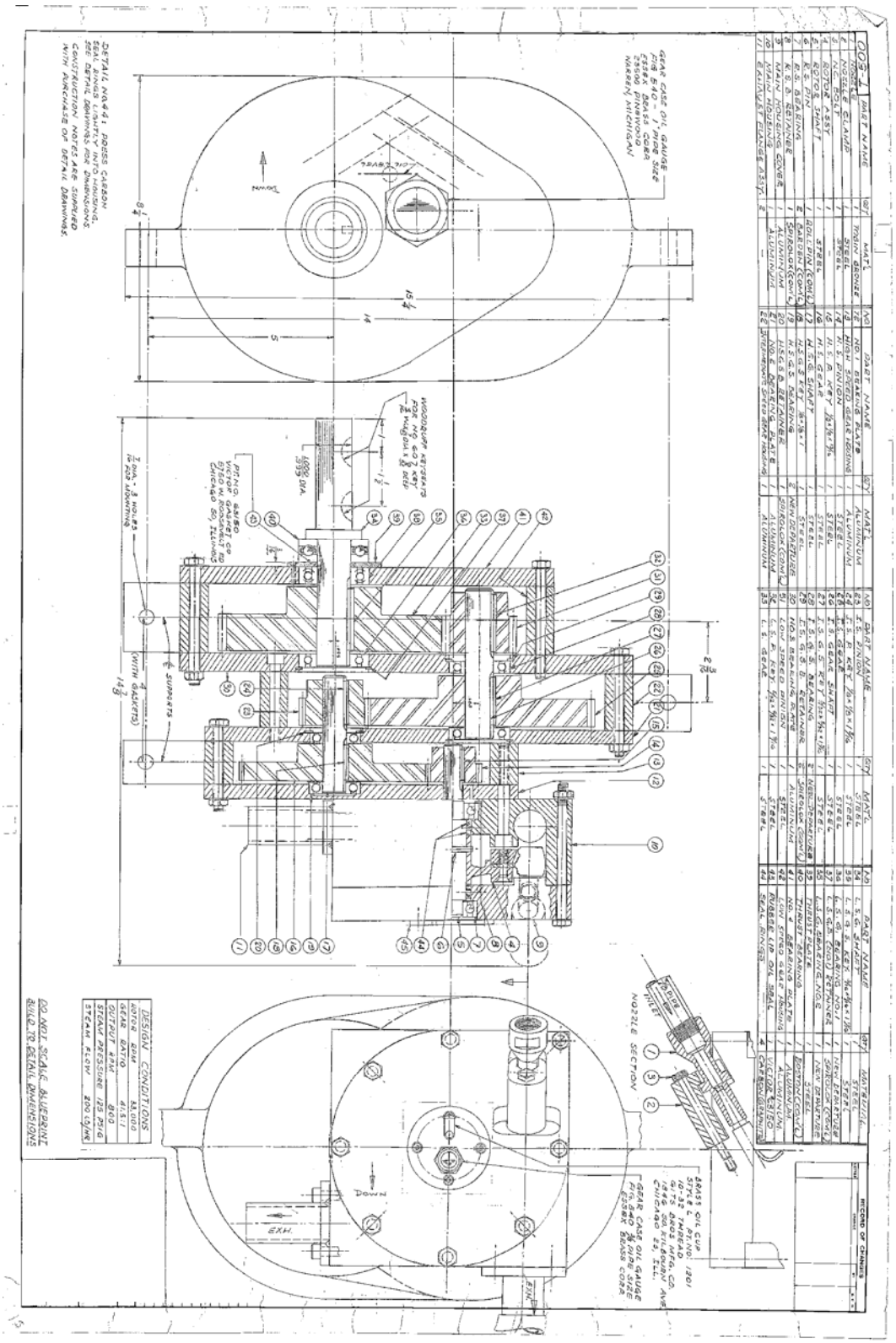

Figure M.1: Detailed drawing for complete assembly of T-500 impulse steam turbine and gear train.

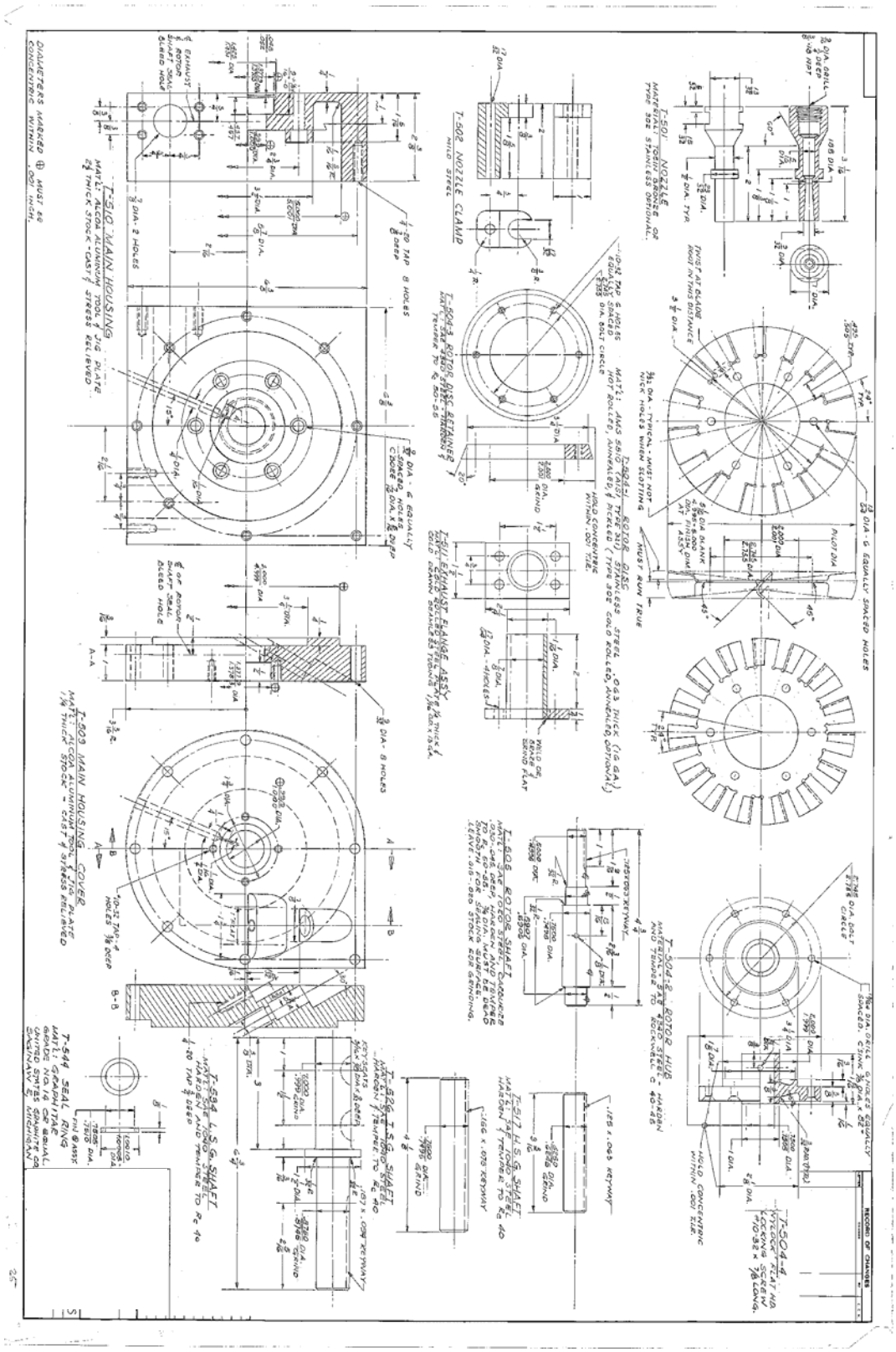

Figure M.2: Detailed drawing of T-500 impulse steam turbine rotor (blades) , housing, and nozzle design.

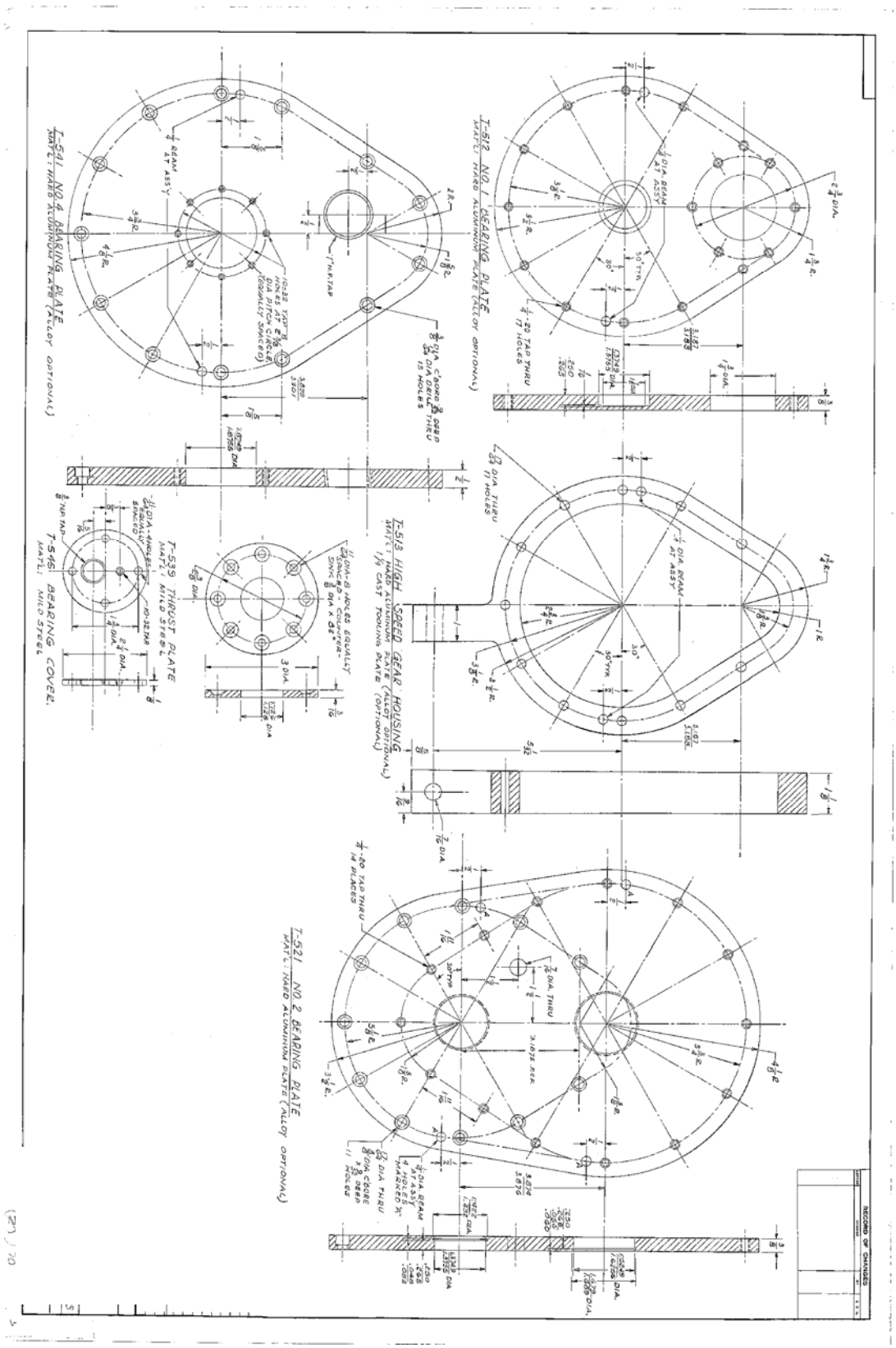

Figure M.3: Detailed drawing for first section of gear train; bearing plates one, two, and four, thrust plate, bearing cover, and high speed gear housing.

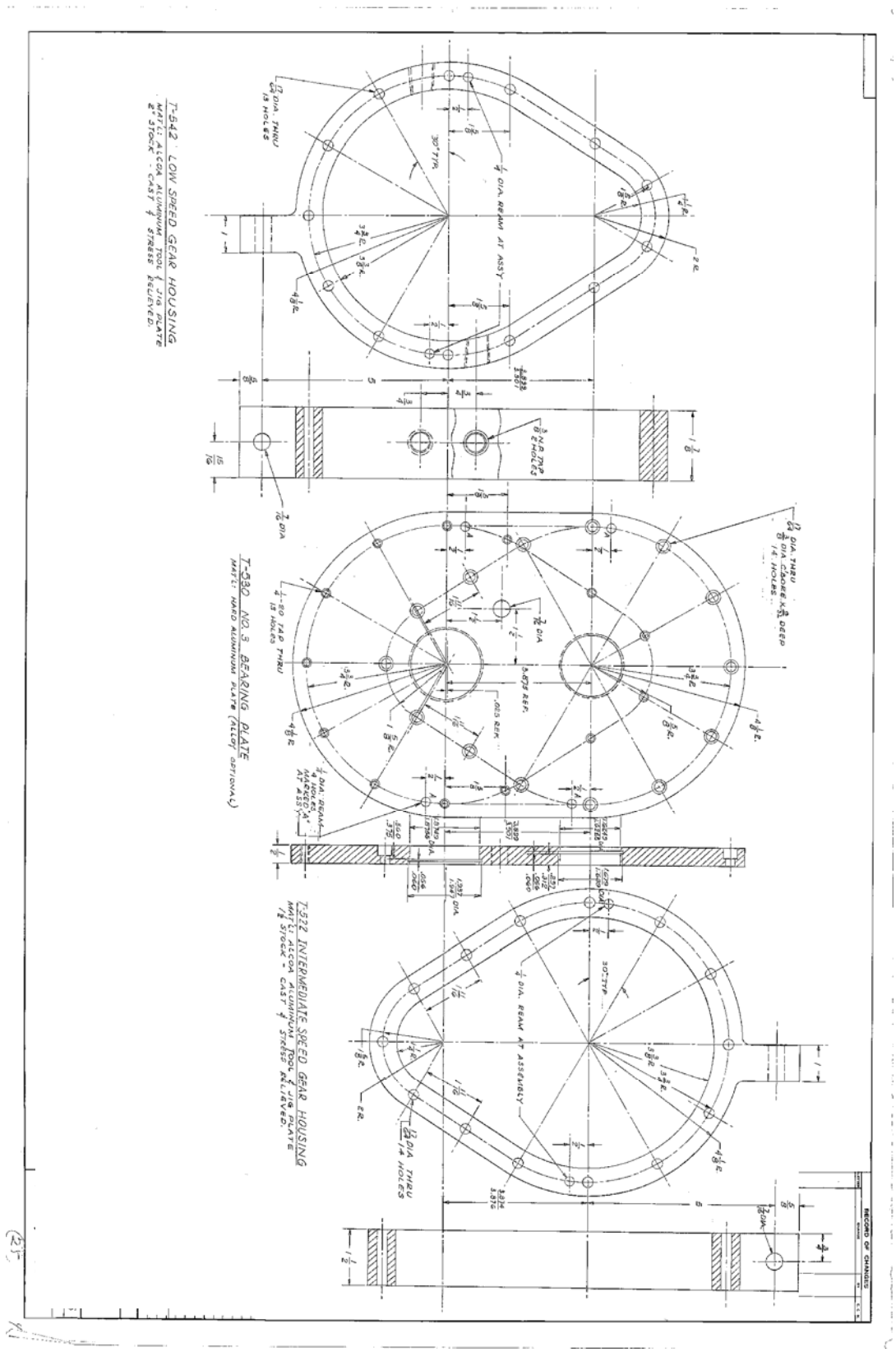

Figure M.4: Detailed drawing of bearing plate three, low speed gear housing, and intermediate speed gear housing.

APPENDIX N

RECEIVER/BOILER
DETAILED DRAWINGS AND IMAGES

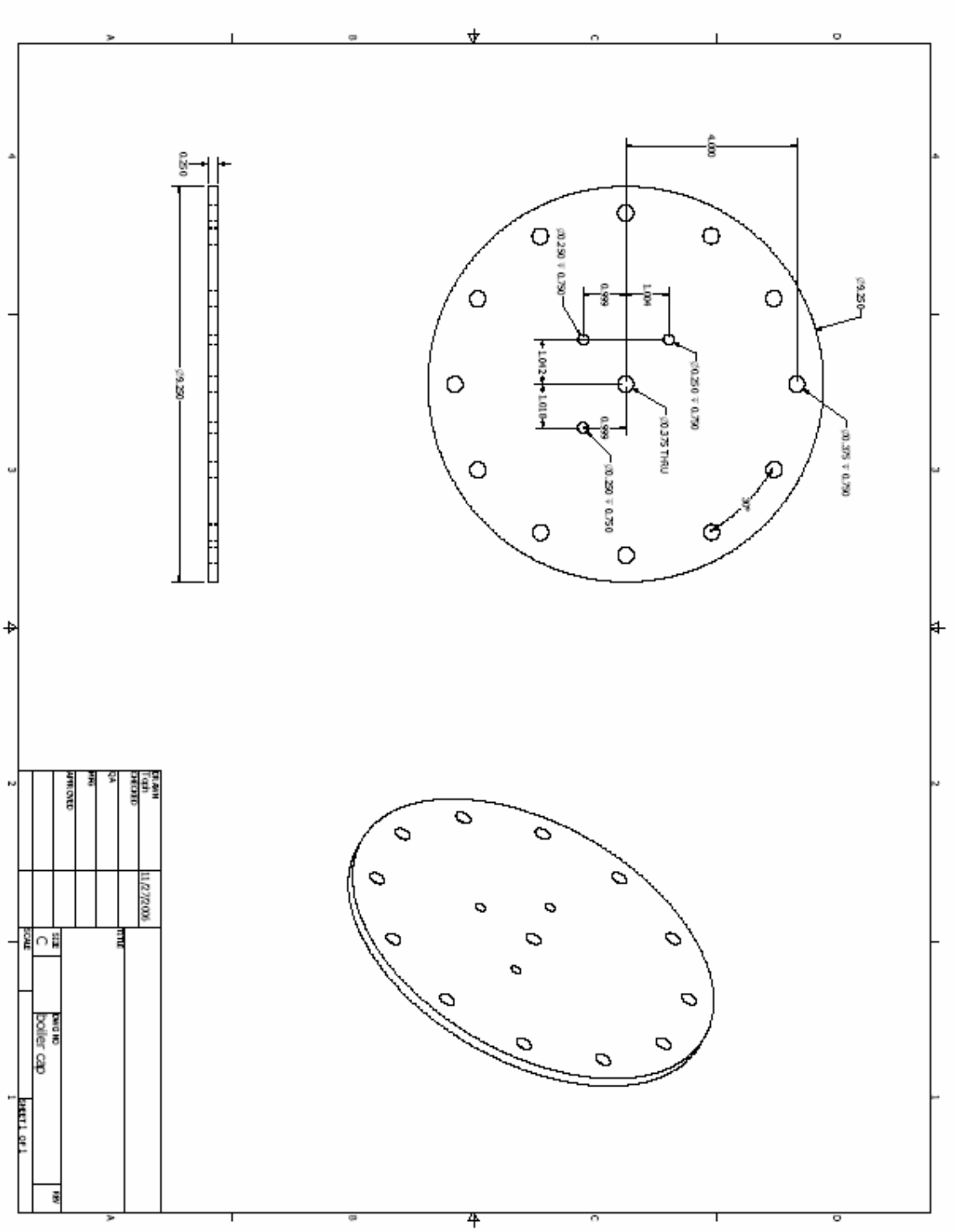

Figure N.1: Dimensioned diagram of the Receiver/Boiler Cap.

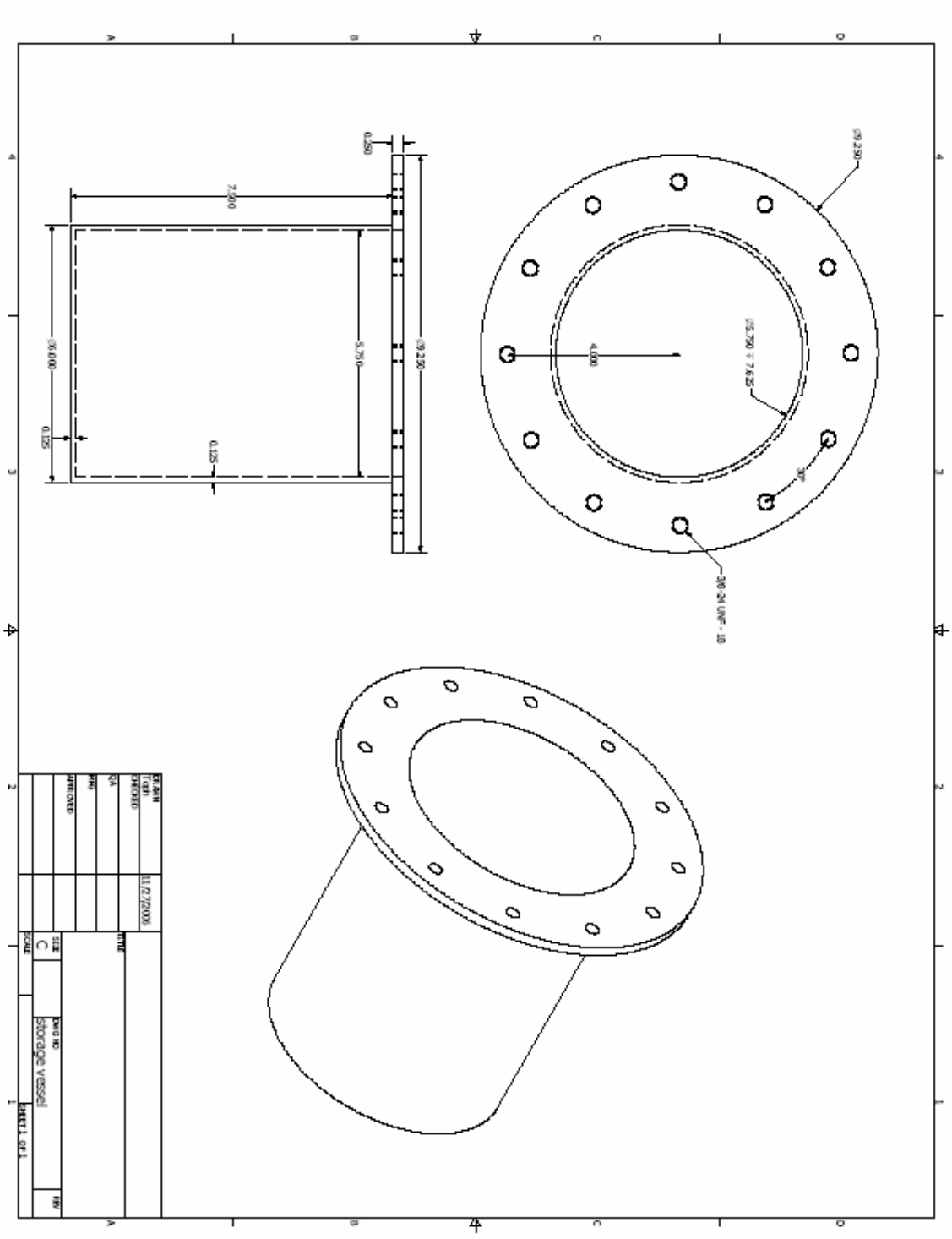

Figure N.2: Dimensioned diagram of the main body of the Receiver/Boiler.

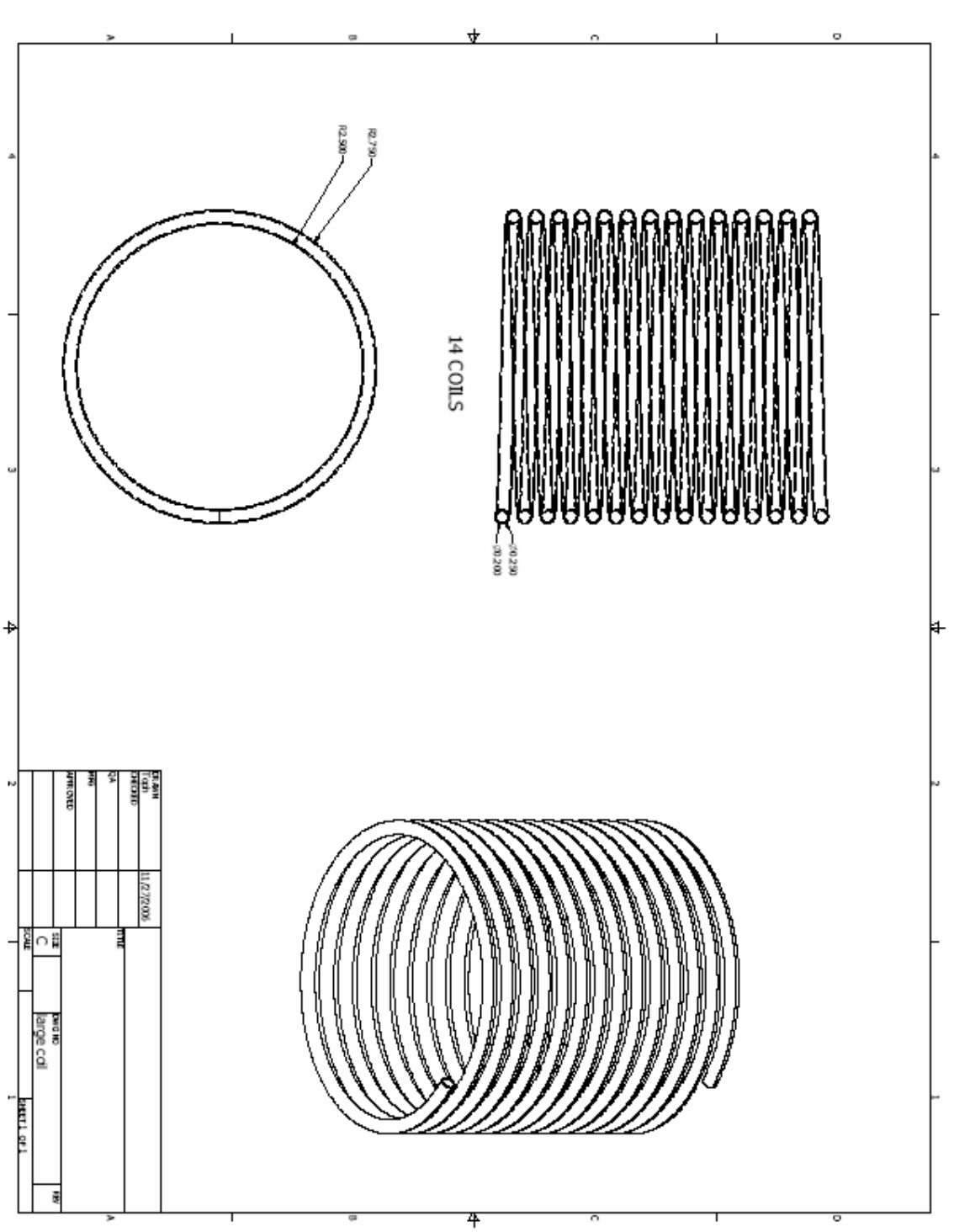

Figure N.3: Dimensioned diagram of the outer coils contained within the receiver.

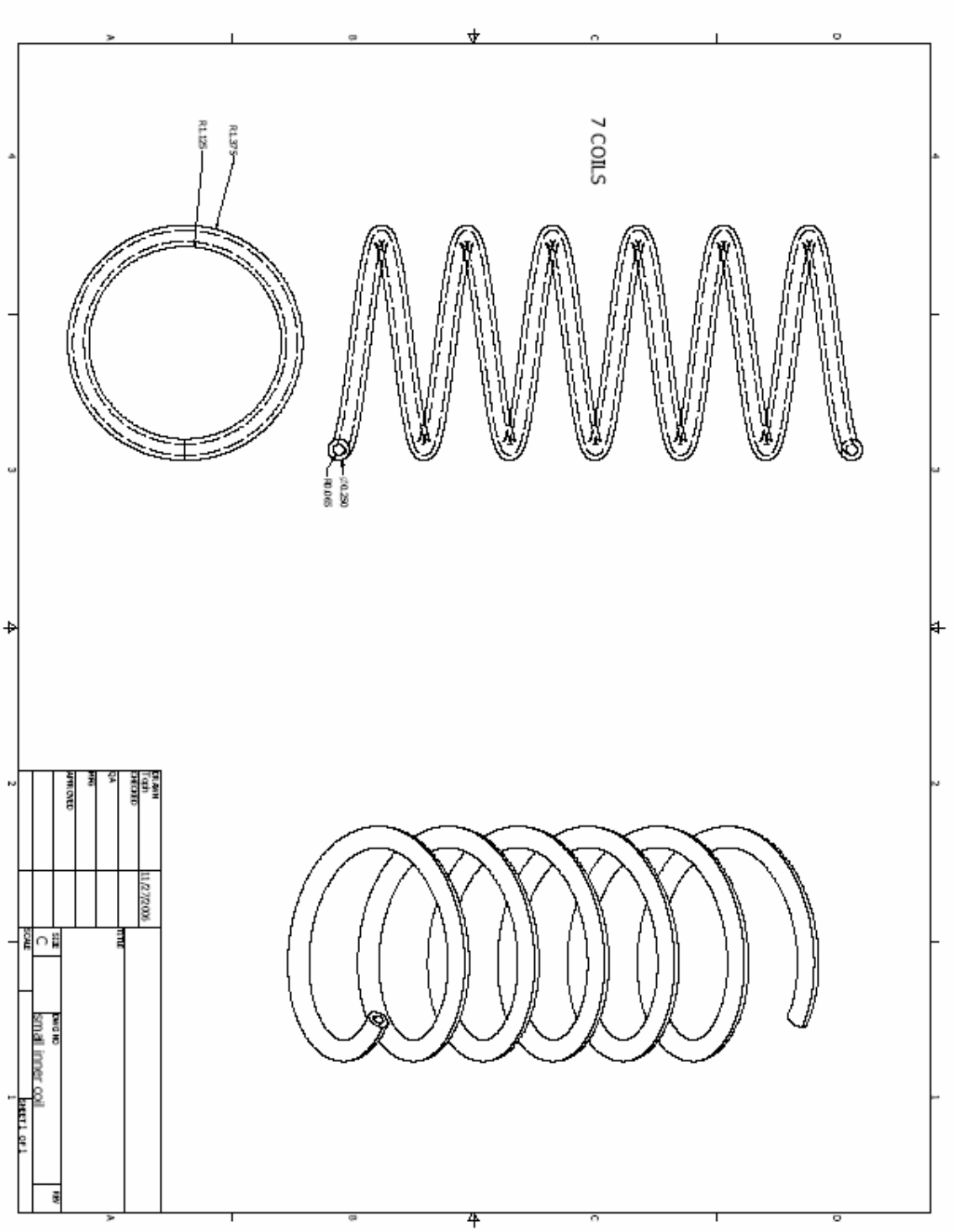

Figure N.4: Dimensioned diagram of the inner coils housed within the receiver.

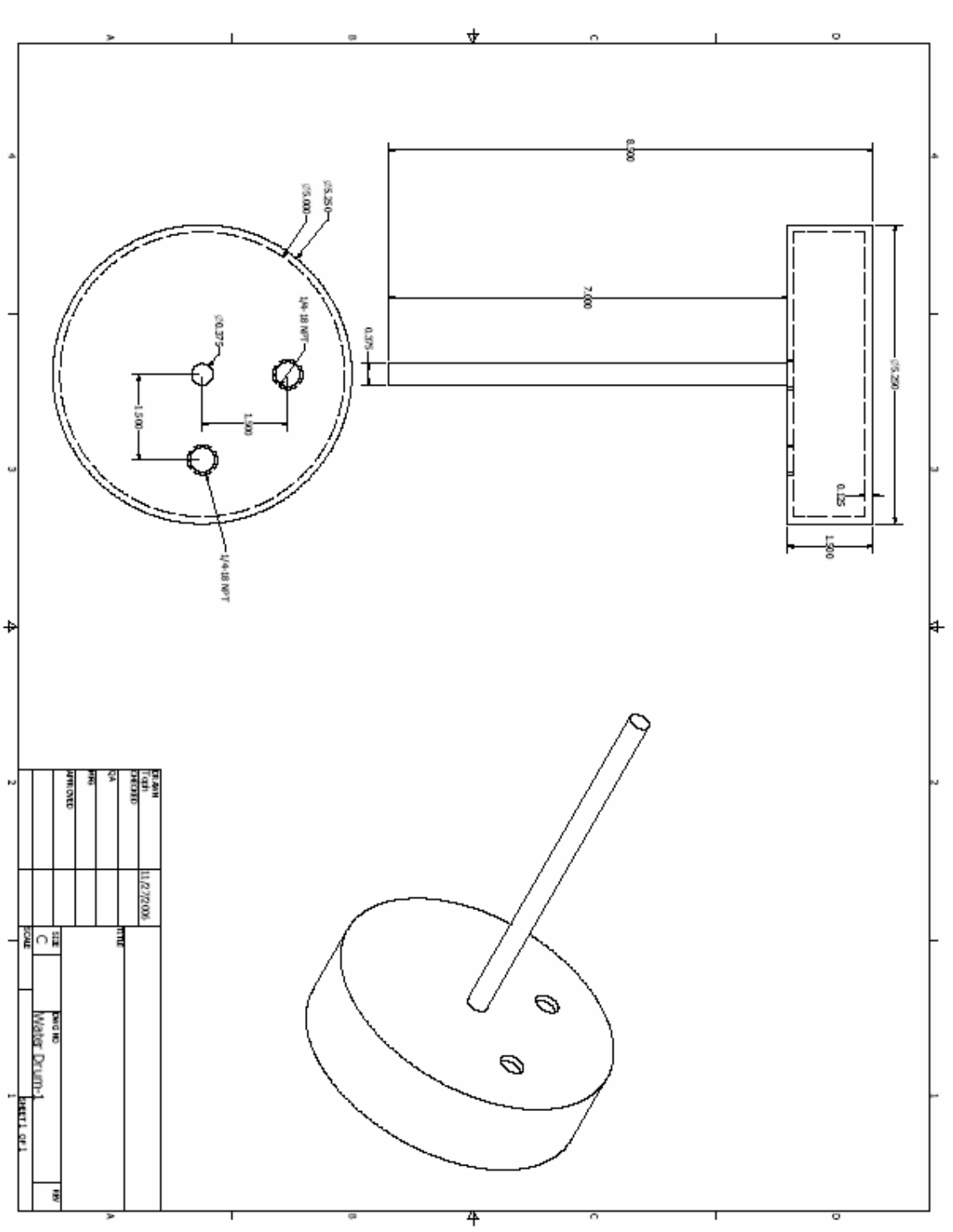

Figure N.5: Dimensioned diagram of the water drum located in the receiver.

Figure N.6: a) Exploded ¾ view of receiver/boiler. b) ¾ view of assembled receiver/boiler.

Figure N.7: Image of the actual receiver cap, inner and outer coils, and water drum assembled.

Figure N.8: Main body of the receiver/boiler.

Figure N.9: Assembled receiver/boiler being heated on electric burner for initial mixing of the draw salt thermal bath.

Figure N.10: Receiver/boiler assembled with thermocouple and feed-tubes.

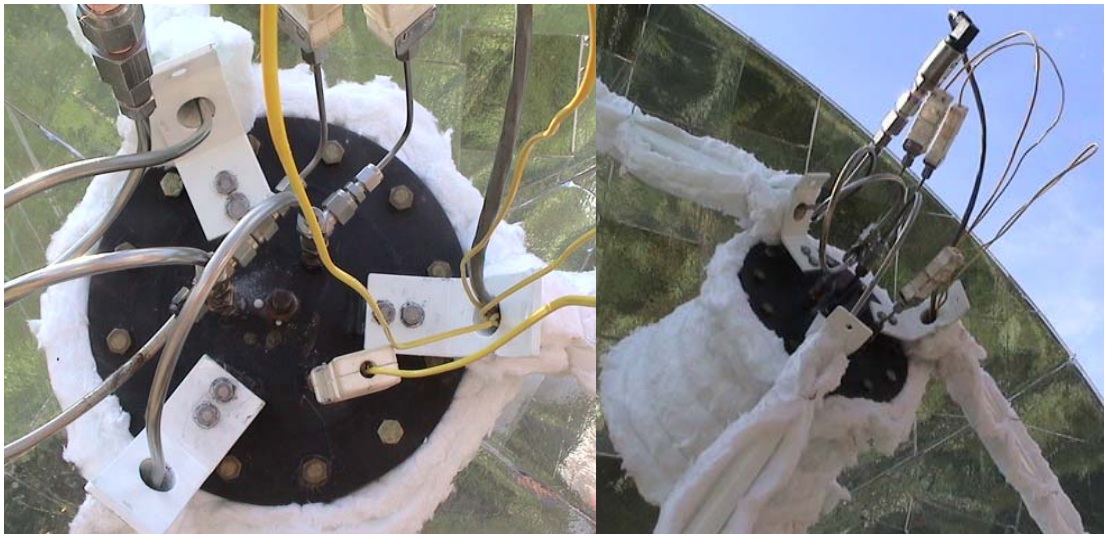

Figure N.11: Receiver/boiler assembled at the focal region of concentrator.

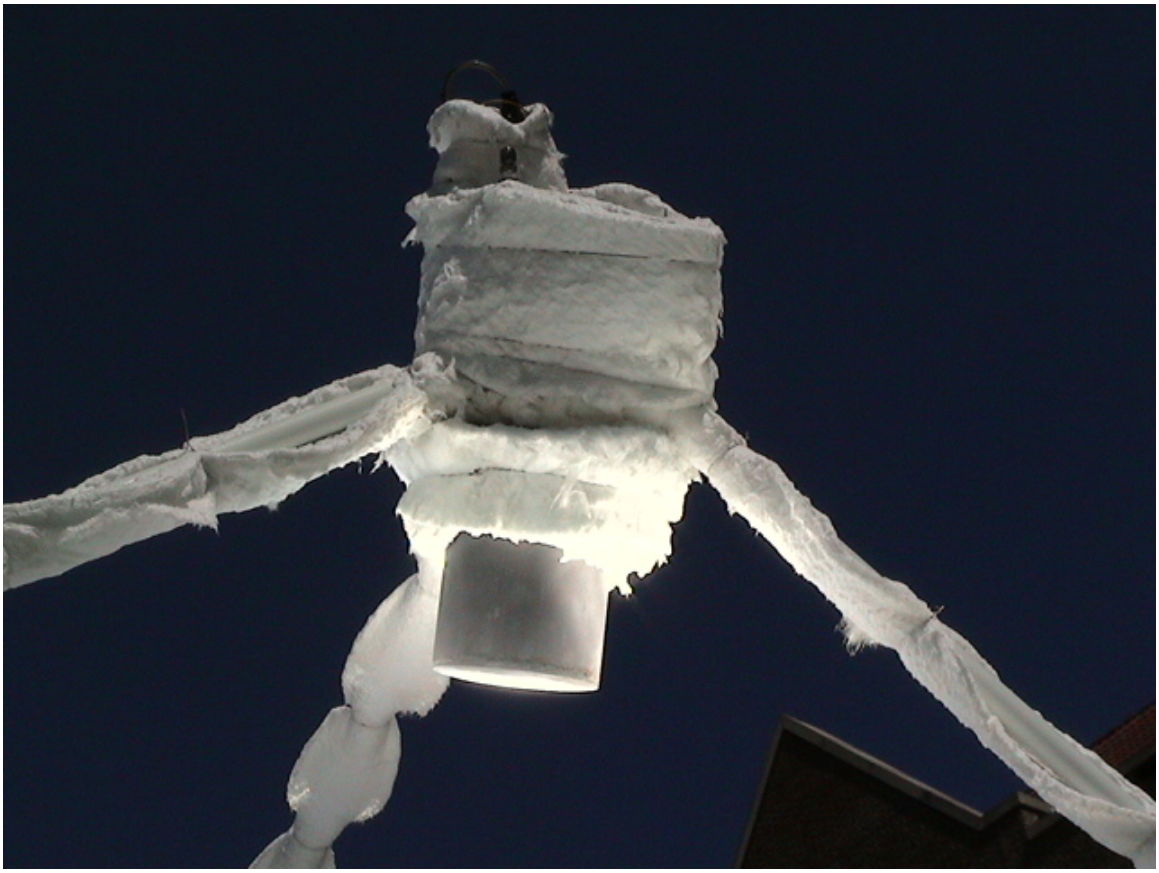

Figure N.12: Receiver/boiler being submitted to concentrated solar insolation.

APPENDIX O

SOLAR CHARGER CONTROLLER
ELECTRICAL DIAGRAM

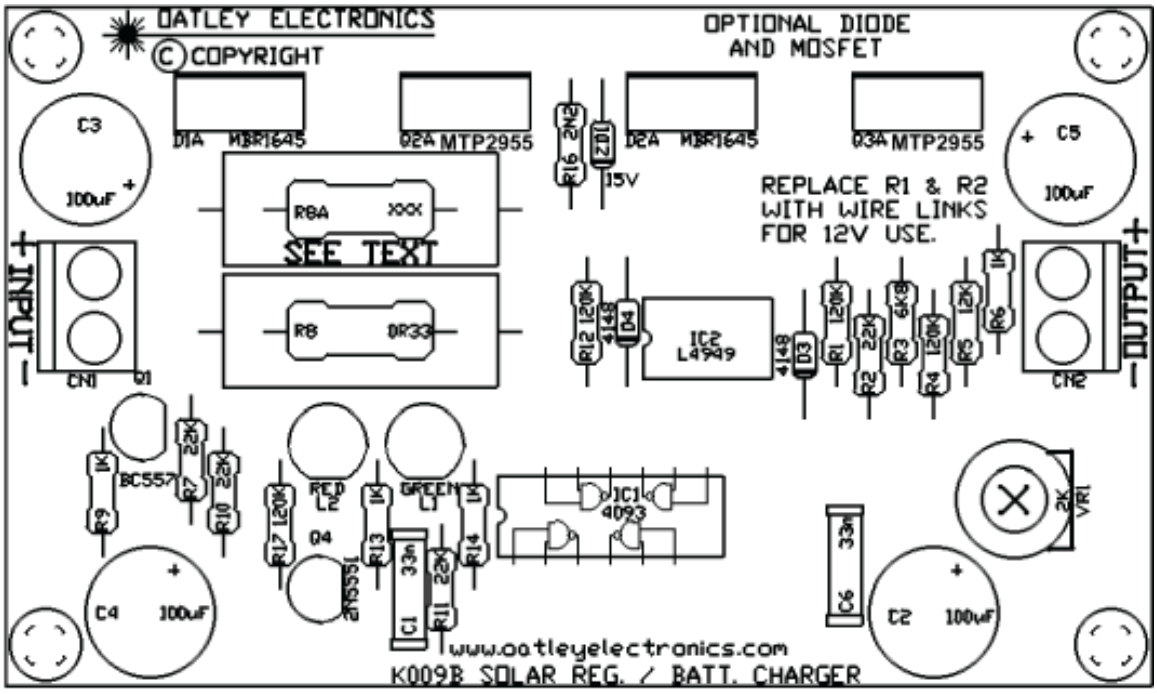

Figure O.1: Diagram of the solar charger controller circuit board layout.

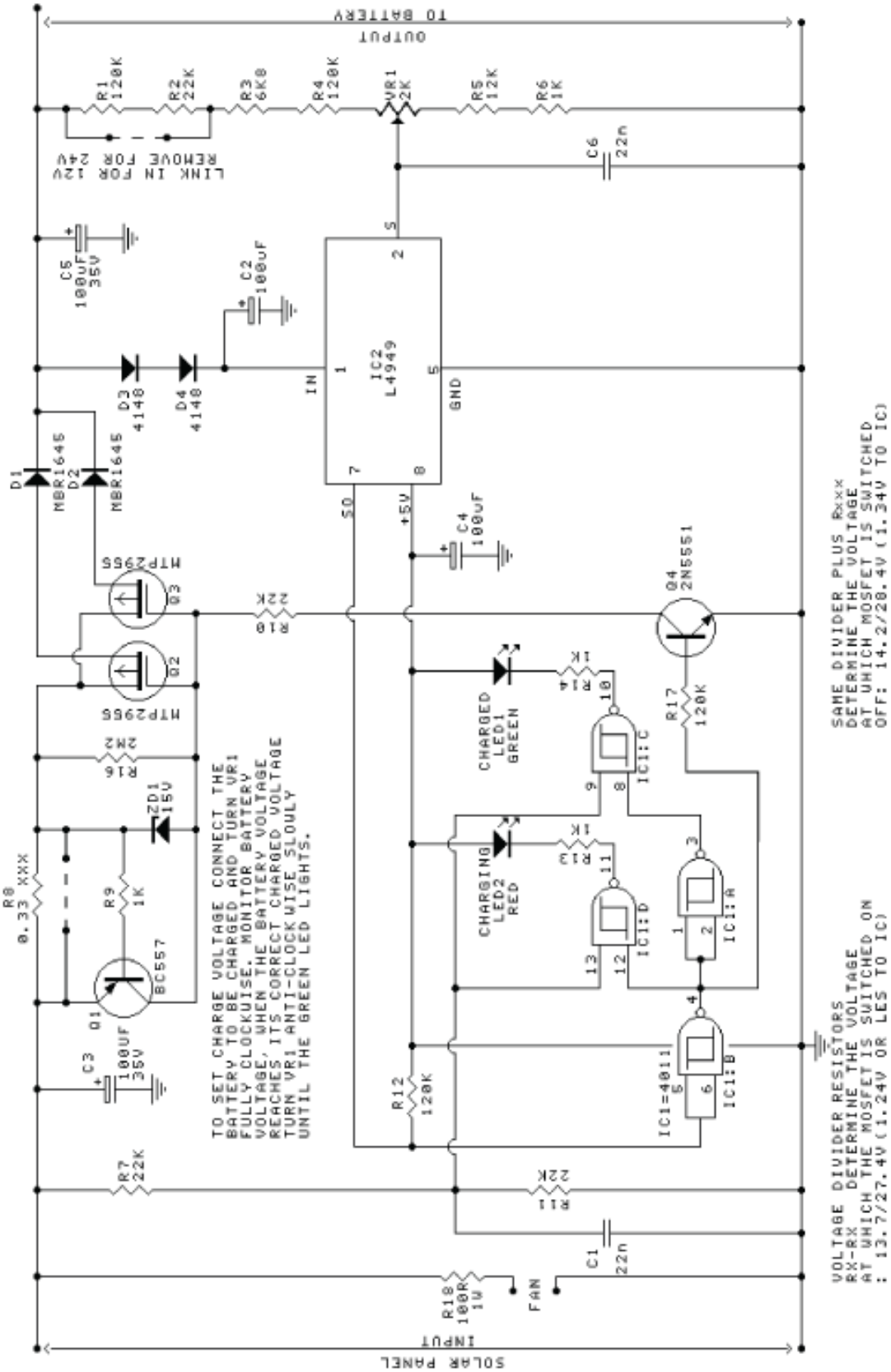

Figure O.2: Solar charger controller wiring schematic.

APPENDIX P

WINDSTREAM POWER LOW RPM PERMANENT MAGNET DC GENERATOR

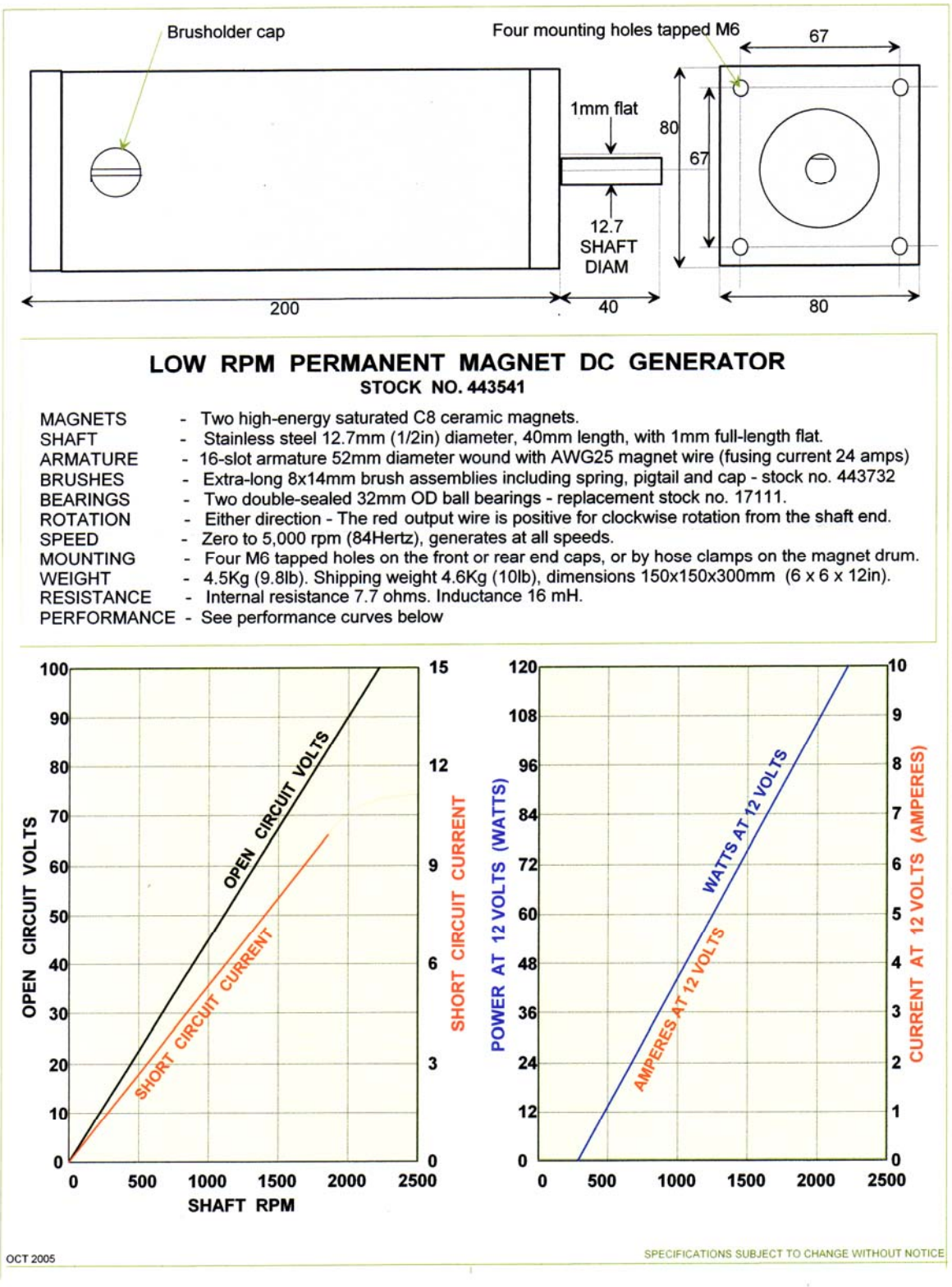

Figure P.1: Diagram, specifications, and performance curves of generator.

REFERENCES

[1] Goswami, D. Yogi, Kreith, Frank, and Kreider, Jan F., *Principles of Solar Engineering*, 2nd edition. Taylor and Francis, Philadelphia, PA, 2000.

[2] Duffie, John A., and Beckman, William A., *Solar Engineering of Thermal Processes*, 2nd edition. Wiley, New York, 1991.

[3] Rapp, Donald, *Solar Energy*. Prentice-Hall, Englewood Cliffs, NJ, 1981.

[4] Geyer, Michael, and Stine, William B., *Power From the Sun* (Powerfromthesun.net). J.T. Lyle Center, 2001.

[5] Hulstrom, Roland, *Solar Resources, Solar Heat Technologies: Fundamentals and Applications*. Massachusetts Institute of Technology, Cambridge, Massachusetts, 1989.

[6] Cheremisinoff, Paul N., and Regino, Thomas C., *Principles and Applications of Solar Energy*. Ann Arbor Science Publishers, Ann Arbor, Michigan, 1978.

[7] Sorenson, Bent, *Renewable Energy: Its physics, engineering, environmental impacts, economics and planning*, 3rd edition. Elsevier Academic Press, Burlington, MA, 2004.

[8] Fay, James A. and Golomb, Dan S., *Energy and the Environment*. Oxford University Press, New York, 2002.

[9] Power Systems Group/Ametek Inc., *Solar Energy Handbook: Theory and Applications*. Chilton Book Company, Radnor, PA, 1979.

[10] Kryza, Frank, *The Power of Light*. McGraw-Hill, New York, 2003.

[11] Stine, William B., *Progress in Parabolic Dish Technology*. Solar Energy Research Institute, SERI/SP 220-3237, 1989.

[12] Hsieh, Jui Sheng, *Solar Energy Engineering*. Prentice-Hall, Englewood Cliffs, NJ, 1986.

[13] Rabl, Ari, *Active Solar Collectors and Their Applications*. Oxford University Press, New York, 1985.

[14] Kribus, A., Doron, P., Rachamim, R., and Karni, J., A Multistage Solar Receiver: The Route to High Temperature. *Solar Energy*, 67:3-11, 1999.

[15] Kribus, A., A High-Efficiency Triple Cycle for Solar Power Generation. *Solar Energy,* 72:1-11, 2002.

[16] Kribus, A. and Ries, H., LiMoNAED: A Limited Motion, Non-shading, Asymmetric, Ecliptic-tracking Dish. *Solar Energy,* 73:337-344, 2002.

[17] Lane, George A., *Solar Heat Storage: Latent Heat Material*, Volume 1. CRC Press, Boca Raton, FL, 1983.

[18] Cannon, Joseph N., Carsie, A. Hall, Glakpe, Emmanuel K., *Modeling Cyclic Phase Change and Energy Storage in Solar Heat Receivers.* NASA/TM-107487. *AIAA Paper 97-2452*, 1997.

[19] Karni, J., Kribus, A., Doron, P., Rubin, R., Fiterman, A., and Sagie, D., The DIAPR: A High-Pressure, High-Temperature Solar Receiver. *Journal of Solar Energy Engineering,* 119:74-78, 1997.

[20] Bertocchi, R., Karni, J., and Kribus, A., Experimental evaluation of a non-isothermal high temperature solar particle receiver. *Energy,* 29:687-700, 2004.

[21] Saunders, E. A. D., *Heat Exchanges: Selection, Design, and Construction*. Wiley, New York, 1988.

[22] Hall, Carsie A., Glakpe, Emmanuel K., and Cannon, Joseph N., *Thermal State-of-Charge in Solar Heat Receivers*, NASA/TM-1998-207920/Rev1. *AIAA Paper 98-1017*, 1998.

[23] Van Wylen, Gordon, Sonntag, Richard, and Borgnakke, Claus, *Fundamentals of Classical Thermodynamics*, 4th edition. Wiley, New York, 1994.

[24] Cengal, Yunus A., *Introduction to Thermodynamics and Heat Transfer*. McGraw-Hill, New York, 1996.

[25] Teir, Sebastian, *Basics of Steam Generation*. Helsinki University of Technology Department of Mechanical Engineering, Energy Engineering and Environmental Protection Publications, eBook, 2002.

[26] Kruse, Alfred and Wagner, Wolfgang, *Properties of Water and Steam*. Springer-Verlag, Berlin Heidelberg New York, 1998.

[27] Fruchter, E., Grossman, G., and Kreith, F., An Experimental Investigation of a Stationary Reflector/Tracking Absorber Solar Collector at Intermediate Temperatures. *Journal of Solar Energy Engineering,* 104:340-344, 1982.

[28] Grossman, Gershon, and Fruchter, Eliezer, Development of a Spherical Reflector/Tracking Absorber Solar Energy Collector. *Israel Journal of Technology*, 17:5-11, 1979.

[29] Forristall, R., *Heat Transfer Analysis and Modeling of a Parabolic Trough Solar Receiver Implemented in Engineering Equation Solver*. National Renewable Energy Laboratory, 2003.

[30] Salisbury, J. Kenneth, *Steam Turbines and Their Cycles*. Krieger Publishing Company, Malabar, FL, 1974.

[31] Fox, Robert W., and McDonald, Alan T., *Introduction to Fluid Mechancis*, 5th edition. Wiley, New York, 1998.

[32] Kulla, Antto, and Teir, Sebastian, *Boiler Calculations.* Helsinki University of Technology Department of Mechanical Engineering, Energy Engineering and Environmental Protection Publications, eBook, 2002.

BIOGRAPHICAL SKETCH

C. Christopher Newton

Charles Christopher Newton was born on April 11, 1982, in Washington, Indiana, to Michelle Eskridge and Chris Newton. He began his undergraduate studies in 2000 at the Florida State University in Tallahassee, FL. In 2004, he received his Bachelors degree in Mechanical Engineering. Shortly after graduation, he began his graduate studies research work under the advisement of Professor Anjaneyulu Krothapalli and Dr. Brenton Greska in the pursuit of his Masters degree in Mechanical Engineering.